

UCLA

UCLA Electronic Theses and Dissertations

Title

Electromagnetic Devices Based on Periodic Structures

Permalink

<https://escholarship.org/uc/item/4qb6h3k0>

Author

Choi, Jun Hwan

Publication Date

2014

Peer reviewed|Thesis/dissertation

UNIVERSITY OF CALIFORNIA

Los Angeles

Electromagnetic Devices Based on Periodic Structures.

A dissertation submitted to in partial satisfaction of the
requirements for the degree Doctor of Philosophy
in Electrical Engineering

by

Jun Hwan (Brandon) Choi

2014

ABSTRACT OF THE DISSERTATION

Electromagnetic Devices Based on Periodic Structures.

by

Jun Hwan (Brandon) Choi

Doctor of Philosophy in Electrical Engineering

University of California, Los Angeles, 2014

Professor Tatsuo Itoh, Chair

Recent research advances based on periodic structures and antenna array systems are presented. In the first part of the dissertation, state-of-the-art retrodirective array (RDA) capable of retransmitting predictable polarization with respect to any received polarization state is proposed. RDAs have the unique ability to retransmit the received signal back to the interrogator without prior knowledge of the source location. In addition to this unique feature, the proposed system can receive any polarization and always backscatter the signal that is orthogonally polarized with respect to its received polarization state. This added feature helps to maintain a more secure communication link between the RDA and the interrogator by mitigating the polarization mismatch loss. The second half of the dissertation is dedicated to frequency scanning phased-array feed network and frequency selective surface (FSS) spatial filters based on metamaterial concept. Composite Right/Left-Hand (CRLH) metamaterial transmission lines

provide not only phase delay but also phase advance response that can be systematically engineered. This allows the design of an all-passive phased-array feeding network that supports dual-band and broadband frequency scanning capability over wide spatial angle. In addition, decoupling the radiating antenna elements from the array factor enables better controllability of the radiated characteristics in comparison to the widely known CRLH based leaky-wave antennas. Conventional periodic structures based on purely right-handed unit structures also exhibit metamaterial behaviors when the periodicities are much smaller than the operating wavelength. Incorporating this concept and the coupled filter theory, high performance multi-pole FSS is designed that is less sensitive to incident angles, polarizations, and separation distances between the FSS layers.

The dissertation of Jun Hwan (Brandon) Choi is approved

Warren Mori

Benjamin Williams

Christoph Niemann

Tatsuo Itoh, Committee Chair

University of California, Los Angeles

2014

Table of Contents

INTRODUCTION	1
CHAPTER 1 Polarization Friendly Retrodirective Antenna Array	5
1.1 Introduction.....	5
1.2 System Configuration	9
1.3 Theory.....	10
1.4 Fabricated System and System Performance.....	15
1.5 Measured Radar Cross Section (RCS) Results	16
1.6 Conclusion	22
CHAPTER 2 Phased-Array Feed Network based on Composite Right/Left-Handed (CRLH) Transmission Lines	23
2.1 Introduction.....	23
2.2 Dual-Band CRLH Phased-Array Antenna.....	24
2.3 CRLH Phased-Array Feed Network for Frequency Scanning Antenna	34
2.4 Conclusion	62
CHAPTER 3 An Alternate Technique in Designing a Low-Profile Two- Pole Bandpass Frequency Selective Surface (FSS) using Aperture Coupling Interlayer.....	63
3.1 Introduction.....	63

3.2	Two-Pole FSS with Aperture Coupling Interlayer	65
3.3	Experimental Verification and Measurement Results	71
3.4	Conclusion	75
CONCLUSION		76
BIBLIOGRAPHY		78

List of Figures

Figure 1-1	RDA example.....	5
Figure 1-2	Basic principle of retrodirective array.	6
Figure 1-3	Schematic diagram of a single element Rx and Tx antenna pair with zoomed view of phase-conjugating sub-harmonic mixer.....	9
Figure 1-4	Diagram of the proposed RDA illustrating the two requirements: 1) phase-conjugation ($-\theta$) and 2) 90° Polarization rotation [$R(90^\circ)$].	10
Figure 1-5	Single element pair illustrating even and odd mode analysis for different incident polarization cases: a) vertical-pol, b) diagonal-pol, c) horizontal-pol incident E-fields.....	11
Figure 1-6	Picture of the proposed RDA system (two element array).	11
Figure 1-7	Measurement setup for the undesired co-pol RCS measurement.	16
Figure 1-8	Measurement setup for the desired cross-pol RCS measurement.....	16
Figure 1-9	Measurement bistatic RCS patterns for linearly-pol incident fields.....	19
Figure 1-10	Measured monostatic RCS patters for different linearly-pol incident fields.	19
Figure 1-11	Measured s-parameter for circularly-pol patch antenna.	20
Figure 1-12	Measurement bistatic RCS patterns for circularly-pol incident field.	20
Figure 1-13	Measured monostatic RCS patters for different circularly-pol incident fields.	21
Figure 2-1	Comparison between a) conventional and b) CRLH based all passive dual-band phased-array.....	24
Figure 2-2	Equivalent circuit model of CRLH TL.	26
Figure 2-3	Desired phase response for four element dual-band CRLH feed network.	28
Figure 2-4	Dual-band antenna return loss and mutual coupling for $d = 7.5$ cm ($0.6 \cdot \lambda_{o2}$).	29

Figure 2-5	a) Simulated and b) measured S-parameters of the CRLH dual-band feed network.	30
Figure 2-6	Simulated and measured phase response of the CRLH based phased-array feed network for line 1 (L1) to line 4 (L4): solid symbols (-●-) are simulated results and open symbols (-○-) are measured results.....	31
Figure 2-7	Photograph of the fabricated dual-band CRLH based phased-array system: a) with antenna b) feed network only.....	32
Figure 2-8	Simulated and measured E-plane co-polarized radiation patterns of the dual-band phased array sytem for a) $f_1 = 1.8$ GHz and b) $f_2 = 2.5$ GHz.	33
Figure 2-9	Proposed frequency scanning phased-array based on CRLH feed network.	34
Figure 2-10	Dispersion diagram of balanced CRLH structure.....	36
Figure 2-11	Ideal phase response of four element linear phased-array feed network needed for continuous 1-D frequency scanning.....	38
Figure 2-12	R-band single element quasi-Yagi antenna: a) photograph of the fabricated antenna and b) simulated and measured reflection coefficient plots.	41
Figure 2-13	Four element linear phased-array using quasi-Yagi antennas in collinear configuration: a) figure of the collinear configuration and b) reflection coefficient and mutual coupling values.	41
Figure 2-14	Four element linear phased-array using quasi-Yagi antennas in side-by-side configuration: a) figure of the side-by-side configuration and b) reflection coefficient and mutual coupling values.	42
Figure 2-15	Illustrative layout of the feed lines for four element phased-array.	43

Figure 2-16	Simulated and measured phase response of CRLH dispersive lines only.	44
Figure 2-17	Measured transmission coefficients and reflection coefficients of CRLH dispersive lines only.....	44
Figure 2-18	Photograph of the fabricated linear 1-D phased-array feed network based on CRLH TLs with uniform amplitude distribution.....	46
Figure 2-19	Measured a) S-parameters and b) phase response of CRLH phased-array feed network with uniform amplitude distribution.....	46
Figure 2-20	Photograph of the fabricated linear 1-D phased-array feed network based on CRLH TLs with tapered amplitude distribution.....	48
Figure 2-21	Measured a) S-parameters and b) phase response of CRLH phased-array feed network with tapered amplitude distribution.....	48
Figure 2-22	Photograph of the measurement setup for the proposed CRLH based frequency scanning phased-array in the near field chamber: a) proposed array in collinear configuration and b) proposed array in side-by-side configuration.....	49
Figure 2-23	Measured normalized E-plane co-pol (black) and cross-pol (gray) patterns in dB scale for frequencies: 1.8 GHz, 2.0 GHz, 2.3 GHz, and 2.5 GHz.....	50
Figure 2-24	Measured normalized H-plane co-pol (black) and cross-pol (gray) patterns in dB scale for frequencies: 1.8 GHz, 2.0 GHz, 2.3 GHz, and 2.5 GHz.....	51
Figure 2-25	Measured directivity and gain of the quasi-Yagi antenna.....	52
Figure 2-26	Measured four element array normalized E-plane co-pol (black) and cross-pol (gray) radiation patterns in dB scale for frequencies 1.8 GHz to 2.5 GHz using uniform amplitude CRLH phased-array feed network in collinear configuration.....	54

Figure 2-27	Measured four element array normalized H-plane co-pol (black) and cross-pol (gray) radiation patterns in dB scale for frequencies 1.8 GHz to 2.5 GHz using uniform amplitude CRLH phased-array feed network in side-by-side configuration.	56
Figure 2-28	Measured four element array normalized co-pol (black) and cross-pol (gray) radiation patterns in dB scale for frequencies 2.1 GHz using uniform amplitude CRLH phased-array feed network for: a) collinear (H-plane) and b) side-by-side configuration (E-plane).	56
Figure 2-29	Measured directivity and gain of uniform amplitude CRLH phased array.	57
Figure 2-30	Measured four element array normalized E-plane co-pol (black) and cross-pol (gray) radiation patterns in dB scale for frequencies 1.8 GHz to 2.5 GHz using tapered amplitude CRLH phased-array feed network in collinear configuration.	59
Figure 2-31	Measured four element array normalized H-plane co-pol (black) and cross-pol (gray) radiation patterns in dB scale for frequencies 1.8 GHz to 2.5 GHz using tapered amplitude CRLH phased-array feed network in side-by-side configuration.	61
Figure 2-32	Measured four element array normalized co-pol (black) and cross-pol (gray) radiation patterns in dB scale for frequencies 2.1 GHz using tapered amplitude CRLH phased-array feed network for: a) collinear (H-plane) and b) side-by-side configuration (E-plane).	61
Figure 2-33	Measured directivity and gain of tapered amplitude CRLH phased array.	62

Figure 3-1	Drawing of proposed two-pole FSS based on aperture coupling interlayer. Metal is shown in black color. Dimensions used for this work are: $a = 120$ mil, $b = 115$ mil, $w = 66$ mil, $g = 7$ mil, $s = 2$ mil, $h = 15$ mil, and $r =$ varied.	63
Figure 3-2	Simulated filter response of two layer FSS without the aperture coupling interlayer with $h = 15$ mil.	66
Figure 3-3	Coupling diagram of the proposed dual-pole FSS filter.	66
Figure 3-4	Coupling coefficient between the two FSS resonators.	67
Figure 3-5	Simulated filter response of two layer FSS with the aperture coupling interlayer of aperture dimension $r = 100 \times 100$ mil and the spacing $h = 15$ mil.	67
Figure 3-6	Simulated filter response of two layer FSS with the aperture coupling interlayer of aperture dimension $r = 80 \times 80$ mil and the spacing $h = 15$ mil.	68
Figure 3-7	Simulated filter response of two layer FSS with the aperture coupling interlayer of aperture dimension $r = 60 \times 60$ mil and the spacing $h = 15$ mil.	68
Figure 3-8	Simulated filter response of two layer FSS with the aperture coupling interlayer of aperture dimension $r = 62 \times 62$ mil and the spacing $h = 15$ mil.	69
Figure 3-9	Simulated transmission coefficient for various oblique angle incidences with TE-polarizations.	70
Figure 3-10	Simulated transmission coefficient for various oblique angle incidences with TM-polarizations.	70
Figure 3-11	Fabricated two-pole FSS based on coupling interlayer.	72
Figure 3-12	Experimental set-up.	72
Figure 3-13	Measured transmission coefficient for various oblique angle incidences with TE-polarizations.	73

Figure 3-14	Measured transmission coefficient for various oblique angle incidences with TM-polarizations.....	73
Figure 3-15	Measured transmission coefficient for various oblique angle incidences with Diagonal-polarizations.....	74

ACKNOWLEDGMENTS

I would like to thank Professor Tatsuo Itoh for his guidance and to all my colleagues in Microwave Electronics Lab for their invaluable advices and discussion. I am also indebted to the members of my committee, Professor Warren Mori, Professor Benjamin Williams, and Professor Christoph Niemann, for their valuable comments. Lastly, I would like to dedicate this thesis to my family, especially to my parents and my wife/best-friend Jee Eun (Jamie) Kang for all their loving supports.

VITA

- 2003 B.S. Electrical Engineering, University of California, Irvine.
- 2007 M.S. Electrical Engineering University of California, Los Angeles.
- 2005 - 2007 Graduate Student Researcher, Department of Electrical Engineering,
University of California, Los Angeles.
- 2010 - 2013 Teaching Assistant, Department of Electrical Engineering, University of
California, Los Angeles.
- 2008 - Present Graduate Student Researcher, Department of Electrical Engineering,
University of California, Los Angeles.

PUBLICATIONS

J. Choi and T. Itoh, “Dual-band composite right/left-handed (CRLH) phased-array antenna,” *IEEE Antennas Wireless Propag. Lett.*, vol. 11, pp. 732-735, 2012.

J. S. Sun, H. Lobato-Morales, **J. H. Choi**, A. Corona-Chavez, and T. Itoh, “Multistage directional filter based on band-reject filter with isolation improvement using composite right/left-handed transmission lines,” *IEEE Trans. Microw. Theory Tech.*, vol. 60, no. 12, pp. 3950-3958, Dec. 2012.

J. H. Choi, J. S. Sun, and T. Itoh, “Frequency-scanning phased-array feed network based on composite right/left-handed transmission lines,” *IEEE Trans. Microw. Theory Tech.*, vol. 61, no. 8, pp. 3148-3157, Aug. 2013.

J. H. Choi, Y. Dong, J. S. Sun, and T. Itoh, “Retrodirective array immune to incident waves with arbitrary polarization,” *IEEE Trans. Antennas Propag.*, vol. 61, no. 12, pp. 6006-6013, Dec. 2013.

J. H. Choi, P. W. C. Hon, and T. Itoh, “Dispersion analysis and design of planar electromagnetic bandgap ground plane for broadband common-mode suppression,” *IEEE Microw. Wireless Compon. Lett.*, *Accepted for publication*, 2014.

INTRODUCTION

Periodic arrangements either in the form of antenna array or periodic structures provide an added design freedom in microwave devices and systems. When applied to the radiated applications, collective behavior of the periodic structures offer better control of the radiated waves such as radiating direction, frequency dependent power transfer level, polarization properties, etc. Exploiting the advantages of periodic structures, novel RDA, phased-array feed networks for dual-band and frequency scanning systems, and frequency selective surfaces have been developed.

In chapter 1, polarization immune feature has been incorporated to RDA system to help maintain a more secure communication link between the interrogator and the RDA by mitigating the polarization mismatch loss [1, 2]. It is well known that polarization mismatch loss is unavoidable unless the antennas can maintain the polarization alignment at all times [3]. To minimize the polarization mismatch loss thereby maximizing the power transfer level between the two wireless nodes, RDA systems can be designed to receive any polarization and always retransmits orthogonally polarized signals with respect to the received polarization state back to the interrogator. With this scheme, as long as the interrogator is equipped with one transmitting antenna and a separate receiving antenna that is orthogonally polarized, the loss due to polarization mismatch can always be minimized. Based on the new retrodirective array architecture, the array is able to respond to the interrogator without prior knowledge of the source location as well as the state of the incoming polarization, while providing a more desirably polarized retrodirective signal. Aforementioned features may be applicable for the use

of unmanned satellite systems, remote sensors, and drones that are subject to constant motion or rotation.

In the second chapter, metamaterial transmission line concept is utilized to design dual-band and frequency-scanning phased array system. Periodic structures based on metamaterial concepts have recently attracted much attention. Although the original concept of metamaterial was postulated in 1967 by Russian scientist Viktor Veselago [4], the research toward the development of metamaterial based microwave devices and systems have only recently flourished. Since early 2000, Composite Right/Left-Handed (CRLH) structures that provides metamaterialistic behavior in the microwave domain has been extensively researched in designing novel devise and systems [5]. One of the unique properties of CRLH structure is its inherent dual-band property, where specific phase responses can be assigned to two operating frequencies. In our work, this dual-band concept has been utilized in designing an all passive phased-array system that can direct the radiated beams to two arbitrary spatial angles [6]. Another notable invention of the metamaterial based microwave device is frequency-scanning leaky wave antenna. Unlike its predecessors, metamaterial based antenna provides full frequency scanning capability from backfire-to-endfire, including broadside direction [7]. Furthermore, these antennas can be realized in planar form without the need of complex feed structure. However, the antenna requires a very particular structural requirement to achieve continuous frequency scanning, forfeiting the independent design freedom of the far-field radiated patterns such as directivity, side-lobe-level, and polarization type/orientation. To obtain individual controllability of aforementioned properties, the frequency scanning antenna is designed using array concept. Based on this alternative approach, radiating element can be completely

decoupled from the array factor, offering much flexible engineering capability in designing frequency scanning antennas [8, 9].

In the last chapter, high performance miniaturized-element dual-pole Frequency Selective Surface (FSS) based on filter coupled theory will be presented. Hybrid radomes mounted at the front of an aircraft is regarded as one of the more central applications of the FSS. They are also used for dichroic surfaces for reflectors and subreflectors and absorbers [10]. Aside from military applications, FSSs have also found its niche in the commercial applications where it is integrated into the walls to reduce wireless interference in indoor environment [11]. For practical applications, aside from providing structural rigidity and/or low radar cross section (RCS), FSSs are generally designed to behave as a transparent medium only for the desired communication frequency band. As a rule of thumb, electrically small periodicity, multi-pole response, and thin interlayer spacing are the desired aspects in designing FSS. In our work, high performance spatial bandpass FSS filter is realized by combining all of above mentioned desirable aspects. The band-pass response can be obtained by designing the FSS structures to provide a collective behavior resembling that of the parallel shunt LC tank to the incident plane waves. The proposed uniplanar compact photonic-bandgap (UC-PBG) [12] inspired FSS structure has electronically miniaturized unit lattice dimension. This electrically small resonant structure can be further miniaturized by heavily loading the capacitance of the FSS structure with high dielectric constant substrate. The fabricated structure has miniaturized unit-cell lattice dimensions of $d < \lambda_o/8$. In addition, filter coupling theory is incorporated to control the coupling level of multi-layer FSS to maintain thin form factor while preserving the desired filter transfer function. As will be shown in Chapter 3, merging the miniaturization concept with the coupled filter theory, two-pole FSS bandpass filter that is robust to the incident fields from oblique angle and arbitrary polarization is

realized with the total thickness of $d < \lambda_0/30$ [13]. This idea can be extended to multi-pole filter design and also in designing different types of filters, such as bandstop, low-pass, and high-pass.

CHAPTER 1

Polarization Friendly Retrodirective Antenna Array

1.1 INTRODUCTION

Retrodirective arrays (RDA) have the unique ability to transmit a received signal back toward the interrogator without prior knowledge of the interrogator's location. A typical communication link between the interrogator and the retrodirective responder is shown in (Fig. 1-1). Under a dynamic communication link where either the interrogator or the responder is in motion, the responder equipped with the RDA can track the interrogator, thereby maintaining a more stable communication link. This concept may be applied to remote sensor, identification

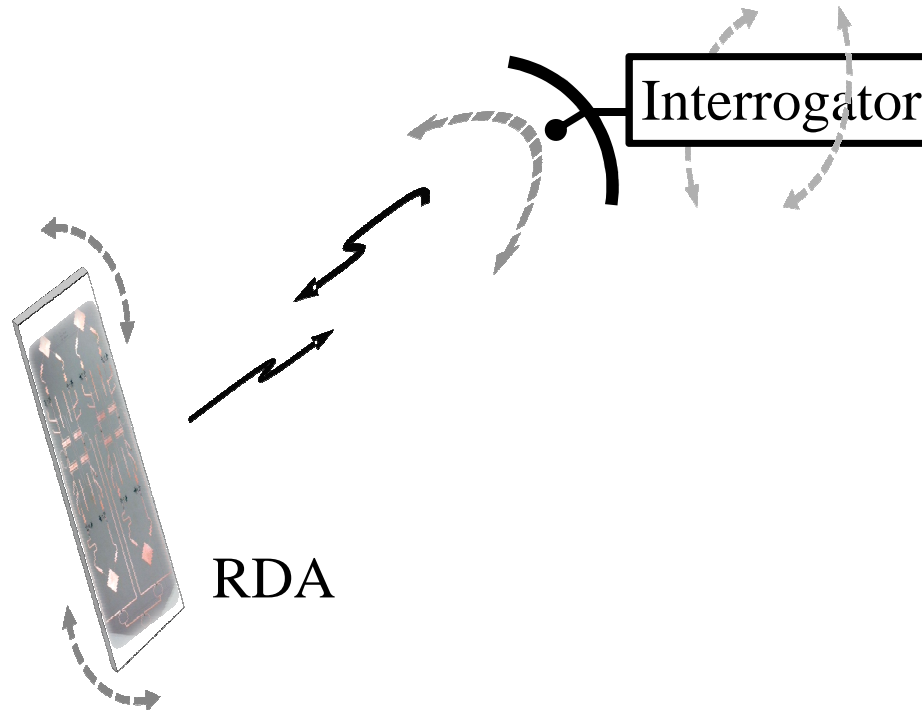


Figure 1-1 RDA example.

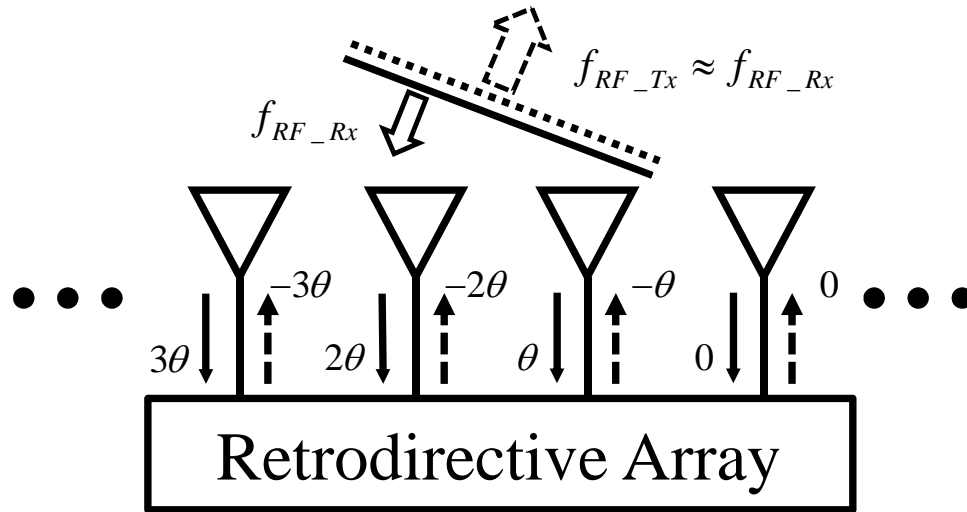


Figure 1-2 Basic principle of retrodirective array.

tags, unmanned space crafts, etc. There are different techniques to achieve this functionality of rescattering the signal back to the interrogator. However, when high link gain and high-speed target tracking is desired, analog self-phasing method has been the candidate of the choice [14]. The invention of the Van Atta array in 1955 paved the notion of creating analog RDA systems in the form of an array [15]. In addition, unlike the traditional corner reflector, Van Atta arrays enabled the devices to be built entirely on planar substrates with a wider retrodirective angle [16]. Novel techniques and devices based on the Van Atta concept are actively being studied [17]-[19].

A different approach is designing a retrodirective antenna array based on the heterodyne technique, originally introduced by C. Y. Pon in 1963 [20]. The working mechanism is essentially similar to that of the Van Atta array where the effective phase gradient across the array is reversed, thereby directing the signal back to the source location. However, instead of pairing the antennas with respect to the symmetric plane of the array using equi-length interconnects; the heterodyne technique retrodirects the signal by conjugating the received phase

at each antenna elements [21]. The basic operating principle of the RDA based on phase-conjugating technique is shown in (Fig. 1-2). This technique has stirred much interest among researches by allowing devices to be built on a conformal surface. The method also allows simpler integration of standard electronic devices, modulation, and amplification of the signals. Endeavors toward building yet more robust RDAs has produced interesting design schemes and techniques. For example, a frequency autonomous RDA has been developed to retrodirect the signal without prior knowledge of source location and source frequency [22], a dual-frequency RDA was proposed where two sets of array are used to receive high frequency signal and retrodirect low frequency signal back to the source or vice versa [23], and a RDA system based on phase-conjugating technique has been implemented using not only through local oscillator (LO) at twice the RF frequency but also using sub-harmonic mixing [20], [24]-[26].

To further improve the system performance, this chapter emphasizes on the polarization properties of the RDA to build a device immune to arbitrary polarizations of the incident waves. Polarization characteristics have been previously studied in conjunction with RDAs. Polarization duplexing has been utilized, where a set of orthogonal polarizations are used for receiving and transmitting operation with high isolation [27]-[28]. However, they operate for linearly polarized case only and require the RDA to be pointing to the interrogator with a particular orientation to minimize polarization mismatch loss. Dual-polarized antennas that can receive any type of polarizations have been utilized in the previous RDAs [29]. Nevertheless, with an ideal dual-polarized square patch, incident waves polarized along the patch diagonal axis returns the same polarization; but all other polarization ellipses flips around this axis. Since the retransmitted polarization state from the RDA is highly dependent on the received polarization state and

unpredictable, it is difficult to maintain low polarization mismatch loss unless the orientation of the RDA with respect to the interrogator can be tracked at all times.

The Friis equation (Eqn. 1.1) shows that the ratio between the received power over the transmitted power between the two antennas depends on gain of the transmitting (G_t) and receiving antennas (G_r), distance between the antennas (R), and lastly, on the polarization alignment between the transmitting and receiving antennas [3],

$$\frac{P_r}{P_t} = \left(\frac{\lambda}{4\pi R} \right)^2 G_t(\theta_t, \phi_t) G_r(\theta_r, \phi_r) |\hat{p}_t \cdot \hat{p}_r|^2 \quad (1.1)$$

Unless the antennas can maintain the polarization alignment at all times, polarization mismatch loss is unavoidable. This loss is much detrimental in the RDA system since the signal travels a roundtrip from the interrogator to RDA and back to the interrogator. In order to alleviate this problem, a polarization friendly RDA system may be used, which has the capability to receive any polarization and always retransmits a predictable polarization back to the interrogator. If the interrogator knows the polarization state of the back-scattered signal from the RDA beforehand, it can pre-adjust or pre-rotate its receiving antennas to minimize the loss due to polarization mismatch. The proposed RDA is capable of retransmitting the retrodirective signals polarized orthogonal to any received polarization states. Therefore, as long as the interrogator is equipped with a polarization duplexing antenna or a set of separate Tx and Rx antennas that are orthogonally polarized with respect to each other, the loss due to polarization mismatch can always be minimized. Using the new retrodirective array architecture, the array is able to respond to the interrogator without prior knowledge of the source location as well as the state of the incoming polarization, while providing a more desirably polarized retrodirective signal.

The following sections will present detailed working mechanism of the proposed structure originally presented in [1]. In addition, circular polarization cases are discussed along with the measured results. Chapter 1 is organized as follows. A brief overview of the proposed system configuration is described in Section 1.2. Section 1.3 provides the theory of the proposed system. In the last two sections, a fabricated system is used to verify the proposed method with the experimental results.

1.2 SYSTEM CONFIGURATION

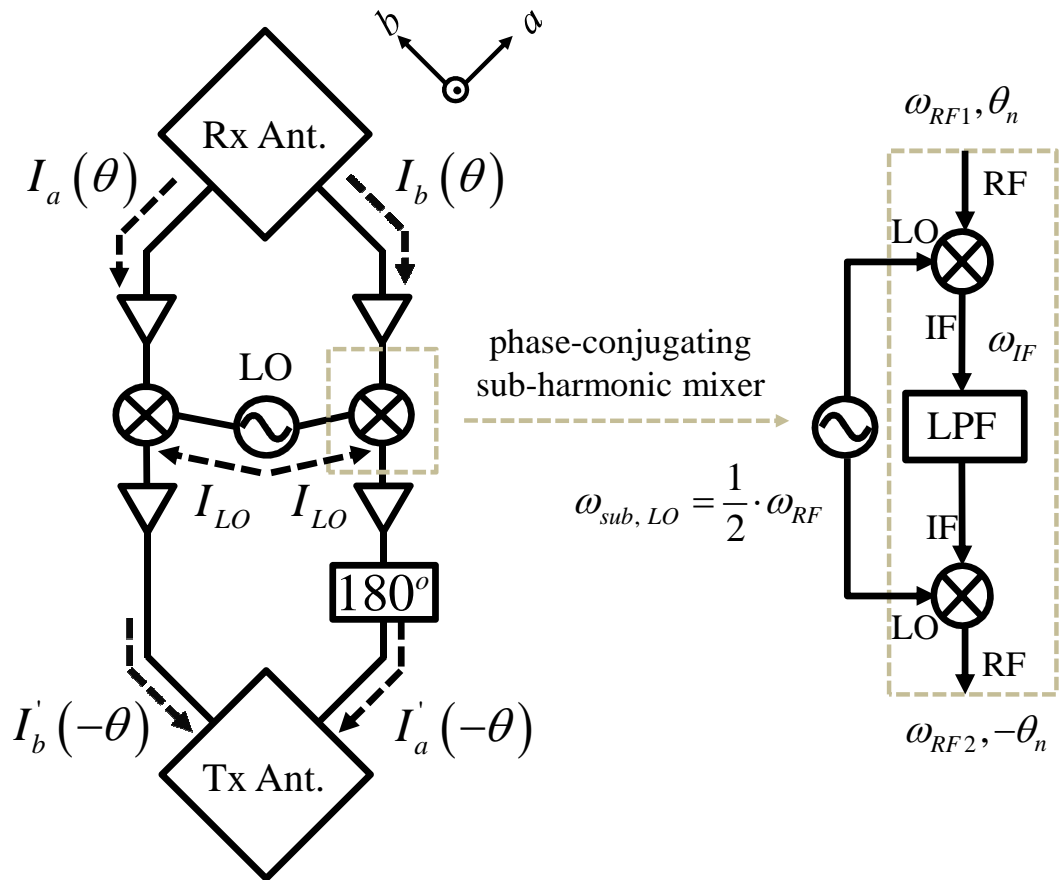


Figure 1-3 Schematic diagram of a single element Rx and Tx antenna pair with zoomed view of phase-conjugating sub-harmonic mixer.

The proposed RDA is realized with a set of dual-polarized Rx and Tx antennas linked by non-radiating phase-conjugating circuits as shown in (Fig. 1-3). Each pair of Rx and Tx dual-polarized antennas are linked by two interconnecting arms. Phase-conjugation needed to direct the signal back to the interrogators is attained through two-stage sub-harmonic mixing. Amplifiers are added before and after the phase-conjugating mixer to compensate the conversion loss of the mixers and provide the signal amplification. Prior to reaching the input ports of the Tx dual-polarized antenna, the signal traveling in one of the linking arms travels through the delay line to flip the phase of the signal by 180 degrees. As will be shown in Section 1.3, this delay line, in addition to the two interconnecting arms arranged in this particular fashion, are required to provide the orthogonally polarized Tx-signal with respect to any received polarization states. The proposed system is a 1-D RDA that can track the interrogator parallel to the array scanning direction.

1.3 THEORY

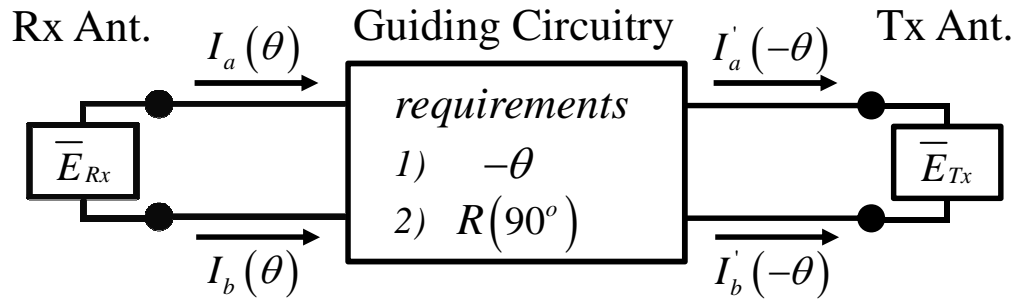


Figure 1-4 Diagram of the proposed RDA illustrating the two requirements: 1) phase-conjugation ($-\theta$) and 2) 90° Polarization rotation [$R(90^\circ)$].

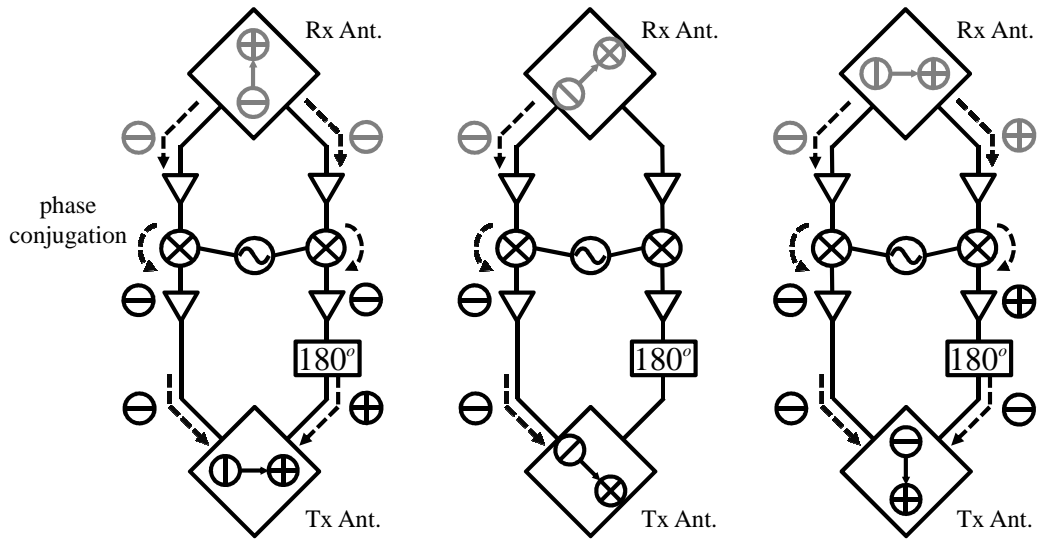


Figure 1-5 Single element pair illustrating even and odd mode analysis for different incident polarization cases: a) vertical-pol, b) diagonal-pol, c) horizontal-pol incident E-fields.

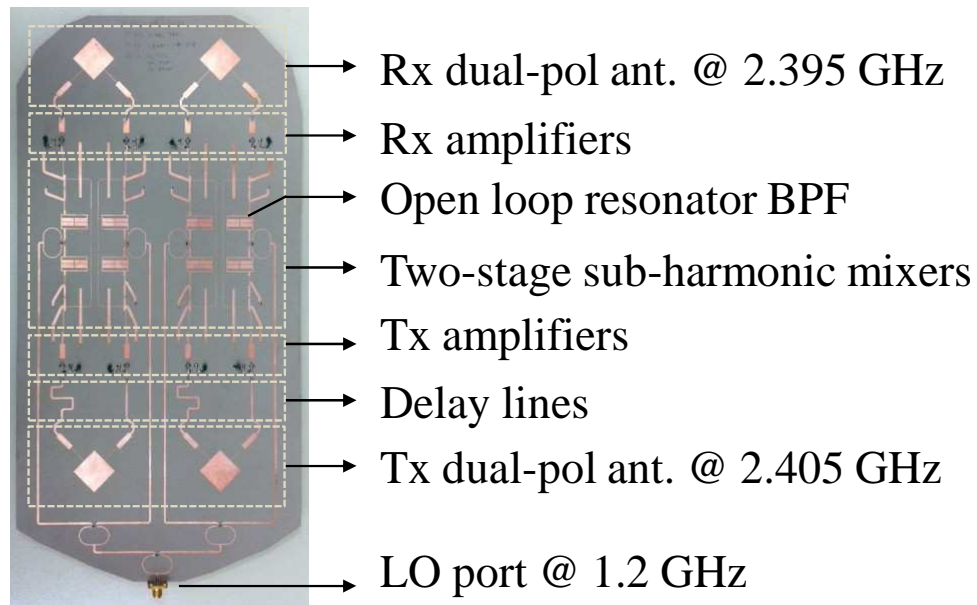


Figure 1-6 Picture of the proposed RDA system (two element array).

Two main requirements needed to ensure orthogonally polarized retrodive signals with respect to any incident polarization states are shown in (Fig. 1-4). The system has to reverse the phase gradient seen by each antennas element and vector rotation of the E-field needs to be

performed prior to re-radiating the received signal. The proposed systems can achieve both requirements completely in analog fashion.

Phase-conjugation may be achieved in several ways. The simpler method to achieve phase-conjugation is by mixing the received RF signal with the LO that has a frequency twice the RF frequency [20], [29]. Once these signals are mixed, the sum frequency can be filtered out using a lowpass filter while the difference frequency that contains the desired phase-conjugated signal is used to retrodirect the signal back to the source location. This technique is particularly advantageous because the operation is not limited to plane wave excitation. Unlike the Van Atta array where all the antenna elements work together as a unit, each radiating element works independently in the phase conjugating method. However, the drawbacks of this simpler method are as follows: 1) since it requires $f_{LO} = 2 \times f_{RF}$, the *LO* becomes less stable and more expensive as the operating RF frequency increases, 2) a reliable isolating circuit is needed to remove the undesired reflection of the RF signal. Several methods have been developed to relieve the latter drawback [24], [30], while sacrificing the bandwidth of the system.

In order to alleviate the high LO frequency, phase-conjugation through sub-harmonic mixing is widely used [25]-[26], [31]. The schematic diagram of the sub-harmonic mixer used in the proposed RDA is shown in (Fig. 1-3). This is a two-step process where in the first mixing process, the received RF signal is first down converted to the *IF* frequency band. The phase is conjugated during this process. After lowpass filtering, the signal is upconverted back to the RF frequency band as shown below

$$I_{RF_Tx} = \frac{I_{RF_Rx} I_{LO}^2}{4} \left[\cos \left((\omega_{LO} + \omega_{IF}) t - \theta_n \right) \right], \quad (1.2)$$

before being retransmitted to the interrogator. Sub-harmonic mixing is advantageous for the proposed RDA not only to reduce the overall system cost and provide higher port isolations, but also to reduce the phase error by lowering the LO frequency. In order to provide proper polarization rotation, it is critical to minimize any phase errors within the system.

The proposed system is equipped with dual-polarized receiving patch antennas that orthogonalize the excited currents with magnitude proportional to the incident E-field projected onto each orthogonal spatial coordinate axis a and b (Fig. 1-5). The above relation and the reverse relation for the transmitting operation can be expressed as

$$\overline{E}_{Rx} \rightarrow \begin{bmatrix} I_a \\ I_b \end{bmatrix}, \quad \overline{E}_{Tx} \leftarrow \begin{bmatrix} I'_a \\ I'_b \end{bmatrix}. \quad (1.3)$$

The subscripts a and b represents the direction of the currents flowing along the respective orthogonal spatial coordinates. To ensure that the retransmitted signals are always orthogonally polarized with respect to the incident polarization, a simple vector transformation needs to be performed; in this case 90 degrees vector rotation is needed as follows:

$$\begin{bmatrix} I'_a \\ I'_b \end{bmatrix} = \begin{bmatrix} \cos \alpha & -\sin \alpha \\ \sin \alpha & \cos \alpha \end{bmatrix} \begin{bmatrix} I_a \\ I_b \end{bmatrix} \xrightarrow{\alpha=90^\circ} \begin{bmatrix} -I_b \\ I_a \end{bmatrix}. \quad (1.4)$$

The vector rotation is carried out by arranging the interconnecting arms such that the spatial coordinates of the decomposed currents leaving the system is reversed relative to the spatial coordinates of the currents incident in the system, and the negative sign in one of the currents is obtained by simply adding a 180 degree delay line in one of the linking arms, as shown in (Fig. 1-5).

The working mechanism of the proposed system can also be analyzed with even and odd mode analysis. If the linearly polarized E-field is incident along the symmetric plane of the

receiving dual-polarized antenna (vertically-pol), the two linking arms experience even-mode (in-phase) excitation. After the phases are conjugated through sub-harmonic mixers, the signal along one of the branches travels through the delay line, creating odd-mode (out-of-phase) excitation to the transmitting dual-polarized antenna. On the other hand, if the field is incident perpendicular to the symmetric plane of the dual-polarized receiving antenna (horizontally-pol), odd-mode excitation is generated at the output of the receiving dual-polarized patch antenna. Similar to the previous case, the delay line in one of the branches provides even-mode excitation to the transmitting antenna. If the incident field is received at a ± 45 degree (diagonally-pol) from the symmetric plane of the dual-polarized antenna, the signals only flow through one of the linking arms. In this case, the retransmitted field will also be orthogonally polarized with respect to the incident polarization as shown in (Fig. 1-5) b). These three linearly-polarized cases along with the circularly-polarized case are verified with measurements.

For circularly or elliptically polarized fields, the proposed RDA will reverse the sense of rotation. Rotational direction of the electric fields incident on the receiving antenna and reradiated from the transmitting antennas will be the same. This can be easily seen by treating (Fig. 1-5) as a sequential time frame. However, received and transmitted fields propagate toward the opposite directions with respect to each other, so the propagation constant will have opposite signs. Therefore, RHCP will become LHCP and vice versa. In summary, the polarization of the retransmitted signal of the proposed architecture will always be orthogonal to any received polarization states. Therefore, as long as the interrogator is equipped with two separate orthogonally polarized antennas, the proposed system is less susceptible to polarization mismatch caused by the motion or rotation of the interrogator and can much alleviate the communication link loss. In addition, by separating the Rx and Tx antennas, the proposed RDA

can also amplify and modulate the received signal by simply integrating unilateral amplifiers and modulating the LO signal respectively.

1.4 FABRICATED SYSTEM AND SYSTEM PERFORMANCE

A two element one-dimensional RDA based on the proposed architecture operating around 2.4 GHz is fabricated on a low loss, 50 mil thick Rogers RT/duroid 6010 substrate with $\epsilon_r = 10.2$. Prior to fabricating the entire system, each component was fabricated and performances were verified. The return loss and isolation of the dual-polarized antenna are 17 dB and 27 dB respectively. Measured cross-pol level is 10 dB below the co-pol for a single antenna element. To compensate the conversion loss of the mixers, amplifiers with 24 dB gain are added at both receiving and transmitting paths. GaAs monolithic-microwave integrated-circuit (MMIC) amplifiers (HP MGA-86576) biased at 5 V, consuming 100 mA are used to provide the gain around the operating frequency region. Phase-conjugation is realized using a pair of sub-harmonic mixer based on antiparallel diode pairs (APDPs). Agilent beam lead Schottky diode pairs (HSCH-5531) are used for the mixers.

In the first mixing stage, the received RF signal ($f_{RF} = 2.395$ GHz) is down-converted to the IF band with an LO frequency slightly higher than half the RF frequency. The phase conjugation is achieved in this process. The IF signal is then up-converted back to the RF frequency band ($f_{response} = 2.405$ GHz) prior to being retransmitted. The optimized conversion loss of each mixer operating at $f_{LO} = 1.2$ GHz is 11 dB with LO power of 0 dBm. The total LO power of 9 dBm is needed to feed all the mixers in the final fabricated system. Bandpass filters are added at each RF and LO ports of the mixers. Open loop resonator bandpass filters are used in the LO path to reduce the overall size of the system (Fig. 1-6).

1.5 MEASURED RADAR CROSS SECTION (RCS) RESULTS

To validate the retrodirective capability of the proposed system for any incident polarization states, bistatic and monostatic radar cross section (RCS) measurements are conducted for different incident polarizations. The measurement setups for co-pol and cross-pol

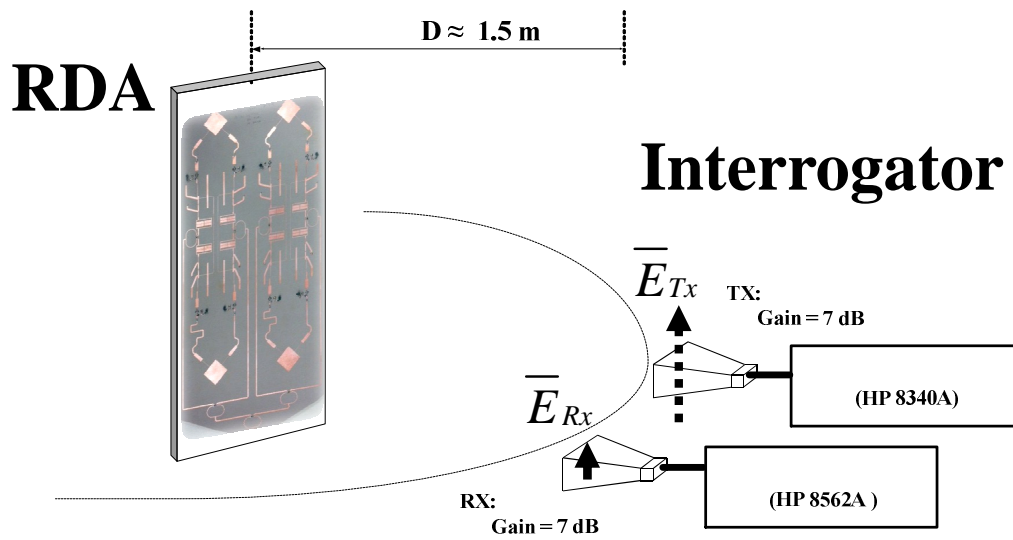


Figure 1-7 Measurement setup for the undesired co-pol RCS measurement.

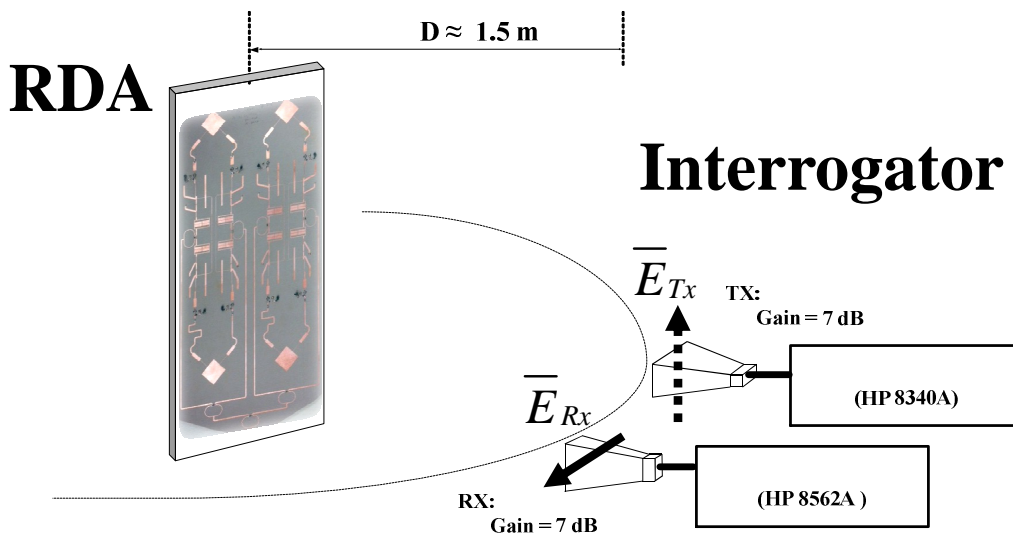


Figure 1-8 Measurement setup for the desired cross-pol RCS measurement.

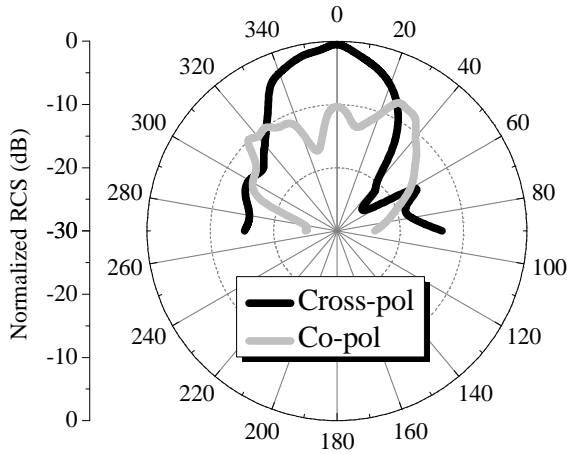
cases are shown in (Fig. 1-7) and (Fig. 1-8) respectively. For the bistatic RCS measurement, an interrogating Tx antenna transmitting a single tone signal (f_{RF}) is placed at fixed positions (0 degrees and 20 degrees) while the reradiated response ($f_{response}$) pattern of the RDA is measured by sweeping Rx horn antenna along the elevation angle parallel to the array scanning plane. For the monostatic RCS, reradiated patterns of the array are measured while simultaneously sweeping the interrogating Tx and Rx antennas. The interrogator antennas and the RDA are maintained at the far-field distance of $d \approx 1.5$ m.

A. Linear Polarization

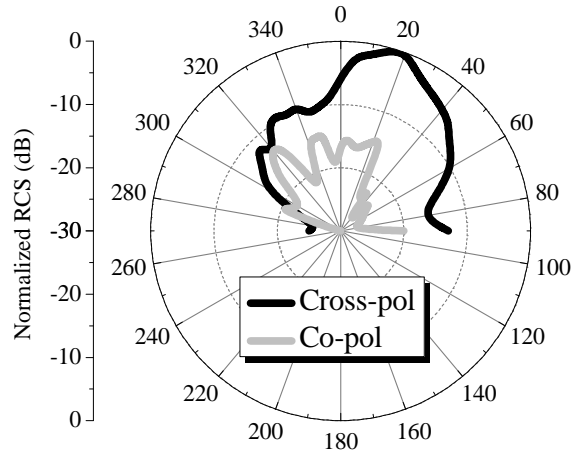
In the linear-pol measurements, the interrogator is composed of two standard gain horn antennas with the gain of 7 dBi. One of the horn antennas is attached to the signal generator and used as the Tx antenna of the interrogator. The other horn antenna attached to the spectrum analyzer to measure the rescattered power from the RDA, thereby acting as the Rx antenna of the interrogator. For each source locations, three sets of linearly polarized RCS measurements were carried out: transmitting horn positioned to illuminate the RDA with 1) vertically-polarized, 2) horizontally-polarized, and 3) diagonally-polarized signals. For each cases, both desired cross-pol and undesired co-pol RCS levels were measured to verify whether the retrodirected signals are properly (orthogonally) polarized with respect to its received polarization state. Retrodirectivity is clearly confirmed in both source angles and for all three linearly-polarized cases (Fig. 1-9). The measured results show the desired cross-pol levels around 10 dB above the co-pol level for all three polarizations and both source locations. Higher than expected co-pol levels in the measurement results may be due to the interference produced by leakage radiation

from the phase-conjugation circuits, fabrication errors, and imperfect measurement setup.

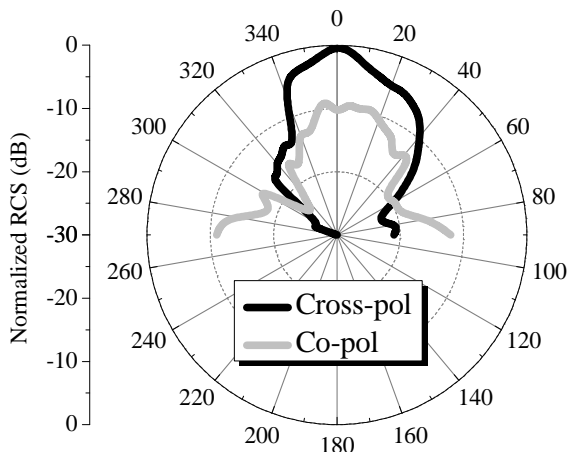
Measured monostatic RCS patterns for linearly-pol case are shown in (Fig. 1-10).



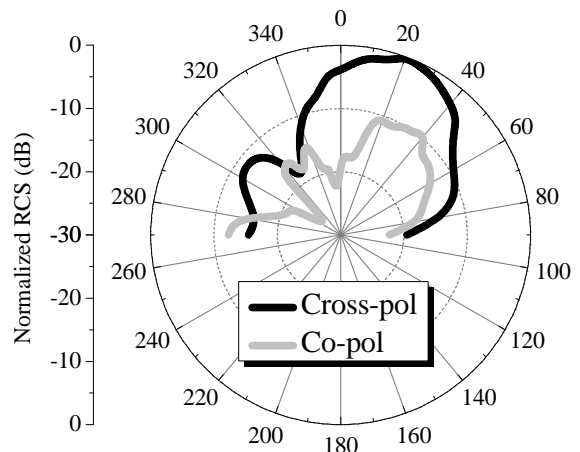
a) Vertically-polarized source at 0°.



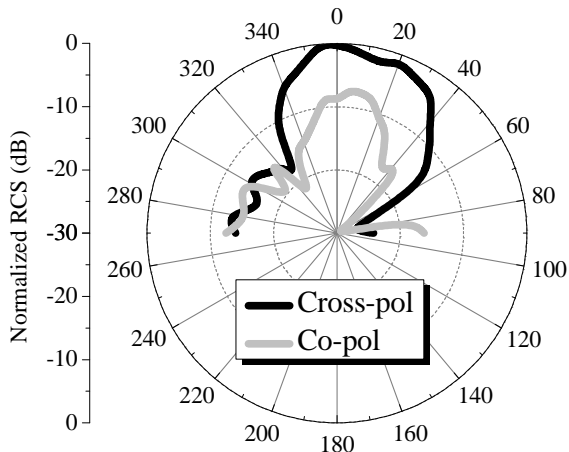
b) Vertically-polarized source at 20°.



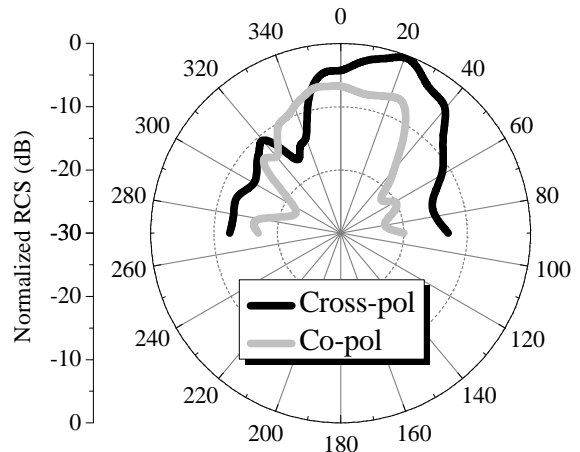
c) Horizontally-polarized source at 0°.



d) Horizontally-polarized source at 20°.



e) Diagonally-polarized source at 0° .



f) Diagonally-polarized source at 20° .

Figure 1-9 Measurement bistatic RCS patterns for linearly-pol incident fields.

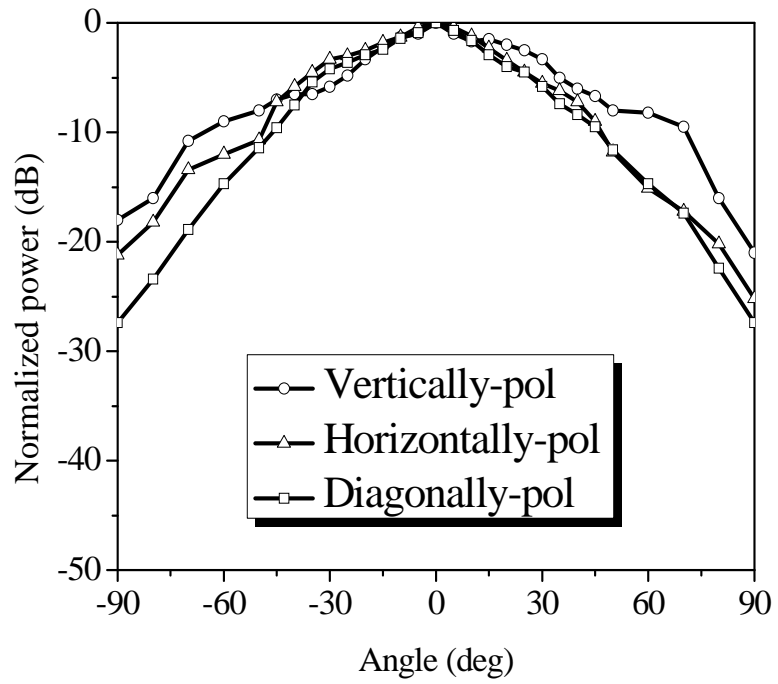


Figure 1-10 Measured monostatic RCS patters for different linearly-pol incident fields.

B. Circular Polarization

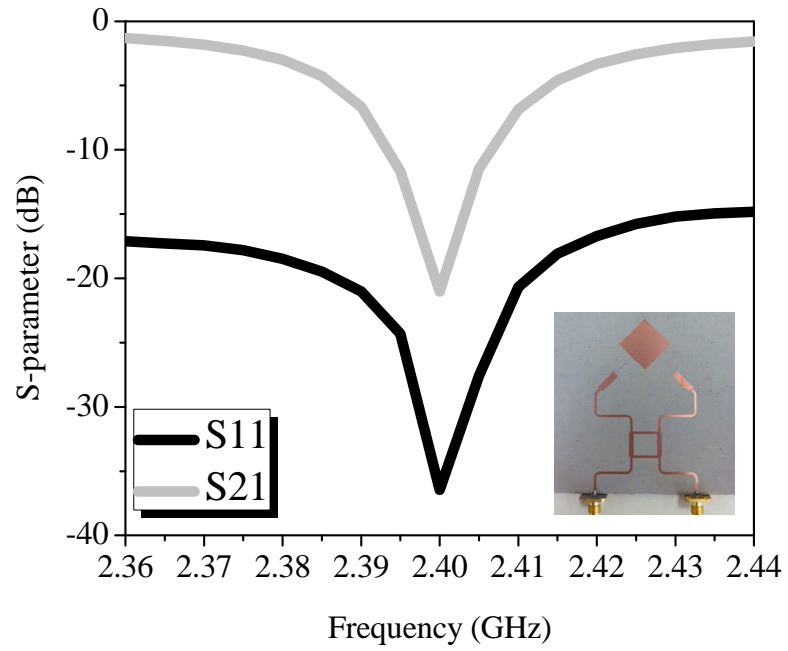
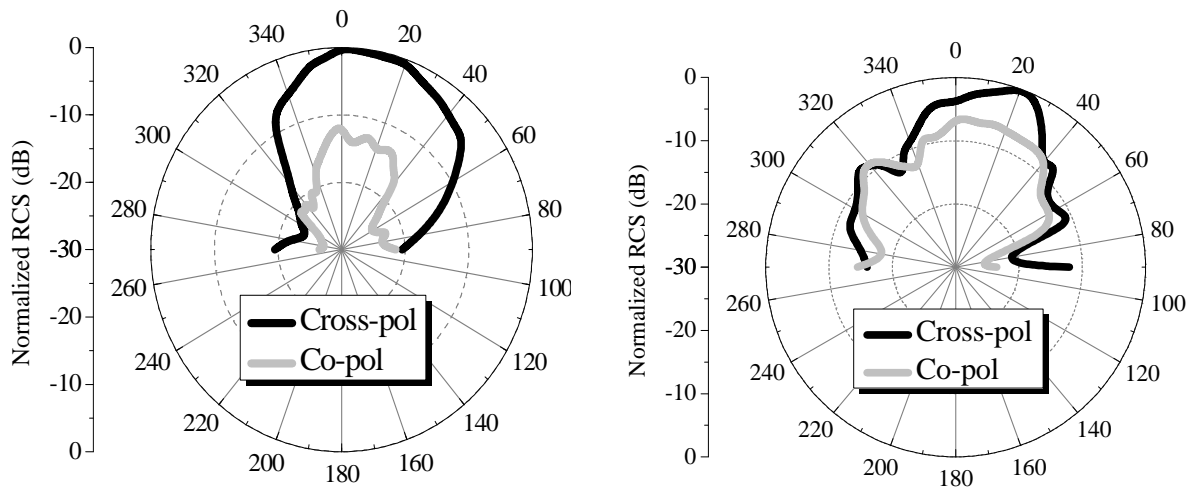


Figure 1-11 Measured s-parameter for circularly-pol patch antenna.



a) Circular-polarized source at 0° .

b) Circular-polarized source at 20° .

Figure 1-12 Measurement bistatic RCS patterns for circularly-pol incident field.

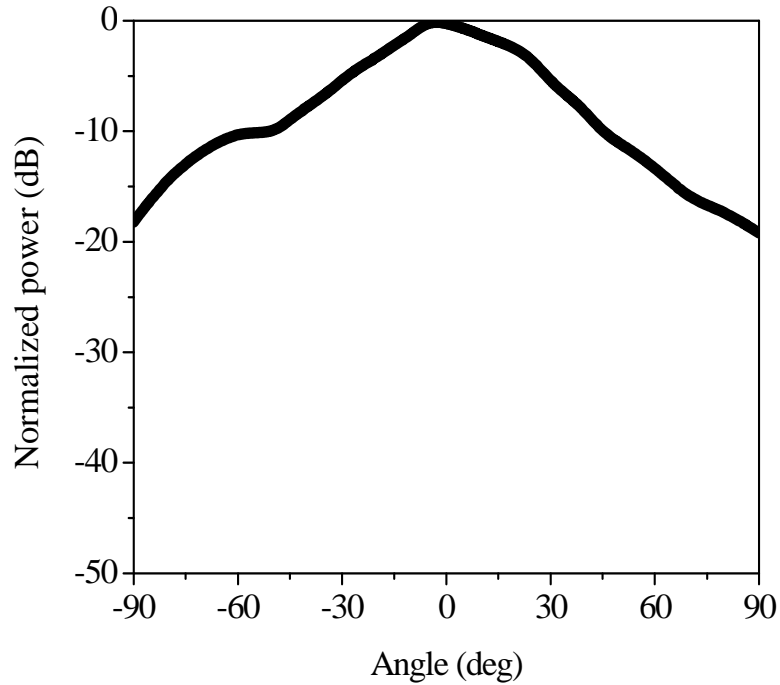


Figure 1-13 Measured monostatic RCS patterns for different circularly-pol incident fields.

RCS measurements for circularly-pol cases are also conducted using a set of circularly-polarized interrogating patch antennas instead of the linearly-polarized horn antennas. Circularly-polarized patch antennas are fabricated using quadrature hybrids as shown in the inset of (Fig. 1-11). Measured bistatic RCS shows the cross-pol level around 15 dB above the co-pol level for the source located at the broadside [Fig. 1-12 a)] and around 8 dB higher when the interrogator is placed at 20 degrees from the broadside [Fig. 1-12 b)]. Similar to that of the linearly-pol case, the measurement results show good retrodirectivity and the desired cross-pol level is higher than the undesired co-pol level. Measured monostatic RCS pattern for circularly-pol case is shown in (Fig. 1-13).

1.6 CONCLUSION

We have demonstrated a RDA that is more robust to the polarization of the communication signal. It can receive any polarization and retransmit a predictable orthogonally polarized signal back to the interrogator. Therefore, as long as the interrogator is equipped with orthogonally polarized receiving antennas, the polarization mismatch loss between the interrogator and the RDA will always be minimized. This device may be especially advantageous for unmanned vehicles, spacecrafts or remote sensors under constant motion or rotation. For the linearly polarized case, the orthogonally polarized backscattered signal also helps to steer away from undesired specular reflection. Lastly, since the system enables the interrogator to use two separate antennas, one for Rx and one for Tx , it allows better isolation and higher Tx power at the interrogator side.

CHAPTER 2

Phased-Array Feed Network based on Composite Right/Left-Handed (CRLH) Transmission Lines

2.1 INTRODUCTION

Composite Right/Left-Handed (CRLH) transmission lines and CRLH based leaky-wave antennas have been rigorously studied and researched for the past decade. Sometimes also commonly known as “Metamaterials”, these periodic microwave structures have attracted much attention due to their physical phenomena that are naturally not available in real world. Dual-band nature of CRLH transmission lines have been implemented in many guided and radiated microwave structures, but have never been implemented in the form of phased-array systems. Also, CRLH based antennas have been built to realize frequency scanning capability, but we have found that the same frequency scanning ability can also be realized by providing CRLH response to the feed network only, rather than integrating CRLH structures directly into the radiating structure. In this chapter, we will demonstrate the two types of all passive phased-arrays system using CRLH feed network. The first system uses the dual-band nature of CRLH dispersive lines to realize the dual-band phased-array that can direct the beam to two arbitrary directions. In the second part of the chapter, similar array network is used along with the wideband antennas to provide full frequency scanning capability.

2.2 DUAL-BAND CRLH PHASED-ARRAY ANTENNA

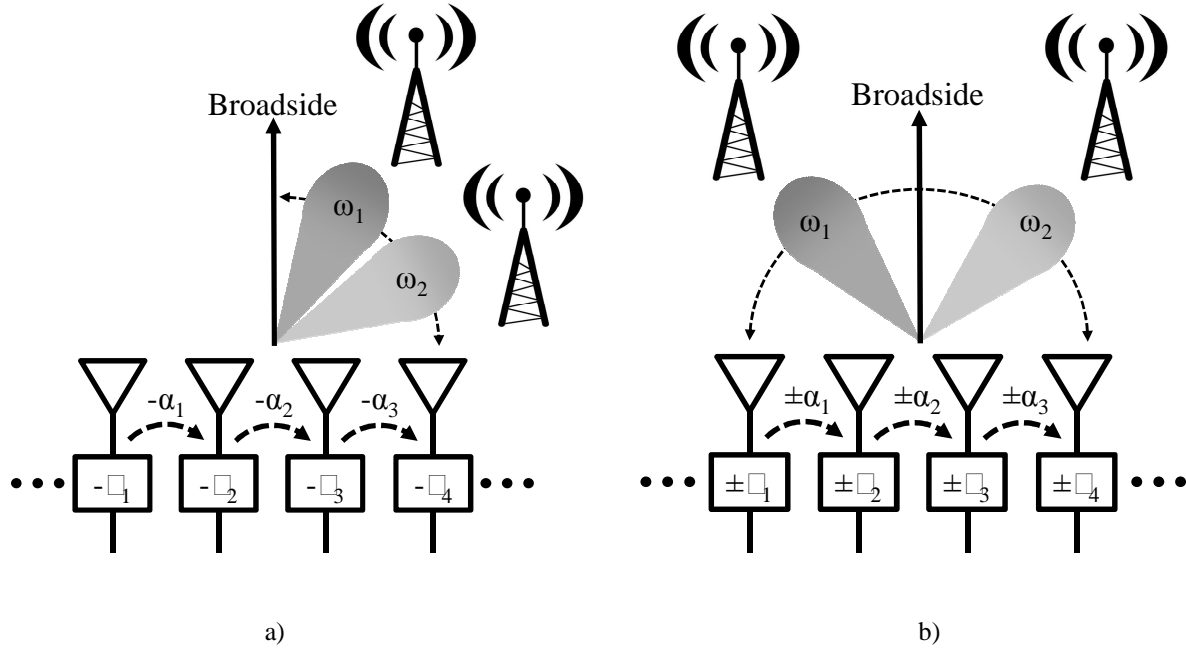


Figure 2-1 Comparison between a) conventional and b) CRLH based all passive dual-band phased-array.

Phased-array antennas are widely used in point-to-point or point-to-multipoint wireless communication links. For fixed communication links, a simple, low cost, all passive phased-array suffice the work. For equally spaced 1-D phased-arrays feed network design, the key factor in directing the radiated beam to the desired main beam angle

$$\theta_o = \sin^{-1}\left(\frac{\alpha}{kd}\right) \quad (2.1)$$

is to provide the appropriate progressive phase shifting (α) between the antenna elements. Here, k is the free-space wavenumber and d is the inter-element spacing. Conventional all passive phased-array systems use delay lines such as quarter-wavelength delay lines [32]. However, due to the linear phase response nature, these types of feed networks are suitable only for single frequency point-to-point operations. In point-to-multipoint communication links (Fig. 2-1), it is

possible to design an all passive dual-band phased array using dispersive delay lines. For example, capacitively loaded dispersive transmission lines may be used to manipulate the phase velocities of different frequencies. If properly designed, the relative phase difference seen at the input of the antennas can be simultaneously controlled for the two operating frequencies. However, the main drawback of this approach comes from the fact that conventional delay lines can only provide phase delay, which bounds the radiated beam angles to only half of the upper hemisphere (Fig. 2-1 a)).

CRLH transmission lines (TLs) on the other hand inherently possess the dual-band nature; thereby provide the phase advance in addition to phase delay. The dual-band nature of CRLH TL has been implemented in many microwave circuits including couplers, filters, etc. [33]-[35]. This additional phase leading feature enables the design of an all passive, single phased-array network that can simultaneously provide positive and negative relative phase difference values ($\pm\alpha$) for two arbitrary operating frequencies, thus enabling the array system to direct the radiated beams in the entire upper hemisphere (Fig. 2-1 b)). Hence, unlike the conventional all passive phased array networks, a CRLH based all passive single feed network is capable of directing the radiated beams of two arbitrary operating frequencies toward two arbitrary directions.

2.2.1. Principle of Phase Advance/Delay Feed Network

The equivalent circuit model for a unit length of the ideal lossless CRLH transmission line is comprised of L_R , C_R , L_L , and C_L (Fig. 2-2). The subscripts indicate the right- and left-handed constituents of the reactance values comprising the unit element response. Under the balanced condition ($L_R C_L = L_L C_R$), the characteristic impedance of the CRLH TL simplifies to

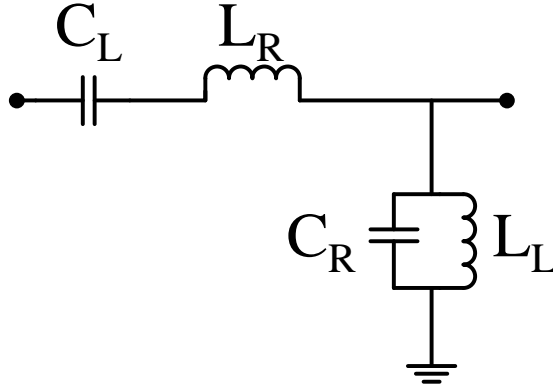


Figure 2-2 Equivalent circuit model of CRLH TL.

$$Z_o = \sqrt{\frac{L_R}{C_R}} = \sqrt{\frac{L_L}{C_L}}, \quad (2.2)$$

and results in the phase response of the composite structure that is the sum of the phase responses from the right- and left-handed portions of the CRLH TLs. For a section of CRLH TL consisting of n unit cells, the resulting phase response has the zero phase point shifted to a higher frequency (away from DC) with the positive phase (phase advance) below the zero phase frequency and negative phase (phase delay) above the zero phase frequency.

$$\phi_c = \phi_R + \phi_L \approx -n\omega\sqrt{L_R C_R} + \frac{n}{\omega\sqrt{L_L C_L}}. \quad (2.3)$$

For dual-band operation, the desired phase responses ϕ_1 and ϕ_2 can be expressed in terms of its two operating frequencies ω_1 and ω_2 . These set of equations along with the two characteristic impedance equations (2.4) leads to a consistent solution for the circuit parameters,

$$L_R = \frac{Z_o [\phi_1(\omega_1/\omega_2) - \phi_2]}{n\omega_2 (1 - (\omega_1/\omega_2)^2)},$$

$$\begin{aligned}
C_R &= \frac{\phi_1(\omega_1/\omega_2) - \phi_2}{n\omega_2 Z_o \left[1 - (\omega_1/\omega_2)^2\right]}, \\
L_L &= \frac{nZ_o \left[1 - (\omega_1/\omega_2)^2\right]}{\omega_1 \left[\phi_1 - (\omega_1/\omega_2)\phi_2\right]}, \\
C_L &= \frac{n \left[1 - (\omega_1/\omega_2)^2\right]}{\omega_1 Z_o \left[\phi_1 - (\omega_1/\omega_2)\phi_2\right]}.
\end{aligned} \tag{2.4}$$

The feasibility of above solution is settled if high- and low-pass cutoff frequencies resulting from the lumped element implementation fall outside the operating frequency region [33].

$$f_c^{LH} = \frac{1}{4\pi\sqrt{L_L C_L}}, \quad f_c^{RH} = \frac{1}{\pi\sqrt{L_R C_R}} \tag{2.5}$$

2.2.2. Implementation

Hybrid implementation is utilized to realize the CRLH dispersive lines where the RH portion is realized using microstrip lines and the LH portion is realized using lumped elements. This technique helps to reduce the total number of lumped components while microstrip lines enable much easier tuning.

2.2.3. Dual-Band CRLH Feed Network Design Procedure

For illustrational purpose, a design procedure for an all passive 4 element linear phased-array is demonstrated. Several approaches may be taken when designing the phased array network to achieve the ultimate goal of providing the proper relative phase values for the two operating frequencies. However, if the two main beams need to be pointed toward opposite

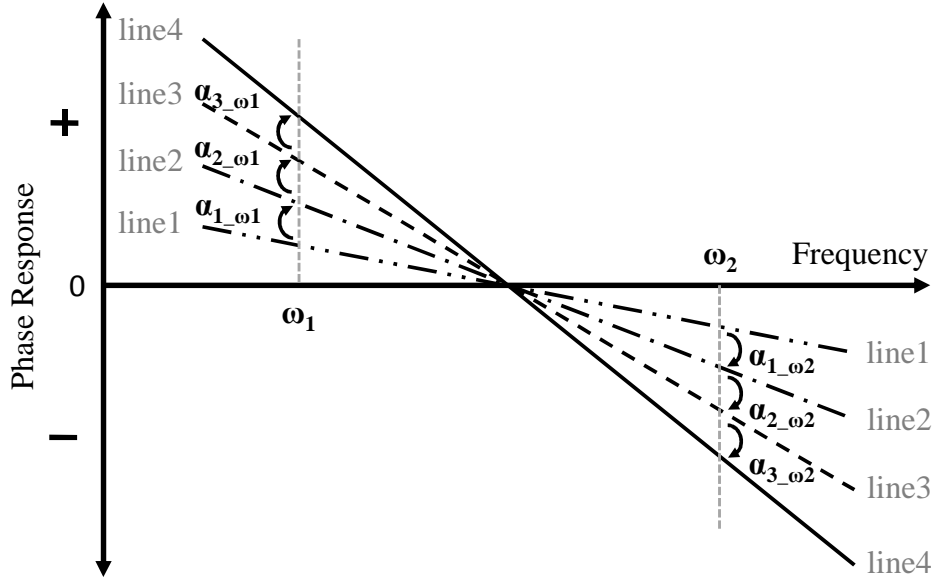


Figure 2-3 Desired phase response for four element dual-band CRLH feed network.

directions from the broadside direction, the phase response of the feed network should resemble those in (Fig. 2-3). Here, the relative phase delays for the two frequencies have opposite signs, thereby enabling the beams to tilt toward the opposite directions from the broadside direction.

The design procedure for the dual-band CRLH feed network which can provide the above requirement is simple and straight forward as follows:

Step 1) Set the desired main beam angle (θ_o) for the two operating frequencies.

Step 2) Find the inter-element spacing (d), considering both the mutual coupling and grating lobe. To avoid the grating lobe, the inter-element spacing is usually set to less than d_{max} [36],

$$d_{max} = \frac{\lambda}{1 + |\sin \theta_o|} \quad (2.6)$$

Step 3) Calculate the required relative phase difference (α) values that provide the desired beam angles for the two design frequencies.

$$\alpha_{\omega_1/\omega_2} = -k_{\omega_1/\omega_2} d \sin \theta_{o_{\omega_1/\omega_2}} \quad (2.7)$$

The desired α values can be attained by providing appropriate phase responses at the input of the antenna elements (ex: $\alpha_{1-\omega_1} = \phi_{2-\omega_1} - \phi_{1-\omega_1}$).

Step 4) Compute the L and C values (2.4) using given design frequencies and pair of required phase values obtained in Step 3).

Step 5) Verify whether the cutoff frequencies (2.5) are outside the operating frequency region. If the cutoff frequencies fall inside the operating region, choose a larger n value in Step 4) and repeat Steps 4) - 5).

Step 6) Determine the phase response produced by the lumped element based $LH TL$ only. The final desired phase response is obtained by adjusting the electrical length of the microstrip line that produces the missing RH phase delay portion.

2.2.4. Dual-Band Antenna

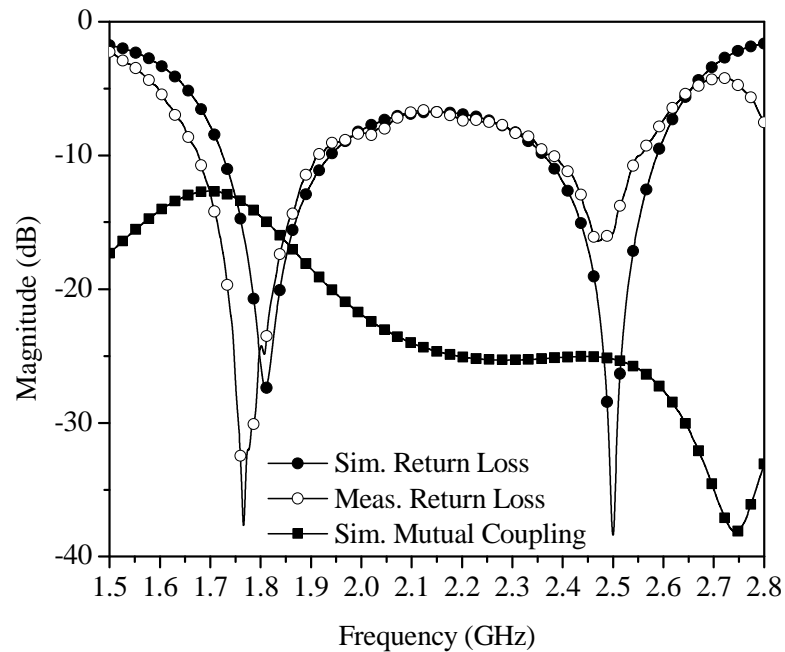


Figure 2-4 Dual-band antenna return loss and mutual coupling for $d = 7.5$ cm ($0.6 \cdot \lambda_{o2}$).

Quasi-Yagi antenna inspired dual-band antenna is designed [37]. Quasi-Yagi antennas are generally used for wideband application, but dual-band operation may be attained by tuning the radiating and parasitic elements and the spacing between them. The simulated and measured return losses are below -15 dB for both operating frequencies. Mutual coupling between the antennas is studied through simulation. The inter-element spacing is reduced while monitoring S21 to determine minimum allowed spacing.

2.2.5. CRLH Feed Network

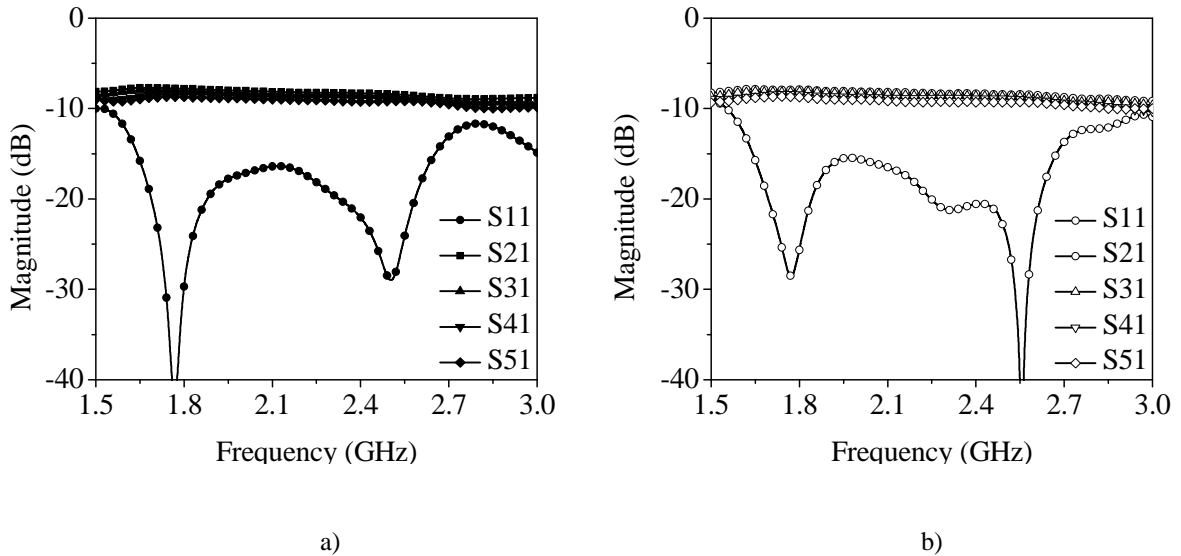


Figure 2-5 a) Simulated and b) measured S-parameters of the CRLH dual-band feed network.

For the demonstrational purpose, the operating frequencies are set to 1.8 GHz and 2.5 GHz and the desired elevation angles for the two operating frequencies are set to $\theta_o = \pm 10$ degrees from the broadside direction. The CRLH dispersive lines are designed using inter-element spacing $d = 7.5$ cm (mutual coupling ≈ -15 dB, as shown in Fig. 2.4). This inter-element spacing is $0.45 \cdot \lambda_{low_freq}$ and $0.625 \cdot \lambda_{high_freq}$ which allows moderate beam tilting for both frequency

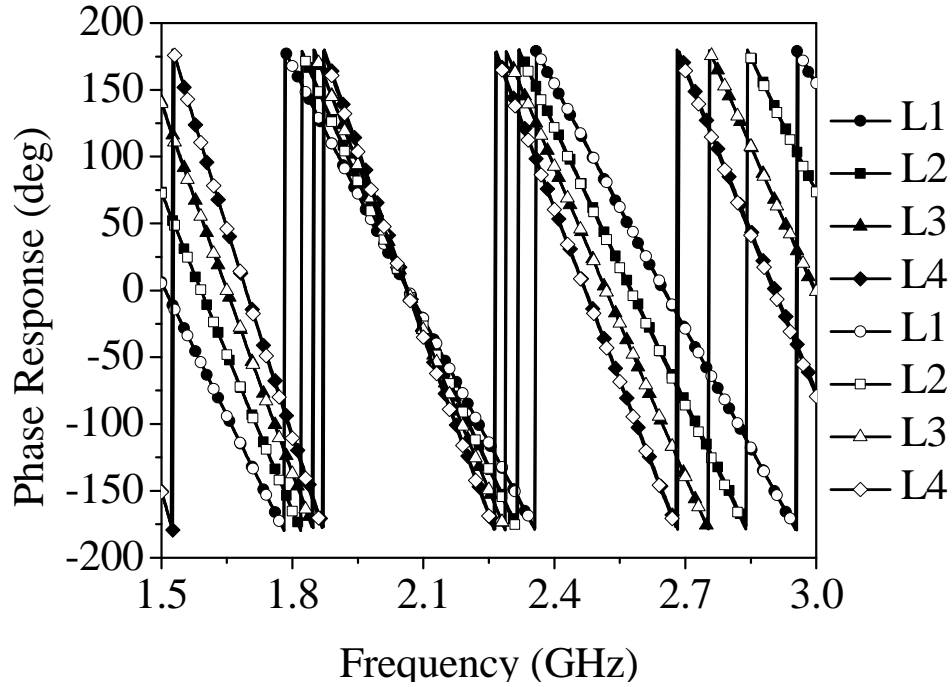


Figure 2-6 Simulated and measured phase response of the CRLH based phased-array feed network for line 1 (L1) to line 4 (L4): solid symbols (-●-) are simulated results and open symbols (-○-) are measured results.

bands prior to the onset of the grating lobes. The computed relative phase difference values are $\alpha_{\omega 1} = +28^\circ$ and $\alpha_{\omega 2} = -39^\circ$ to direct the main beams to $\theta_o = \pm 10^\circ$ for each operating frequencies ($f_1 = 1.8 \text{ GHz}$, $f_2 = 2.5 \text{ GHz}$).

The feeding network is fabricated on FR4 substrate ($\epsilon_r = 4.4$, $h = 31 \text{ mil}$, and $\tan\delta = 0.02$). A two stage Wilkinson power divider is used to evenly divide the power in-phase to the four CRLH dispersive lines. The return loss and insertion loss of the entire feed network including the CRLH TLs are below -15 dB and around -8 dB respectively for both simulation and measurement (Fig. 2-5). The simulated and measured phase responses of the entire feed network show good agreements (Fig. 2-6). Both the simulated and measured results show $\alpha_{\omega 1} \approx +28^\circ$ at $f_1 = 1.8 \text{ GHz}$ and $\alpha_{\omega 2} \approx -39^\circ$ at $f_2 = 2.5 \text{ GHz}$ as desired.

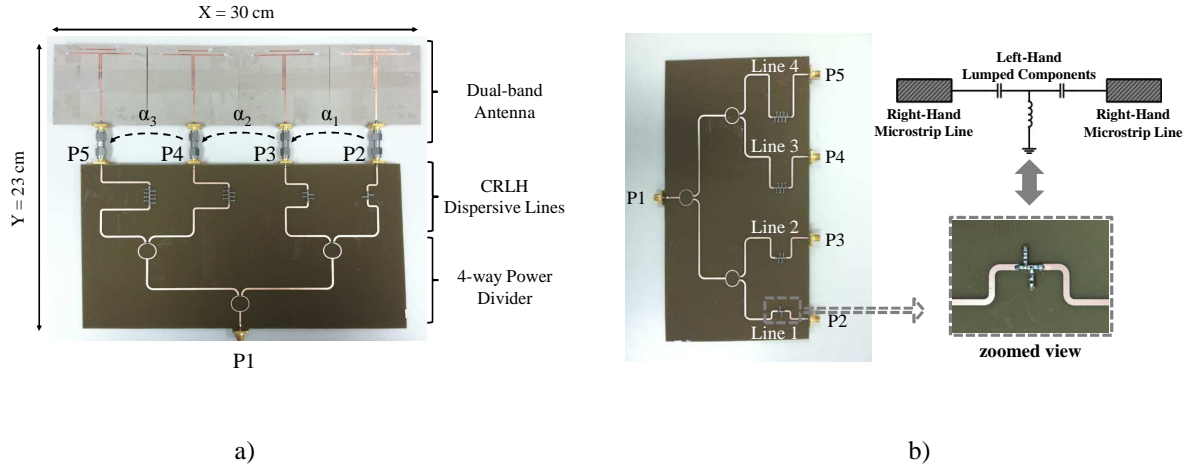


Figure 2-7 Photograph of the fabricated dual-band CRLH based phased-array system: a) with antenna b) feed network only.

2.2.6. Radiation Patterns

Simulated radiation pattern of the 4 element linear array is obtained by simulating a single antenna then plotting the array pattern using array factor calculation. For the measurement, the pattern of the entire circuit (feed network and antennas) is measured in the anechoic chamber. The simulated and measured radiation patterns show the main beam angles toward $\theta_o \approx \pm 10^\circ$ as desired with good agreement between them (Fig. 2-8). The measured gain and efficiency of the entire systems is 6.7 dB and 62% respectively for the lower frequency band and 6.7 dB and 49% respectively for the upper frequency band, as indicated in Table I.

Freq.	Sim. vs. Meas.	α_1	α_2	α_3	Desired α	Direct.	Gain	Efficiency	θ_o	Desired θ_o
1.8 GHz	Sim.	+29.9 deg	+28.5 deg	+28.5 deg	+28 deg	10.5 dB	-	-	+9 deg	+10 deg
	Meas.	+28.3 deg	+27.8 deg	+28.1 deg		8.8 dB	6.7 dB	62 %	+10 deg	
2.5 GHz	Sim.	-38.4 deg	-39.6 deg	-38.2 deg	-39 deg	9.8 dB	-	-	-9 deg	-10 deg
	Meas.	-39.1 deg	-37.8 deg	-38.1 deg		9.8 dB	6.7 dB	49 %	-9.5 deg	

Table 1 Simulated and measured performances of the proposed dual-band CRLH based phased-array.

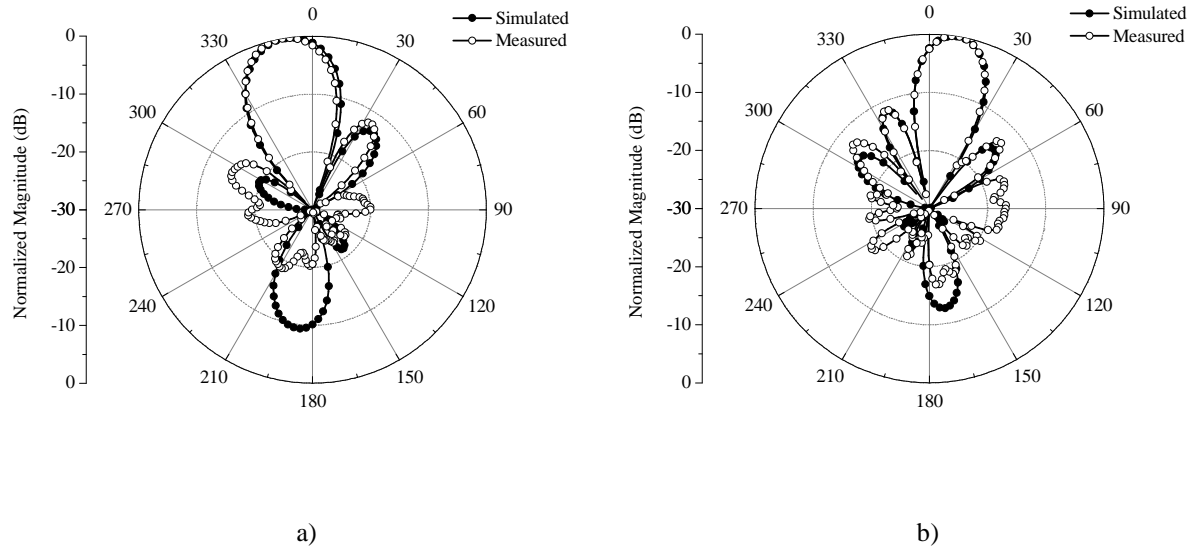


Figure 2-8 Simulated and measured E-plane co-polarized radiation patterns of the dual-band phased array system for a) $f_1 = 1.8$ GHz and b) $f_2 = 2.5$ GHz.

2.2.7. Conclusion

A CRLH dual-band feed network provides both phase advance and delay for arbitrary frequencies thereby providing dual-band operation of the phased array that directs the main beam to two arbitrary radiation angles using a single feed network. This type of feed network works with any conventional dual-band antennas. If broadband antenna is used, the CRLH feed network can also be used to construct a frequency scanning antenna system. However, unlike the CRLH leaky-wave antenna, the frequency scanning functionality is obtained through feed network design and not antenna design.

2.3 CRLH PHASED-ARRAY FEED NETWORK FOR FREQUENCY SCANNING ANTENNA

Composite right/left handed (CRLH) based frequency scanning antennas have attracted much attention in recent years. Unlike the previous generation of frequency scanning leaky-wave antennas that could only scan toward one direction with respect to broadside (excluding broadside radiation) [38, 39], the CRLH concept enable full frequency scanning capability from backfire-to-endfire including broadside while operating in the dominant mode. Popular CRLH based leaky-wave antennas (LWA) can be analyzed using antenna array theory [40]. The antenna is composed of periodic structures with unit dimensions much smaller than the guided wavelength. When the antenna is fed from one end of the leaky wave mechanism, each antenna element contributes a small portion of the radiated power. Careful design of the antenna structure essentially provides both negative and positive phase progressions between each unit element as

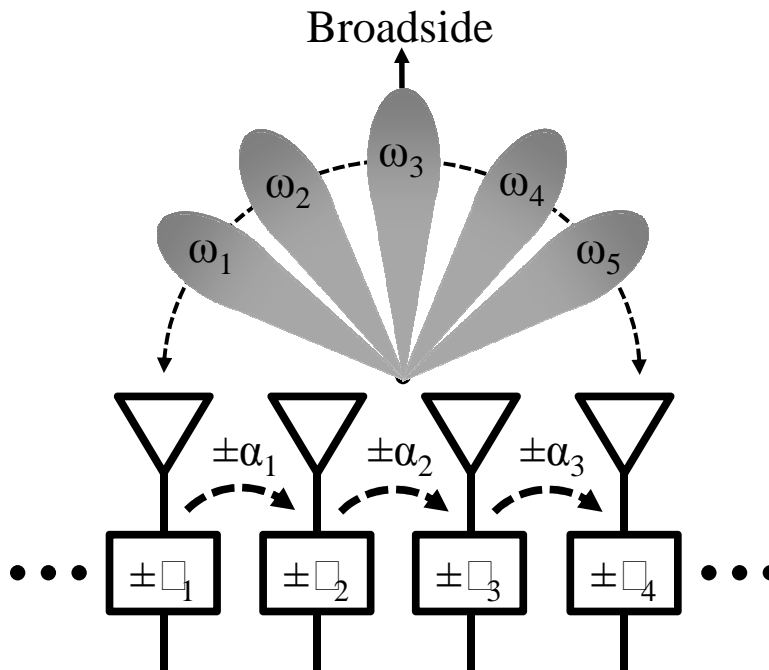


Figure 2-9 Proposed frequency scanning phased-array based on CRLH feed network.

frequency is varied within the radiating frequency band. Since the introduction of CRLH based leaky-wave antennas in 2002 [41, 42], researchers have focused on improving antenna functionalities and performances. For example, common and differential mode feeding is added to control and improve the radiated far-field polarization [43]. Amplifiers are inserted to control the amplitude distribution and increase the radiated gain toward broadside radiation [44]. Substrate integrated waveguide is utilized to increase the quality factor (Q) of the antennas [45]. Despite each novel approach, CRLH based LWAs have an inherent drawback that arises from closely coupled linkage between the radiating antenna elements and the array factor (AF). In order for CRLH LWAs to provide smooth frequency scanning operation, a very specific structural form must be retained. But in doing so, independent control of the antenna parameters, such as polarization and amplitude distribution, are sacrificed.

However, a different approach using array theory can also be used in designing a frequency scanning radiating circuit. The proposed method also uses the CRLH concept, but rather than integrating the approach into the antennas, the phase engineering concept of the CRLH TL is applied to the phased-array feed network, which is completely decoupled from the radiating elements. In doing so, independent design controllability can be obtained to easily alter radiated polarization type, polarization orientation, and cross polarization level. Furthermore, when combined with power dividers that allow simple power ratio adjustments, current amplitude distribution of the array can be easily manipulated to control the directivity and mainlobe-to-sidelobe level of the radiated pattern. To the authors' knowledge, an all-passive full frequency scanning radiating circuit that allows independent controllability of polarization, phase, and amplitude distribution has not yet been demonstrated. To address the similarities and differences with CRLH LWA, we present a brief review of conventional CRLH LWA, followed

by the new design approach for frequency scanning arrays based on the CRLH TL. Finally, the improved radiated performances of the proposed system are highlighted and validated with measured results.

2.3.1. Conventional CRLH LWA

CRLH LWAs are composed of periodic unit cells containing reactive parameters that provide both negative and positive propagation constant (β) values as a function of scanned frequency. For frequencies where $-k_o < \beta < +k_o$, the guided mode couples to air and radiates with a main beam at an angle

$$\theta_o = \sin^{-1} \left(\frac{\beta(\omega)}{k_o} \right) \quad (2.8)$$

where, $\beta(\omega)$ is the frequency dependent propagation constant and k_o is the freespace wave number. Under the balanced condition, a smooth transition from backfire to endfire can be

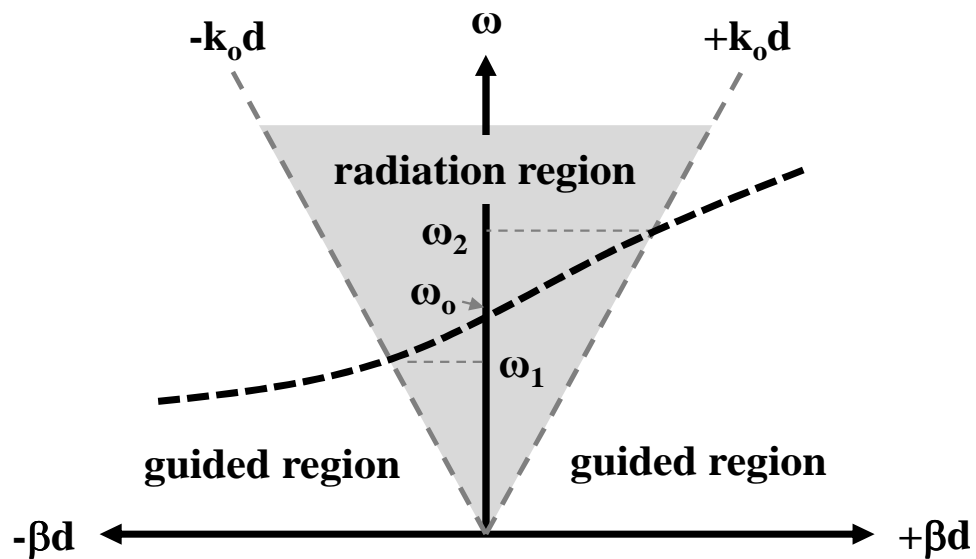


Figure 2-10 Dispersion diagram of balanced CRLH structure.

obtained without introducing the undesired bandgap frequency region [5]. A typical dispersion diagram of a balanced CRLH LWA is shown in (Fig. 2-10). In sum, operating the CRLH structure between the radiation frequency region ($\omega_1 < \omega < \omega_2$), the structure behaves as an antenna with a main beam that scans along the elevation angles as the frequency is varied. However, most planar types of CRLH LWAs [46]-[47] suffer from the difficulties in controlling radiated polarization characteristics and from the non-ideal exponentially decaying amplitude distribution profile. For transmission-line based CRLH LWA structures, non-ideal polarization traits have been remedied by combining a set of antennas side-by-side and feeding common/differential mode signals [43]. Different structural types such as SIW have demonstrated relatively better polarization characteristics for a particular E-plane orientation [45]. However in all cases, directivity/side lobe level (SLL) controllability remains unresolved. To add the amplitude controllability and increase directivity, unidirectional amplifiers have been added to the CRLH LWA [44]. In doing so, tapered amplitude distribution has been provided for broadside radiation, but frequency scanning capability has not been demonstrated. Also, integrating amplifiers adds both design and fabrication complexity, in addition to forfeiting bilateral ($Tx.$ and $Rx.$) operation. However, to simultaneously address polarization and amplitude distribution properties, CRLH TLs may be used in the form of a phased-array feed network as described in the following.

2.3.2. CRLH Phased-Array Feed Network for Frequency Scanning Antenna

Arrays

The essential property required in continuous frequency scanning is obtained by gradually increasing the relative phase progression between the antenna elements toward both

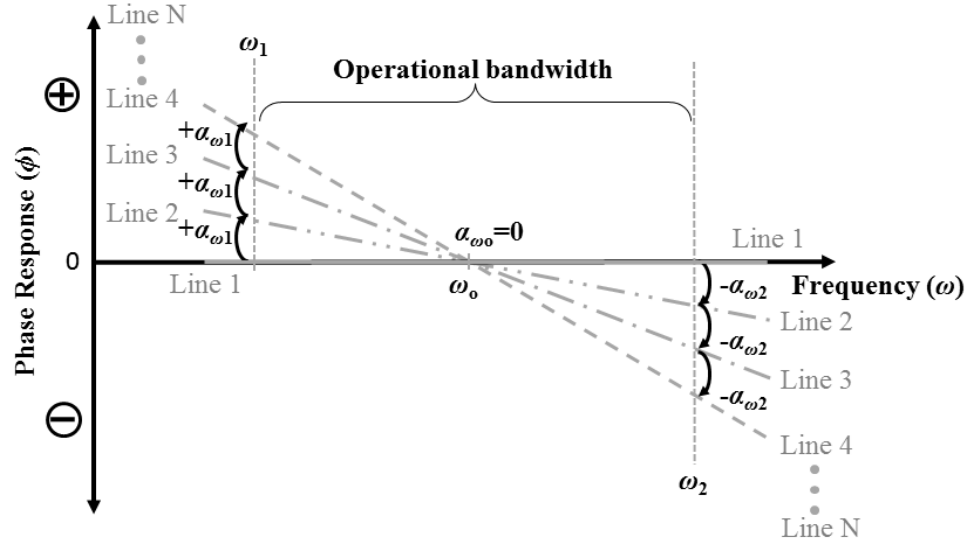


Figure 2-11 Ideal phase response of four element linear phased-array feed network needed for continuous 1-D frequency scanning.

negative and positive directions as frequency is shifted away from the center frequency ω_o (Fig. 2-11). The equation for the main beam angle describing the phased-array has the same form as that of the CRLH LWA,

$$\theta_o = \sin^{-1} \left(\frac{\alpha}{kd} \right) \quad (2.9)$$

Here, if the progressive phase shifting (α) between the antenna elements can be both negative/positive and dispersive [$\pm\alpha(\omega)$] for a fixed inter-element spacing (d), the same full 1-D frequency scanning feature obtained in CRLH LWAs can also be achieved, but all in passive phased-array form. The idea is similar to that of the dual-band case, but rather than using two edge frequencies, we can also use the entire CRLH spectrum band as long as they are comprised of non-radiating CRLH transmission lines. Unlike the conventional transmission lines, CRLH TL allows simpler systematic manipulation of the phase response between the input and output ports of the line. The equivalent circuit model is the same as that of the CRLH LWA, but when

lumped devices are used, radiation is suppressed. In this section we further improved the feeding structure designed for dual-band case [8], where larger scanning angle is provided by eliminating the CRLH lines in one of the feeding path and also amplitude distribution is examined to demonstrate mainlobe-to-sidelobe controllability. Unlike [44], bilateral operation is allowed in this system since only passive elements are utilized to control the radiated parameters.

To obtain full 1-D frequency scanning, the final phase response should resemble (Fig. 2-11). CRLH dispersive lines only contribute to the phase component of the array system. Slight amplitude perturbation may be created between the lines due to the lossy nature of lumped elements, but the amplitude imbalance can be easily compensated by adding an unequal power divider in the first power division step.

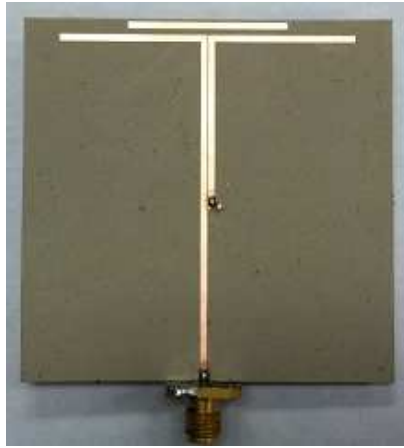
2.3.3. Implementation of CRLH based Phased-Array

When the CRLH lines are combined with proper power dividers, a more versatile frequency scanning phased-array feed network can be designed. As noted in the previous section, the phase component is mainly dictated by the dispersive CRLH lines. On the other hand, amplitude distribution can be controlled by the power dividers and radiated polarization properties depend purely on the antenna elements used along with the proposed network. Therefore, independent design freedom is allowed by simply selecting and combining the independent functional blocks (power divider, dispersive feed lines, and antenna elements) to meet most design specifications, such as the type and orientation of the radiated polarization, cross-polarization levels, mainlobe-to-sidelobe level, and frequency scanning range. In the following sections, two sets of frequency scanning phased-array feed networks based on CRLH dispersive lines are designed using quasi-Yagi antennas to demonstrate the versatility and simplicity in designing and controlling the

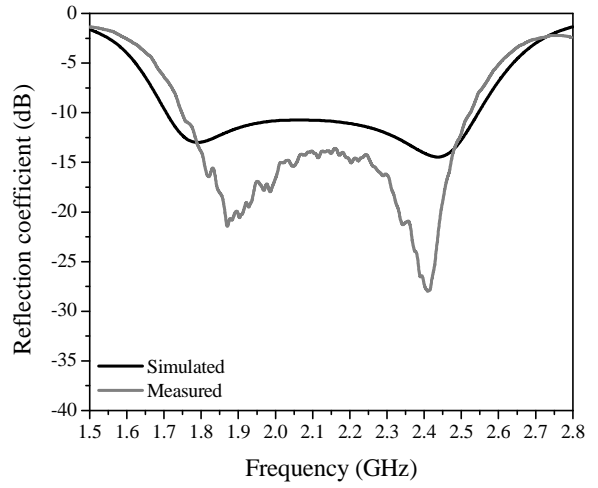
radiated properties of the antenna array. First, a CRLH array feed network is designed to provide uniform amplitude distribution for maximum directivity, and the second network is fed with tapered amplitude distribution to examine the SLL controllability of the radiated pattern. Also, for each feed network, quasi-Yagi antennas are oriented to collinear and side-by-side configurations to show simple polarization controllability of the array system.

A. Wideband Quasi-Yagi Antenna

Wideband Quasi-Yagi antennas have been extensively studied both as a single element and in an array. In both cases, these linearly polarized antennas provide good polarization selectivity, can be designed electrically small, provide directive radiation beam pattern, and offer sufficient bandwidth needed for the frequency scanning operation [37], [48]-[49]. Both simulated and measured results show reflection coefficient values below -10 dB throughout the operating band: $\omega = 1.8$ GHz to 2.5 GHz (Fig. 2-12). The design process of the frequency scanning phased array is same as that of the dual-band case. Similar to the dual-band case, inter-element spacing needs to be carefully determined for a given antenna element to satisfy both maximum tolerable mutual coupling level between the antennas and to avoid the onset of the grating lobe when starting the phased-array network design [36]. However, undesired mutual coupling between the antenna elements at the lower frequencies will limit close placement. Prior to finalizing the inter-element spacing, a mutual coupling study is carried out using full-wave simulation to ensure the levels are kept under reasonable value. In the proposed design, inter-element spacing of $d = 64$ mm ($\approx 0.4 \times \lambda_{0_1}$ and $\approx 0.5 \times \lambda_{0_2}$) is used. In both collinear and side-by-side four element linear array configuration, reflection coefficient and mutual coupling levels are maintained below -10 dB as shown in (Fig. 2-13) and (Fig. 2-14). Extra optimization may further enhance both levels.

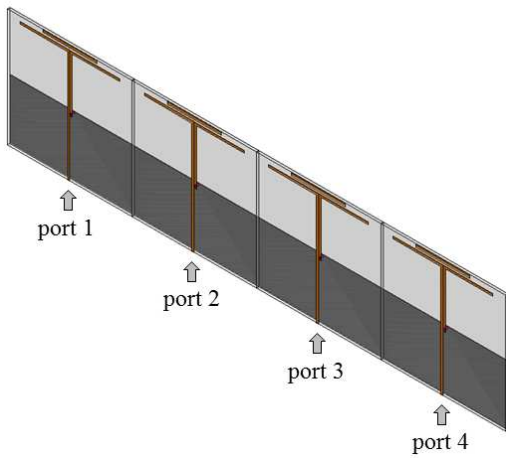


a)

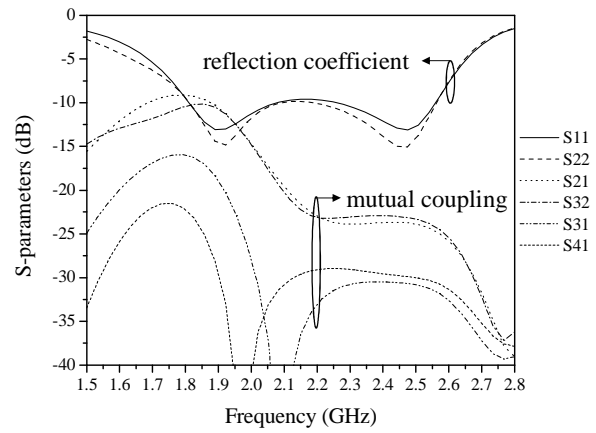


b)

Figure 2-12 R-band single element quasi-Yagi antenna: a) photograph of the fabricated antenna and b) simulated and measured reflection coefficient plots.



a)



b)

Figure 2-13 Four element linear phased-array using quasi-Yagi antennas in collinear configuration: a) figure of the collinear configuration and b) reflection coefficient and mutual coupling values.

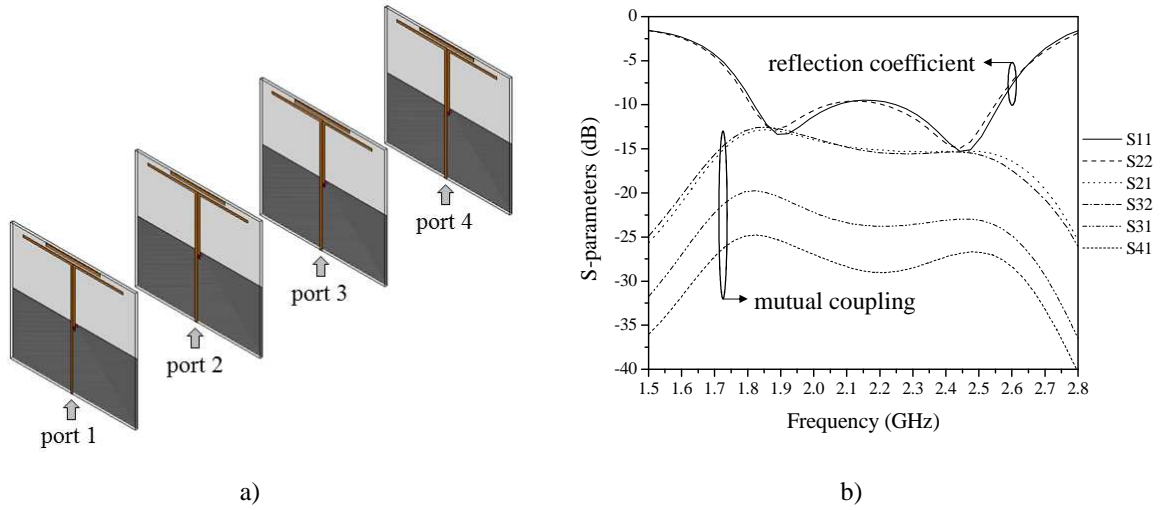


Figure 2-14 Four element linear phased-array using quasi-Yagi antennas in side-by-side configuration: a) figure of the side-by-side configuration and b) reflection coefficient and mutual coupling values.

B. CRLH Based Phased Advance/Dealy Lines for Frequency Scanning Phased-Array

Network.

Once the inter-element value is determined, required phase values can be calculated to direct the main beam toward the desired directions. A detailed systematic design guide of CRLH feed lines are explained in Section 2.3 and also in [6]. Although the design guides are geared toward designing dual-band phased array, the same procedure also applies to the frequency scanning phased-array. As a demonstrational purpose, the CRLH feed networks are designed to scan from $\theta_o = -30^\circ$ to $+30^\circ$ between the frequencies $\omega_1 = 1.8$ GHz to $\omega_2 = 2.5$ GHz. Unlike the previous CRLH based phased-array feed network designs [6] and [8], in order to minimize the number of the total lumped element used, phase reference line (line 1) does not have the CRLH components. Instead, if conventional microstrip line is used for the first antenna element (Fig. 2.15), the calculated reactance values of the first CRLH lines (line 2, feeding the second antenna element) using (5) are: $L_L = 2.65$ nH, $C_L = 1.06$ pF, $L_R = 5.61$ nH, and $C_R = 2.24$ pF with $n = 3$. Three unit-cells are needed to push the high- and low-pass cutoff frequencies outside the operating

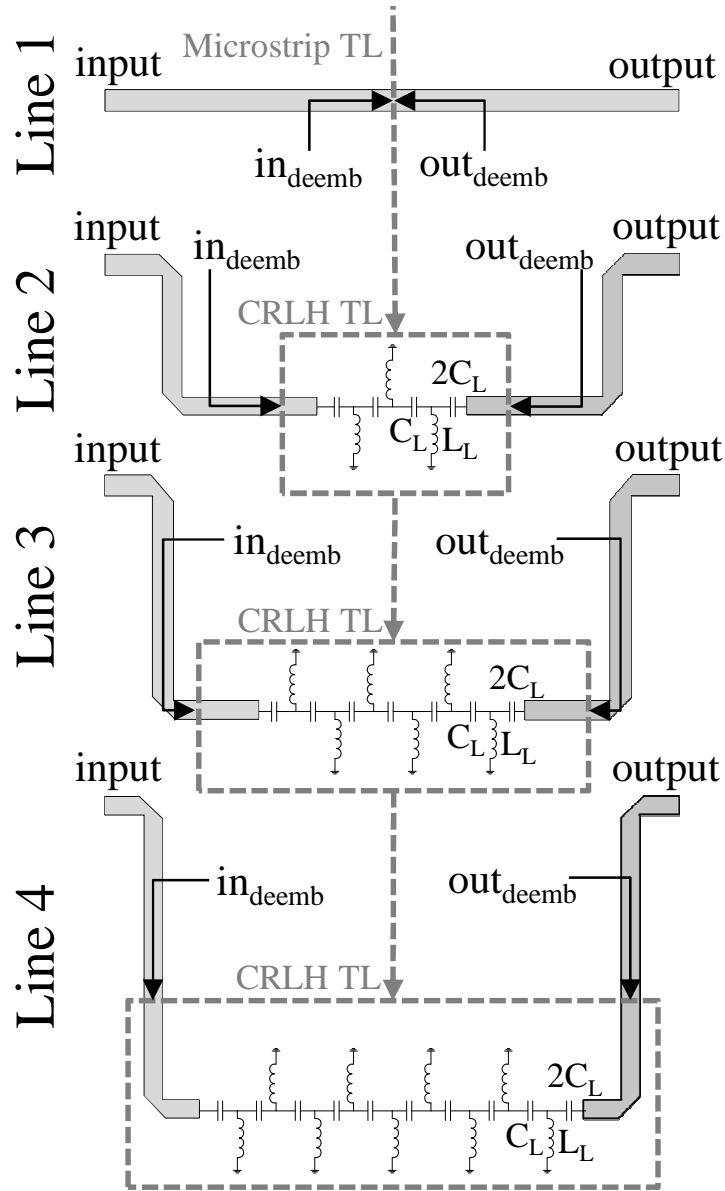


Figure 2-15 Illustrative layout of the feed lines for four element phased-array.

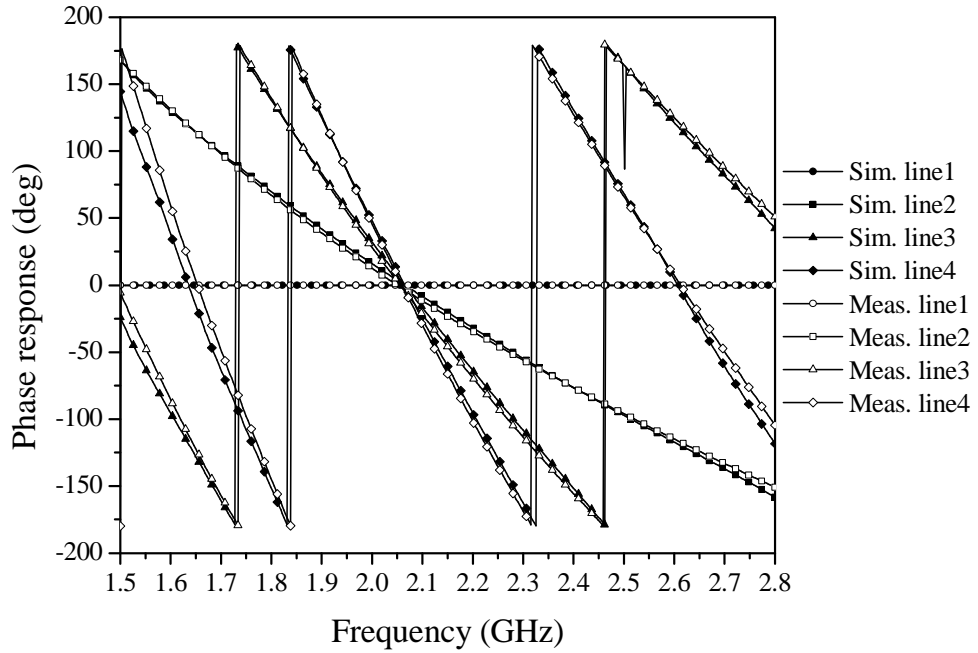


Figure 2-16 Simulated and measured phase response of CRLH dispersive lines only.

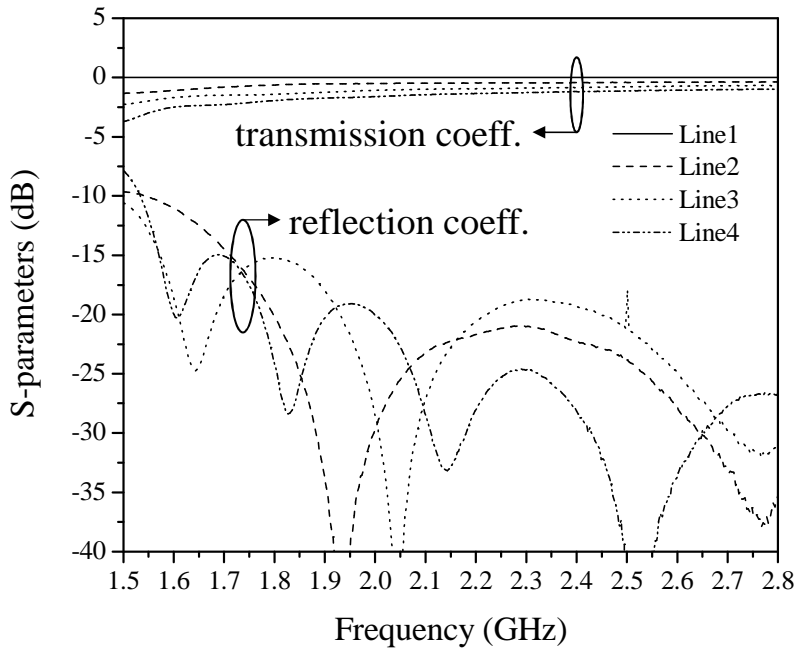


Figure 2-17 Measured transmission coefficients and reflection coefficients of CRLH dispersive lines only.

frequency band [34]. These ideal reactance values will generate the phase response of $\phi_{-\omega_1} = 69.12^\circ$ and $\phi_{-\omega_2} = -96^\circ$ at the two far end frequency points ω_1 and ω_2 , thereby directing the main beams to -30° and $+30^\circ$ respectively. For every added antenna element, the same CRLH sections (in this case, three unit-cells composed of the same reactance values) can be added in a cascaded fashion to ensure the same progressive phase shifting (α) for each operating frequency point within the operating bandwidth. To further reduce the total number of lumped elements and provide better tuning capability, hybrid implementation is used to realize the CRLH lines [34]. *RH* and *LH* portions are realized using microstrip lines and lumped elements respectively. In the final fabricated circuits, $L_L = 3$ nH and $C_L = 1.3$ pF are used, and right-hand microstrip line lengths for each paths are adjusted accordingly to provide the required phase response for the design frequencies. The measured phase response of the phase advance/delay lines match well to the desired simulated data (Fig. 2-16). In both simulated and measured results, the ports are de-embedded to indeemb and outdeemb positions as shown in (Fig. 2-17). Once the phase engineered CRLH dispersive lines are designed, they are combined into two sets of feed networks based on a corporate feeding scheme. One of the circuits uses equal power dividers to provide uniform amplitude distribution that provides maximum directivity while the other feed network is designed to provide tapered current amplitude distribution to minimize the SLL.

C. CRLH Feed Network with Uniform Amplitude Distribution

For a given array size and dimension, uniform current amplitude distribution provides the highest directivity owing to the space-angle Fourier relationship [32]. A simple corporate feeding network can be used to provide uniform amplitude distribution. As mentioned in the previous

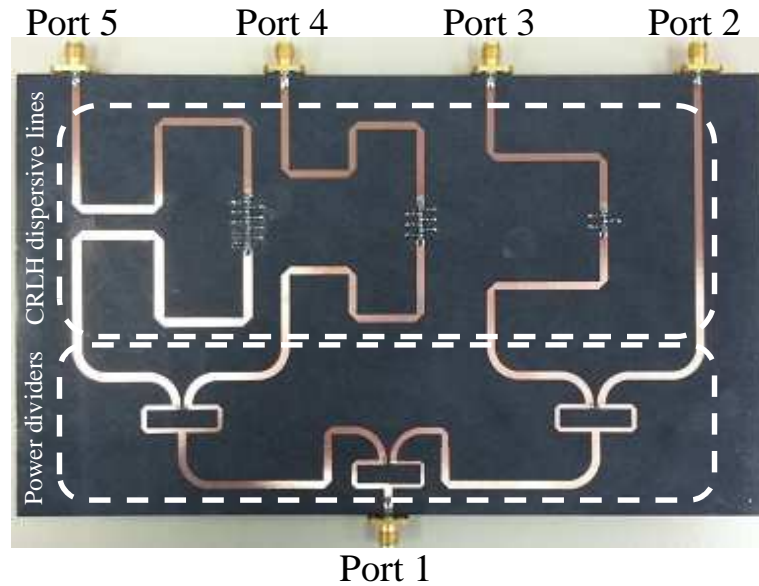


Figure 2-18 Photograph of the fabricated linear 1-D phased-array feed network based on CRLH TLs with uniform amplitude distribution.

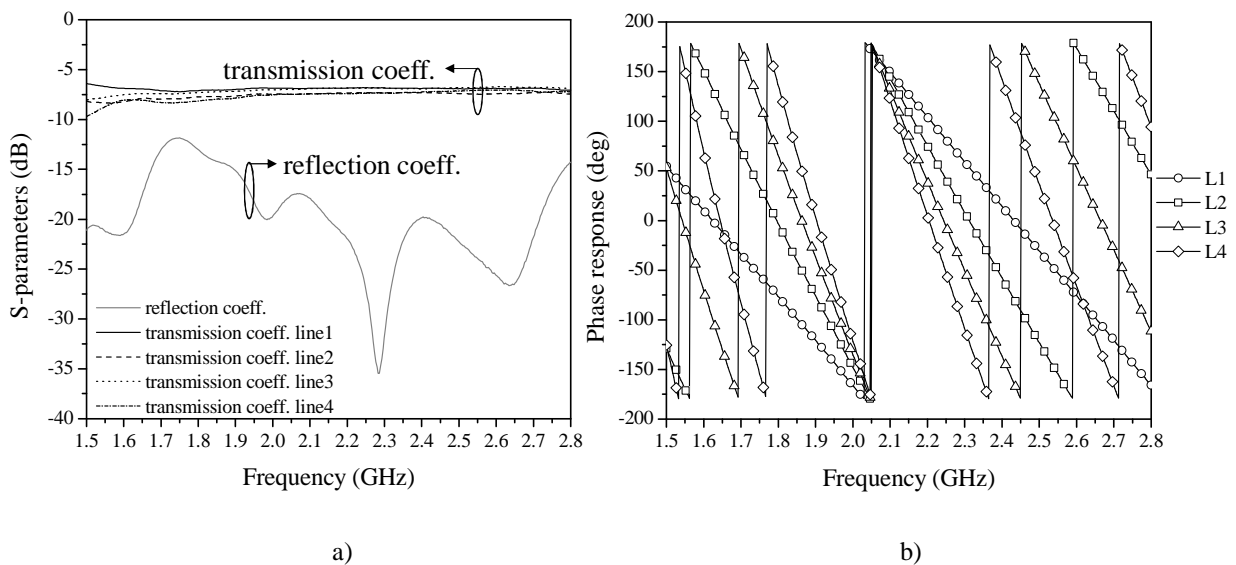


Figure 2-19 Measured a) S-parameters and b) phase response of CRLH phased-array feed network with uniform amplitude distribution.

section, a longer CRLH path introduces more loss, thereby creating amplitude imbalance at the output ports of the feed network. This result is shown in (Fig. 2-17), where larger insertion losses

are produced for longer CRLH lines. Measured results show around 0.2 dB loss per CRLH unit-cell. This loss may be reduced using high-Q lumped elements, but it cannot be completely eliminated. However, the amplitude imbalance can be minimized by adding an unequal power divider at the first power division stage. Using 1dB power divider, the power imbalance is reduced from 2 dB to 1 dB and 1dB to 0 dB at ω_1 and ω_2 respectively. The fabricated uniform amplitude CRLH based phased-array network is shown in (Fig. 2-18). Simulated and measured S-parameters and phase response plots are shown in (Fig. 2-19). Meandered lines are used to efficiently use the substrate area and miniaturize the overall circuit dimension. The entire circuit is fabricated on Rogers RT/duroid 5880 ($\epsilon_r = 2.2$, $h = 31$ mil) substrates.

D. CRLH Feed Network with Tapered Amplitude Distribution

Although uniform amplitude distribution provides the highest directivity, it suffers from undesired larger SLL. To reduce the SLL, tapered amplitude may be used. Theoretically, binomial distribution may be used to completely eliminate the side lobes; however, it requires a relatively more drastic amplitude tapering requirement. For a four-element equally spaced linear array, the binomial current amplitude distribution of 1:3:3:1 (power distribution of 1:9:9:1) is needed to obtain the minimum SLL. Although binomial distribution is achievable, to relax design and fabrication complexity, Dolph-Tschevscheff distribution is selected. Side lobes are

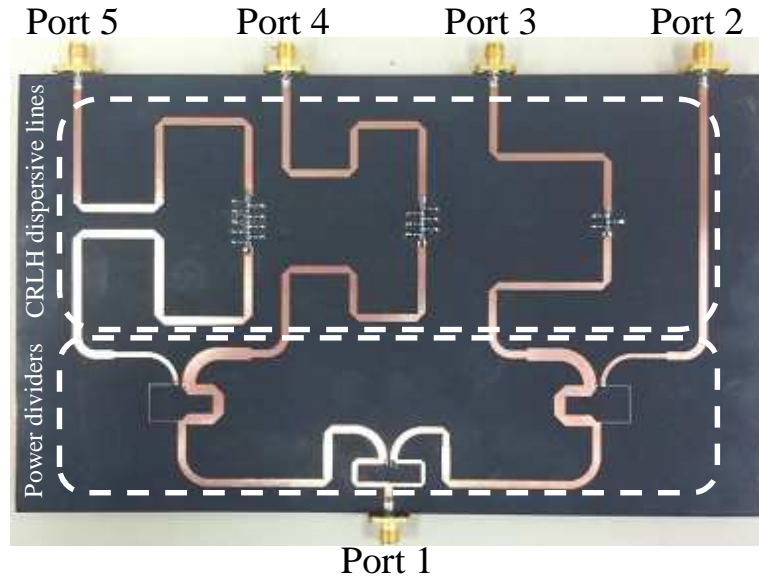


Figure 2-20 Photograph of the fabricated linear 1-D phased-array feed network based on CRLH TLs with tapered amplitude distribution.

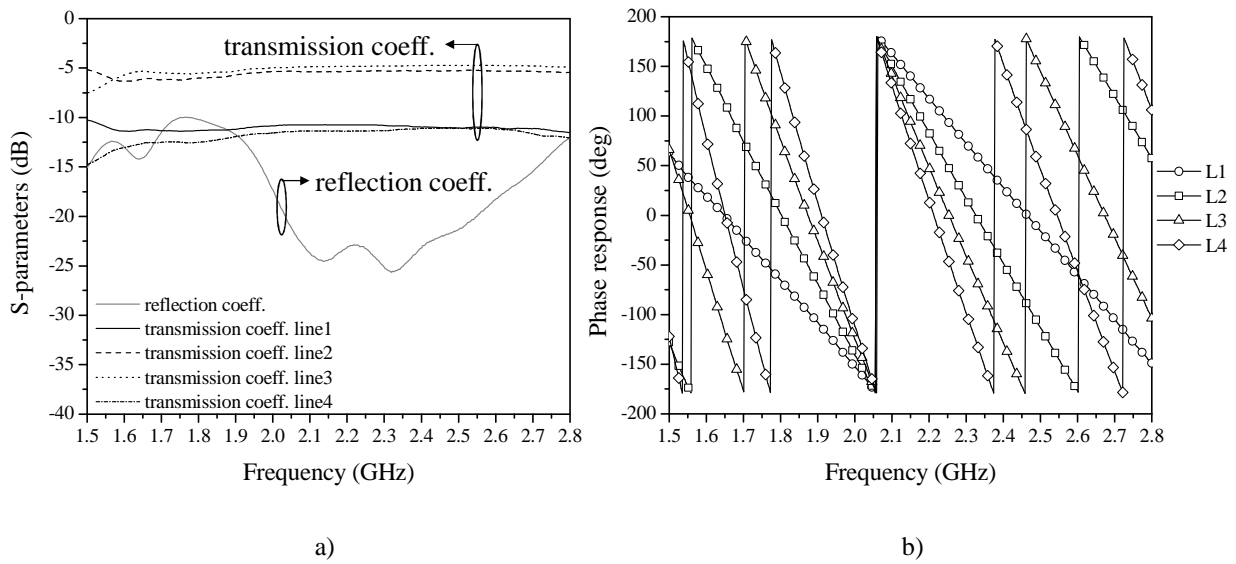


Figure 2-21 Measured a) S-parameters and b) phase response of CRLH phased-array feed network with tapered amplitude distribution.

not completely eliminated, but SLL can be suppressed below the pre-specified level. Standard Doph-Tschevyscheff synthesis with four-element equally spaced linear array for SLL of -26 dB

requires current amplitude distribution of 1:2.13:2.13:1 [3]. To ease both the design procedure and fabrication process, a Wilkinson power divider is designed to provide current amplitude distribution of 1:2:2:1 (power distribution of 1:4:4:1) [50]-[51]. The fabricated tapered amplitude CRLH based phased-array network is shown in (Fig. 2-20). Simulated and measured S-parameters and phase response plots are shown in (Fig. 2-21). Adding 4:1 divider in the second stage shows excellent matching and desired dividing ratio of 6 dB between the inner (ports 3 and 4) and outer (ports 2 and 5) ports.

2.3.4. Radiation Patterns: Measurement Setup and Results

A. Wideband Quasi-Yagi Antenna

Radiation patterns and directivity for quasi-Yagi antenna and phased-array antennas using both uniform amplitude and tapered amplitude CRLH phased-array network are measured in the nearfield chamber with a WR-430 waveguide probe. The measurement setup is shown in (Fig. 2-22). The radiated gain values for each circuit are computed based on the gain comparison method using standard gain horn antenna with the gain of 16 dBi

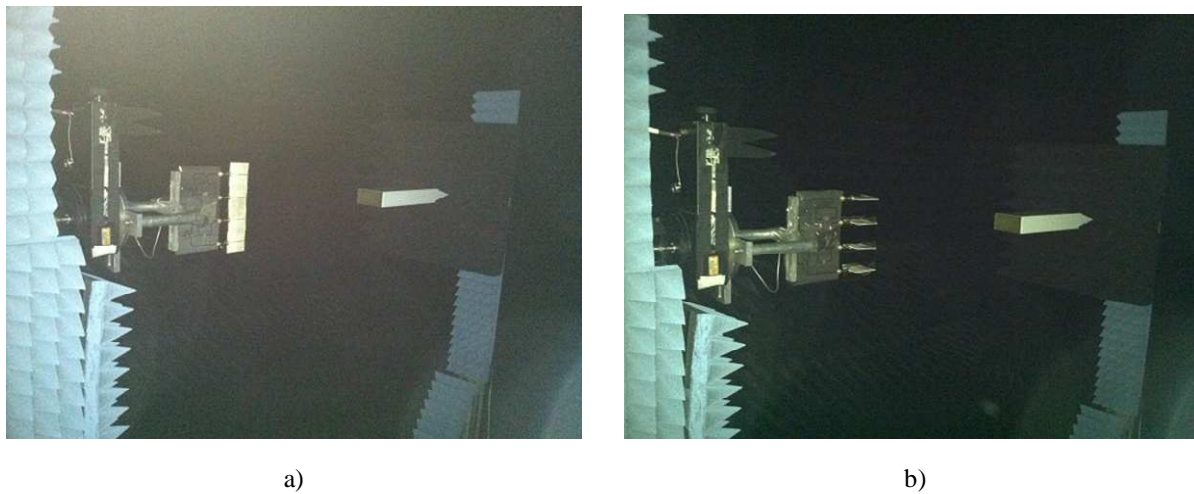


Figure 2-22 Photograph of the measurement setup for the proposed CRLH based frequency scanning phased-array in the near field chamber: a) proposed array in collinear configuration and b) proposed array in side-by-side configuration.

B. CRLH Based Phased Advance/Dealy Lines for Frequency Scanning Phased-Array Network.

The quasi-Yagi antenna has a quasi-dipole radiation pattern that resembles a doughnut shaped radiation pattern. However, the ground plane on the backside acts as a reflector to enhance the directivity toward the opposite direction. Co-pol and cross-pol radiation patterns for both E-plane and H-plane radiation patterns are shown in (Fig. 2-23) and (Fig. 2-24), respectively. Measured directivity and gain plots are shown in (Fig. 2-25).

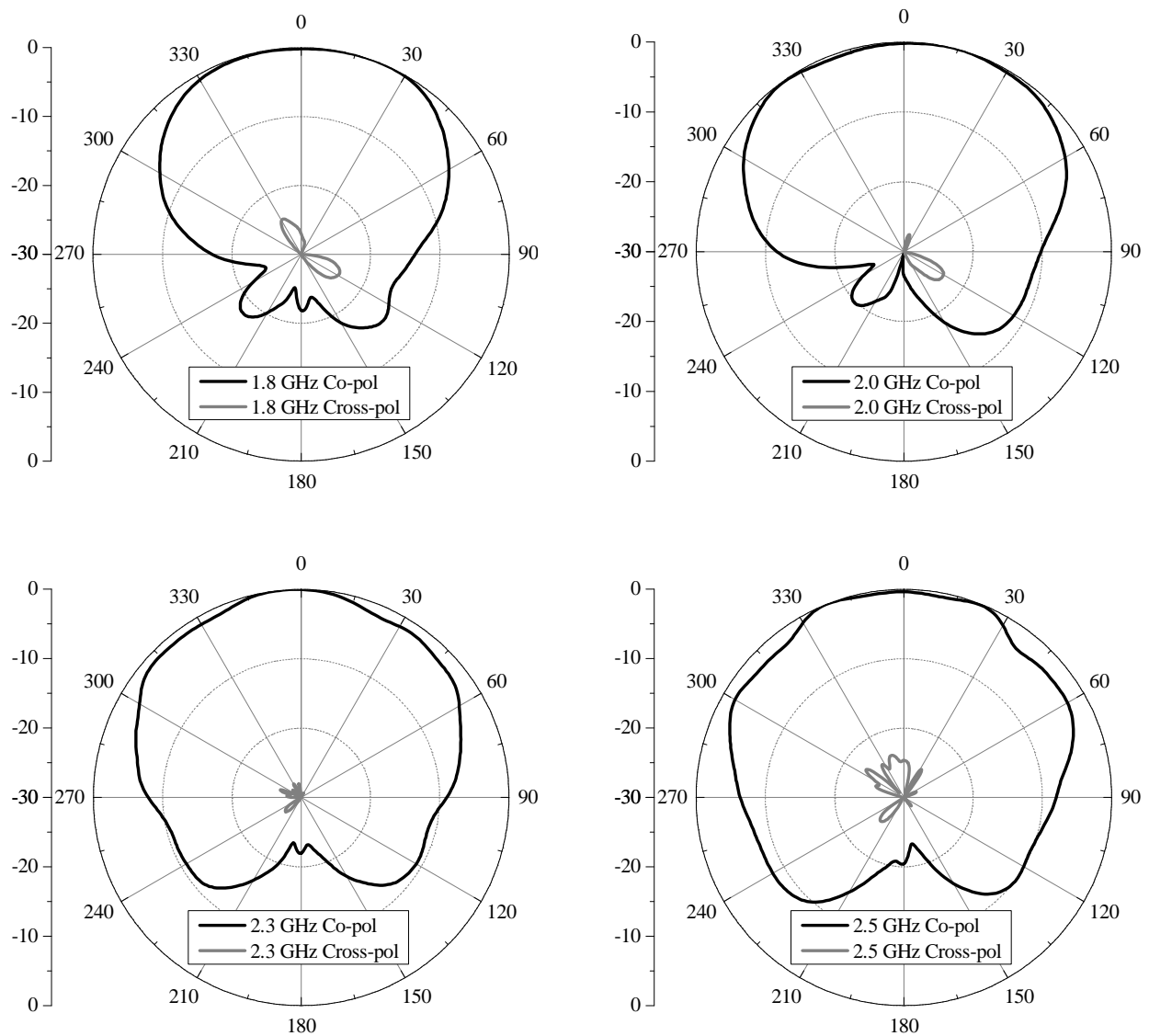


Figure 2-23 Measured normalized E-plane co-pol (black) and cross-pol (gray) patterns in dB scale for frequencies: 1.8 GHz, 2.0 GHz, 2.3 GHz, and 2.5 GHz.

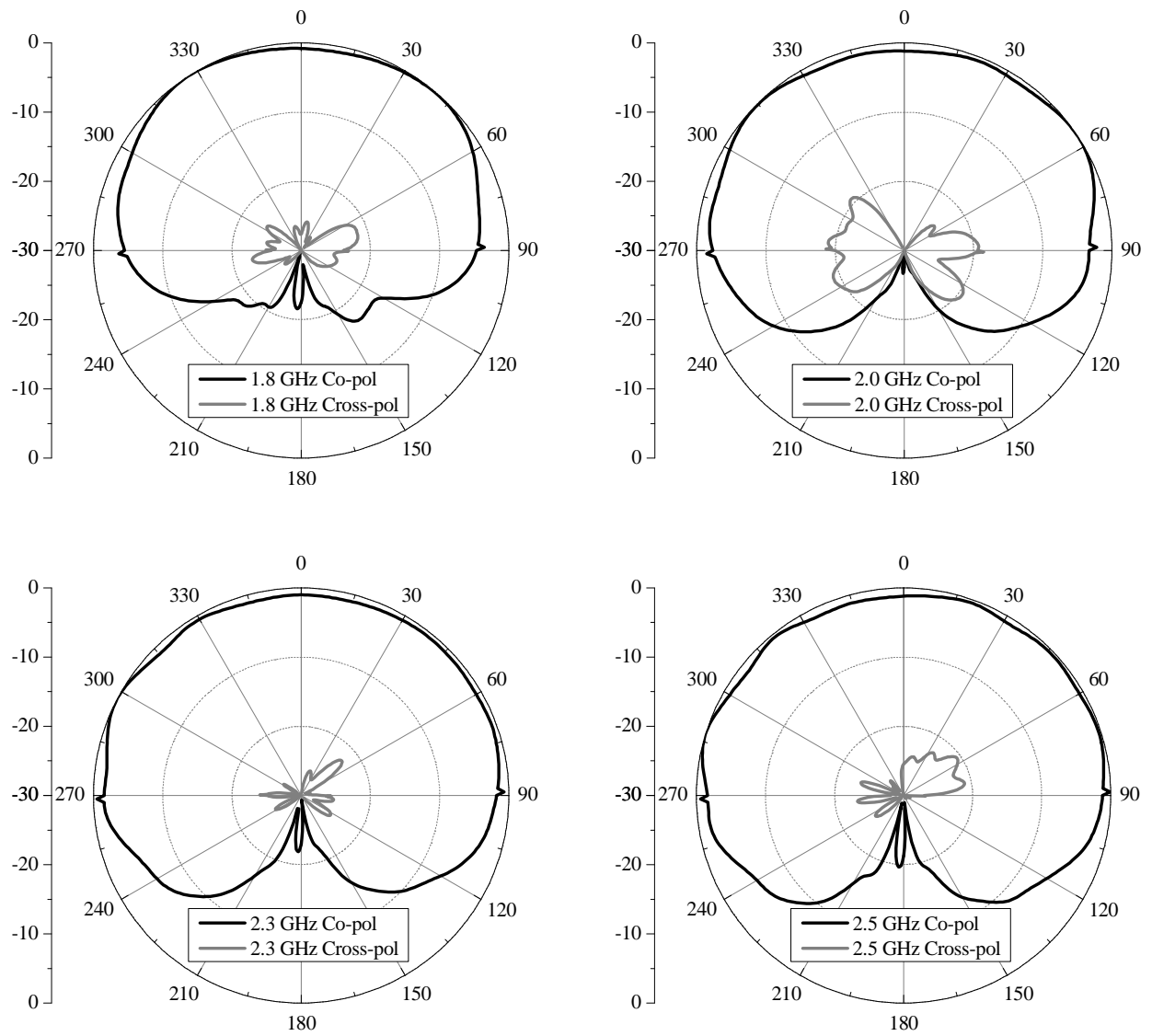


Figure 2-24 Measured normalized H-plane co-pol (black) and cross-pol (gray) patterns in dB scale for frequencies: 1.8 GHz, 2.0 GHz, 2.3 GHz, and 2.5 GHz.

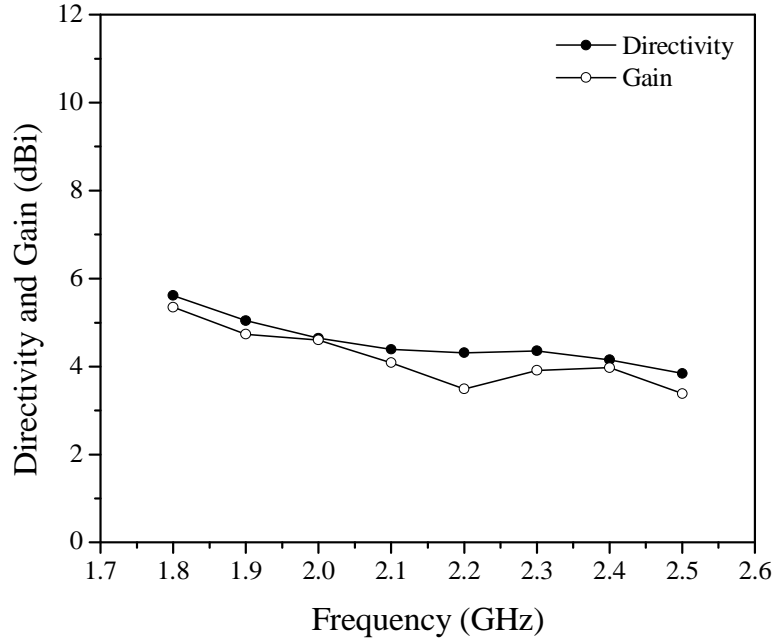
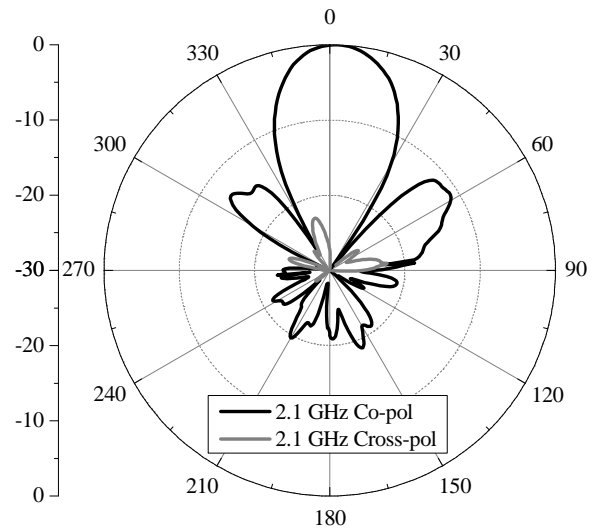
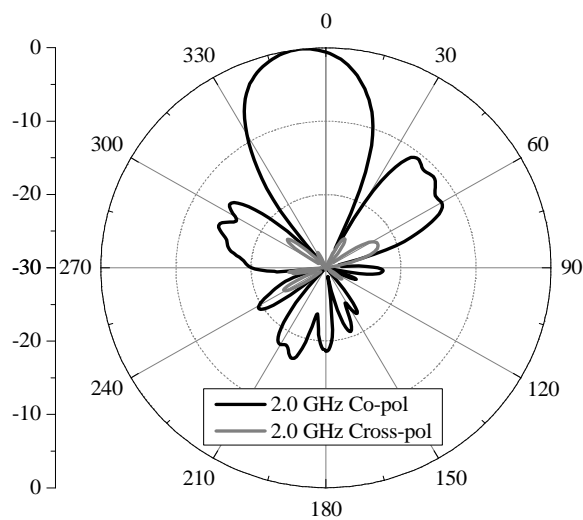
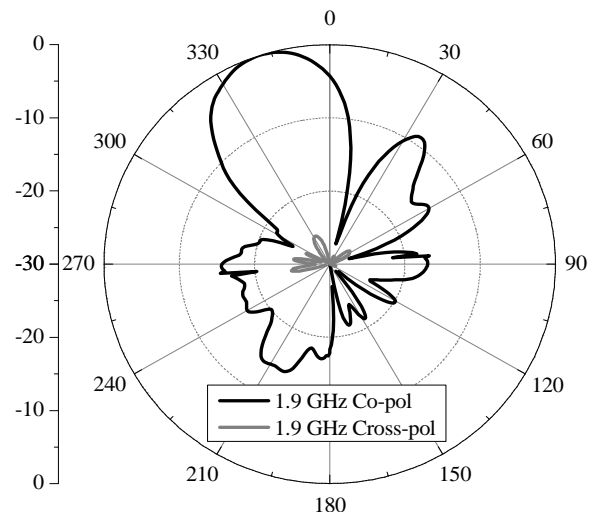
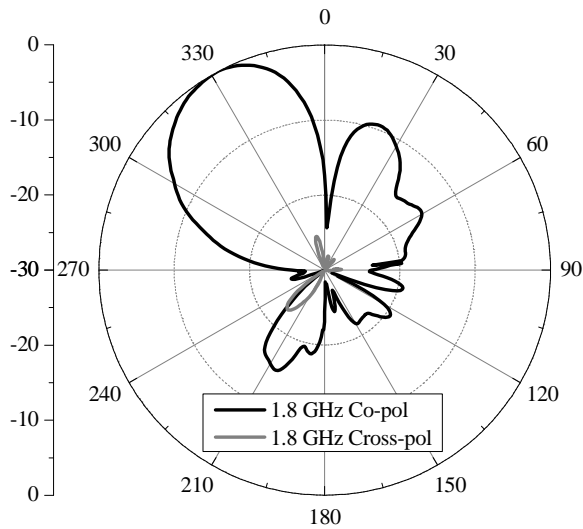


Figure 2-25 Measured directivity and gain of the quasi-Yagi antenna.

C. CRLH Feed Network with Uniform Amplitude Distribution

The measured radiation patterns for both antenna orientations using uniform amplitude distribution show good polarization properties with the scan directions that match well to the designed angles. Measured main beam angles for collinear configuration along the scan angle are $\theta_o = -29^\circ$ and $\theta_o = +28^\circ$ for ω_1 and ω_2 , respectively (Fig. 2-27). For side-by-side configuration, the measured main beam angles steered to $\theta_o = -29^\circ$ and $\theta_o = +28^\circ$ for ω_1 and ω_2 , respectively (Fig. 2-28). E-field is oriented parallel to the scanning angle in collinear configuration and E-plane is orthogonally oriented in side-by-side configuration. The SLL is around 10 dB below the main lobe. Cross-pol level is below 20 dB throughout the entire scan frequency for both E-cut and H-cut patterns. Similar to the CRLH LWAs, fan-beam radiation pattern is generated. However, the H-plane beamwidth may also be controlled by selecting antennas that are electrically long along the H-plane direction or orienting the antenna to align the element pattern

null location along the H-plane. For a quasi-Yagi antenna, the H-plane beamwidth can be squeezed when the array is arranged in side-by-side configuration (Fig. 2-29). Measured directivity and gain values are shown in (Fig. 2-30). Compared to the tapered amplitude case, uniform amplitude CRLH phased-array antenna show more directive radiation pattern.



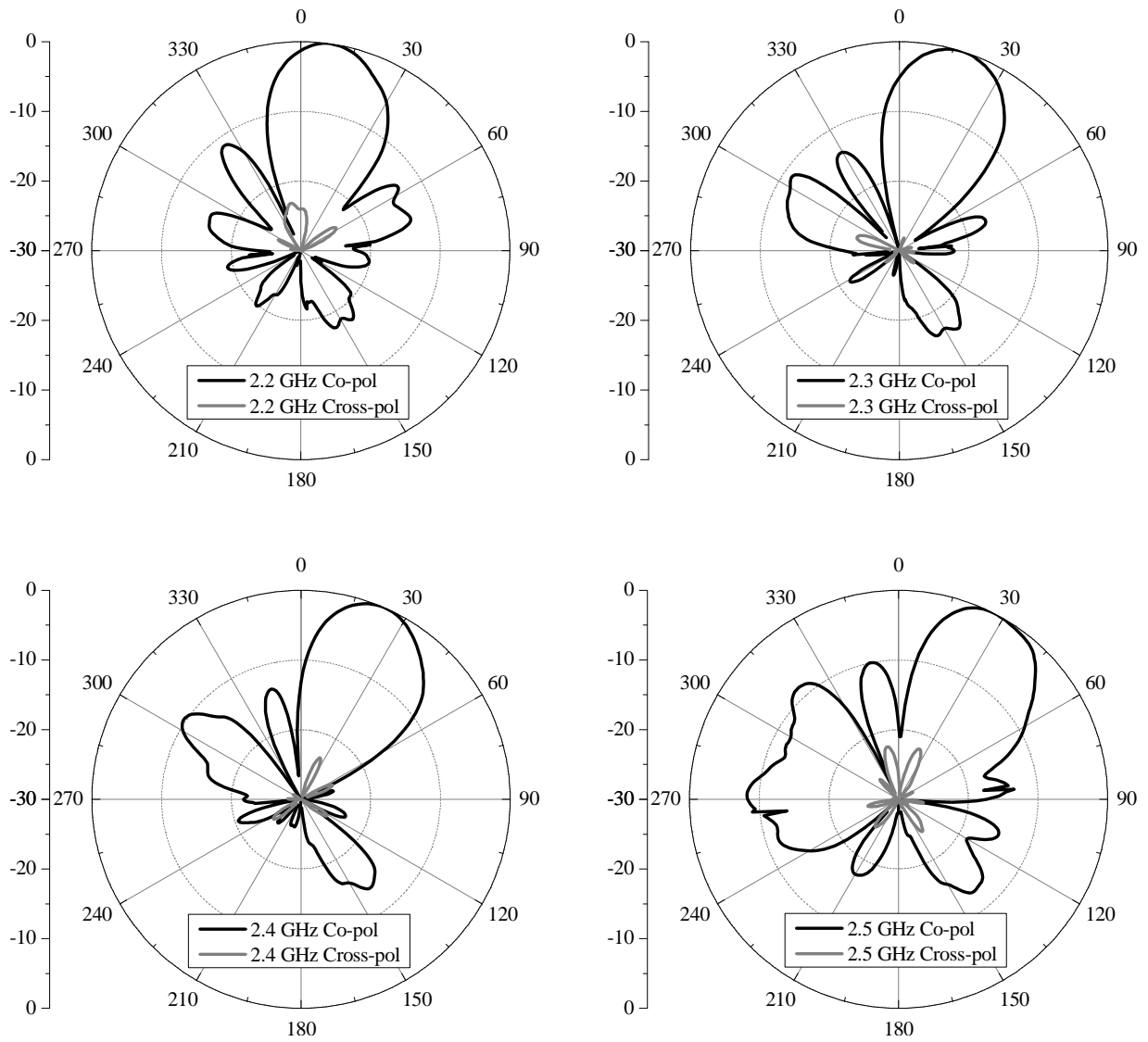
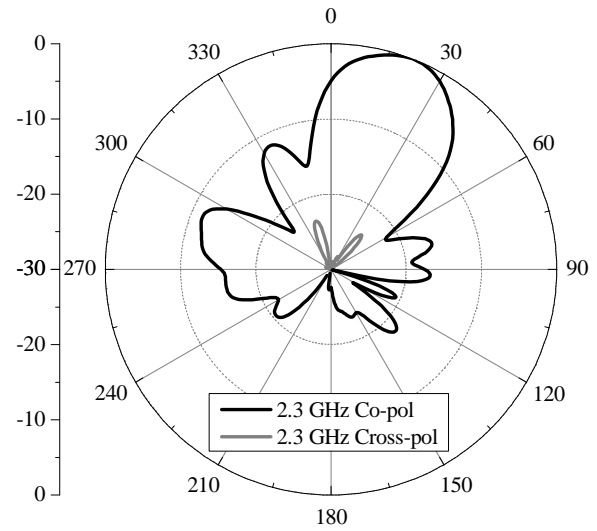
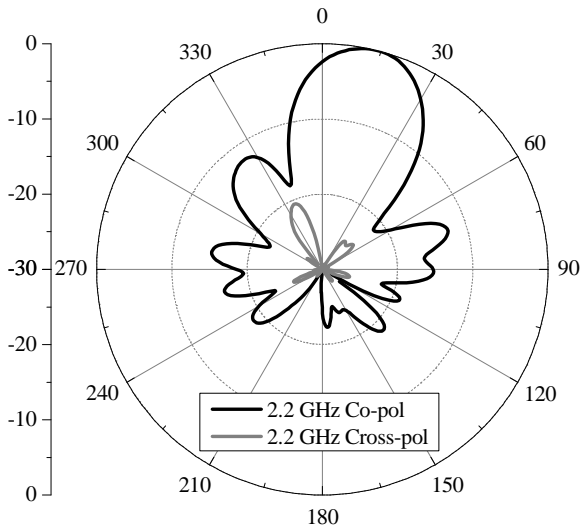
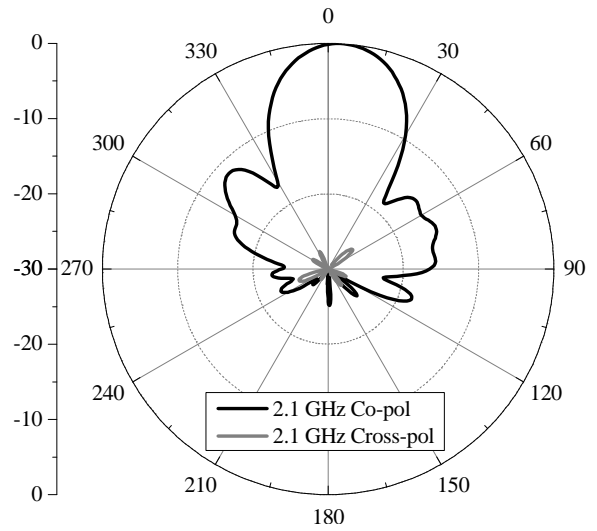
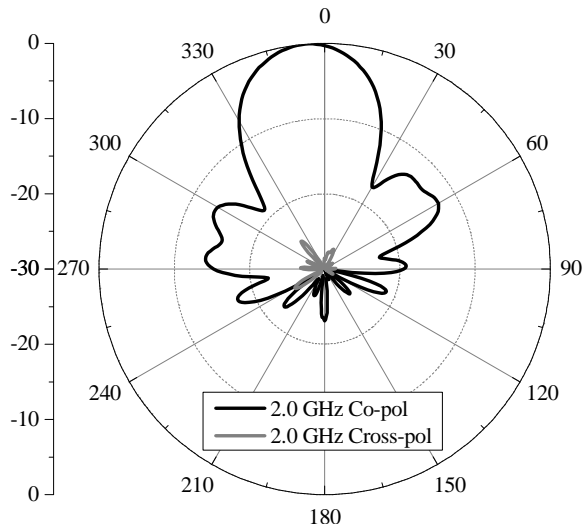
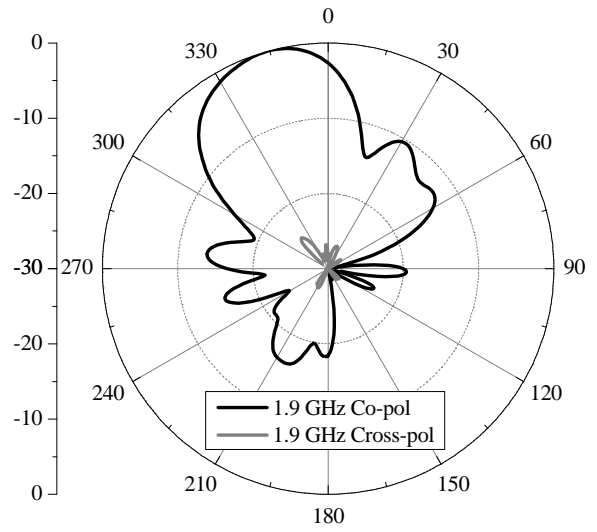
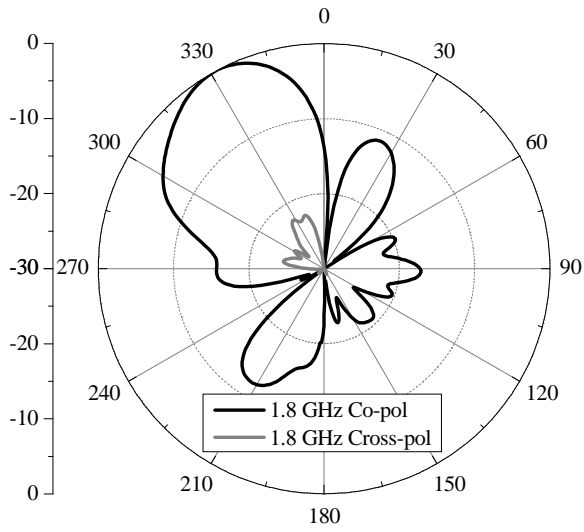


Figure 2-26 Measured four element array normalized E-plane co-pol (black) and cross-pol (gray) radiation patterns in dB scale for frequencies 1.8 GHz to 2.5 GHz using uniform amplitude CRLH phased-array feed network in collinear configuration.



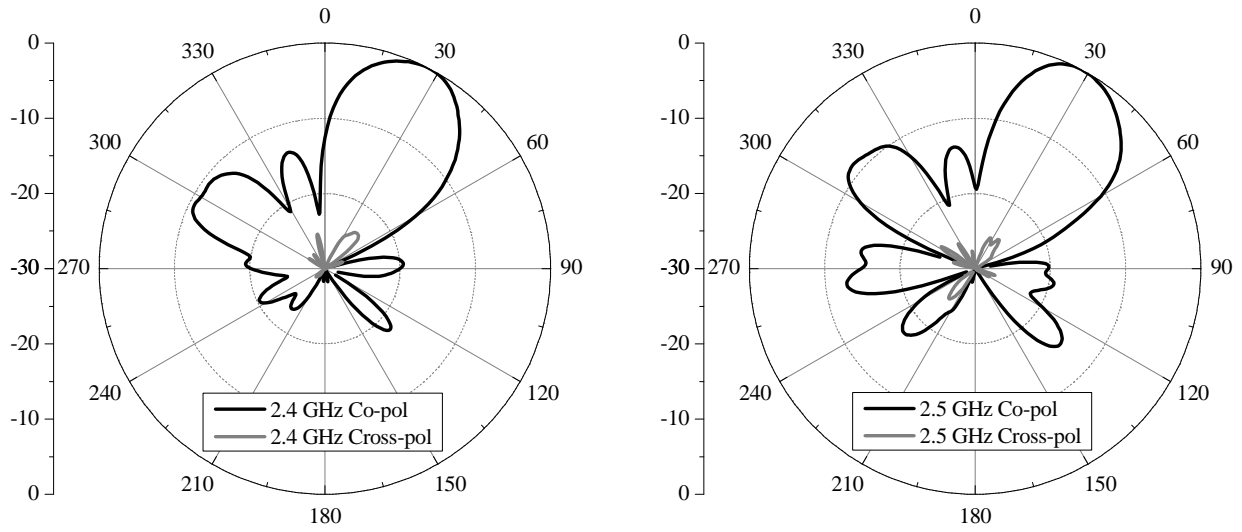


Figure 2-27 Measured four element array normalized H-plane co-pol (black) and cross-pol (gray) radiation patterns in dB scale for frequencies 1.8 GHz to 2.5 GHz using uniform amplitude CRLH phased-array feed network in side-by-side configuration.

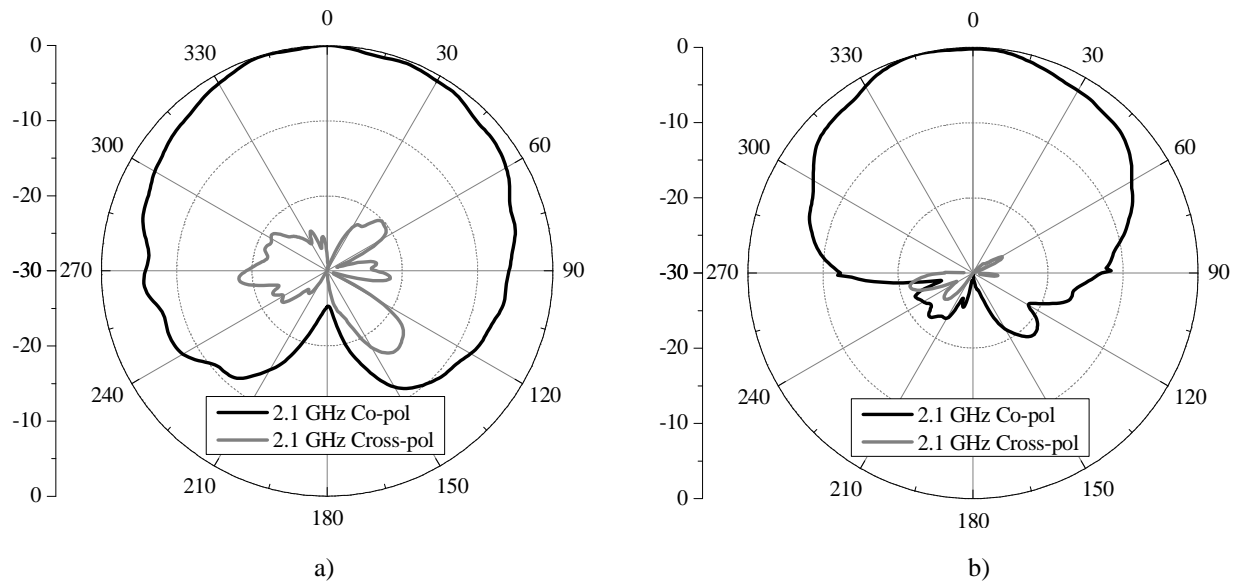


Figure 2-28 Measured four element array normalized co-pol (black) and cross-pol (gray) radiation patterns in dB scale for frequencies 2.1 GHz using uniform amplitude CRLH phased-array feed network for: a) collinear (H-plane) and b) side-by-side configuration (E-plane).

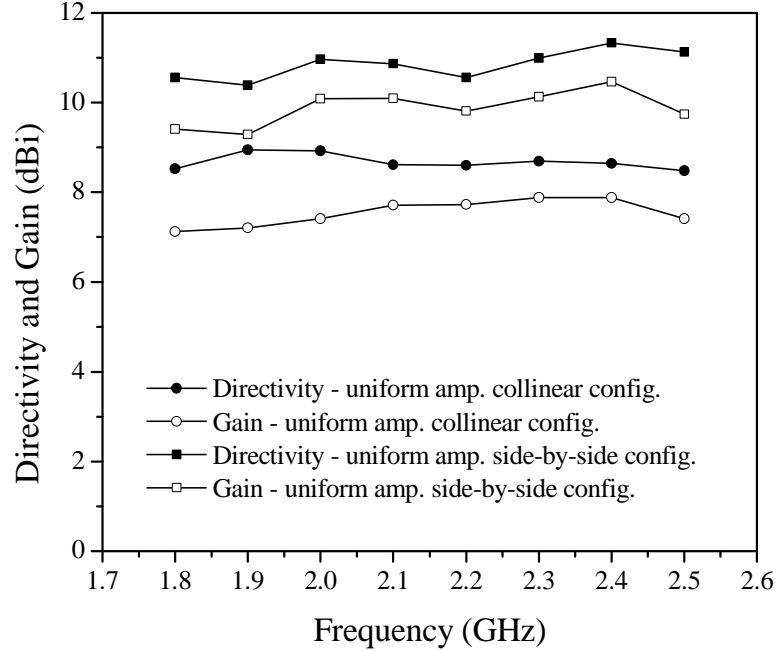
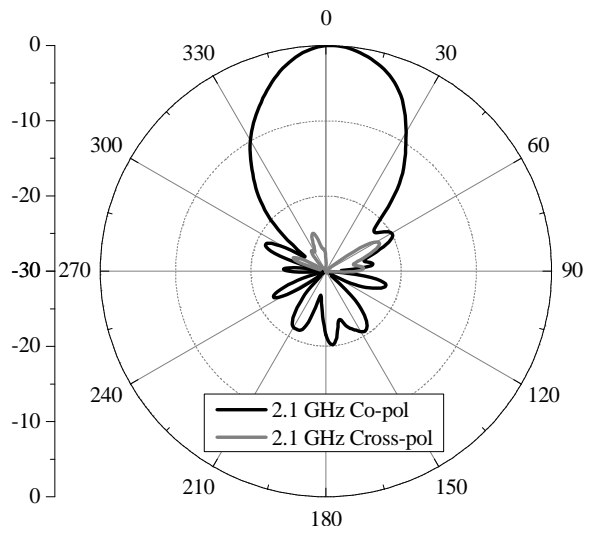
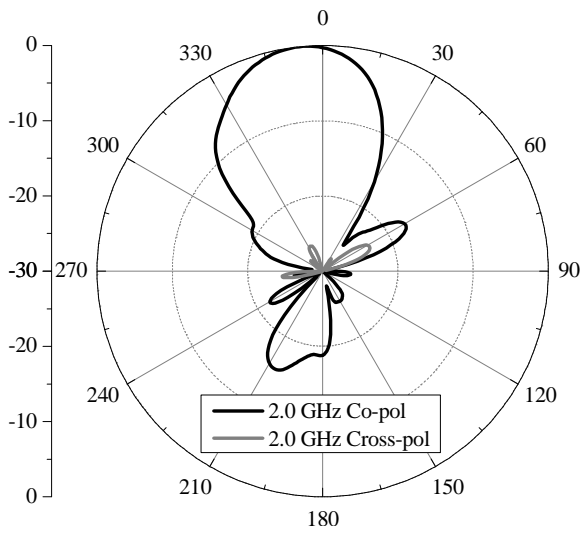
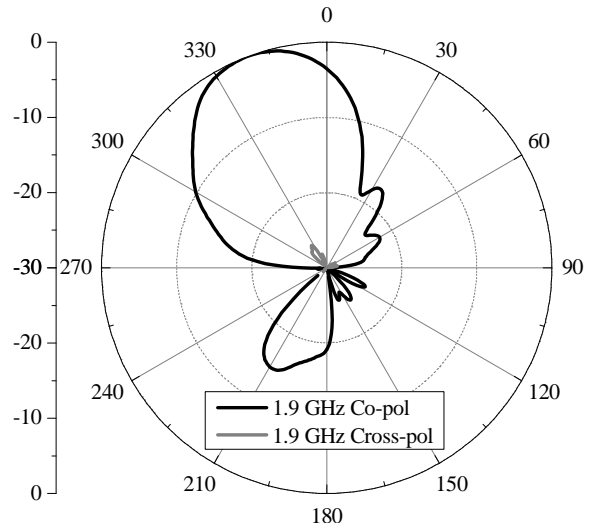
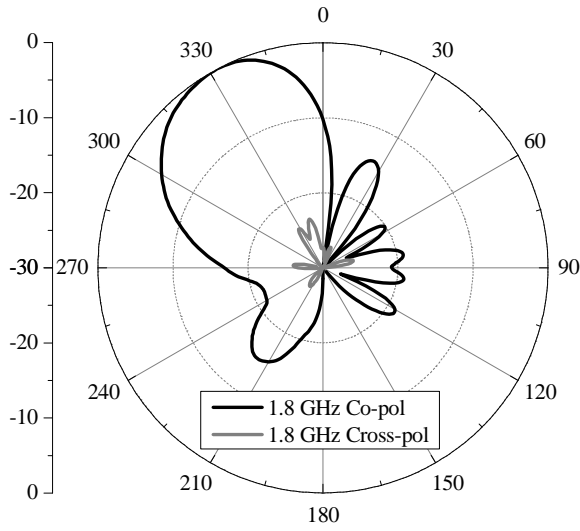


Figure 2-29 Measured directivity and gain of uniform amplitude CRLH phased array.

D. CRLH Feed Network with Tapered Amplitude Distribution

Although the main beam width is wider than that of the equal amplitude case, the SLL are much reduced in the tapered amplitude case. The SLL is below 20 dB near the center frequency, but tend to be relaxed as the frequency shifts away from the designed center frequency. Early onset of the grating lobe shown at $\omega = 2.5$ GHz in (Fig. 2-31) and (Fig. 2-32) is due to widening of the main lobe (in the AF universal pattern) resulting from tapered amplitude distribution. If desired, this grating lobe may be eliminated by placing the antenna elements closer to each other. Similar to the uniform amplitude case, the cross-pol level is suppressed below 20 dB throughout the scan frequency. Measured main beam angles for collinear configuration are $\theta_o = -28^\circ$ and $\theta_o = +27^\circ$ for ω_1 and ω_2 , respectively. For side-by-side configuration, the measured main beam angles are $\theta_o = -30^\circ$ and $\theta_o = +29^\circ$ for ω_1 and ω_2 , respectively. The H-plane main beamwidth is

also narrower for the side-by-side configurations (Fig. 2-33). Measured directivity and gain values are shown in (Fig. 2-34).



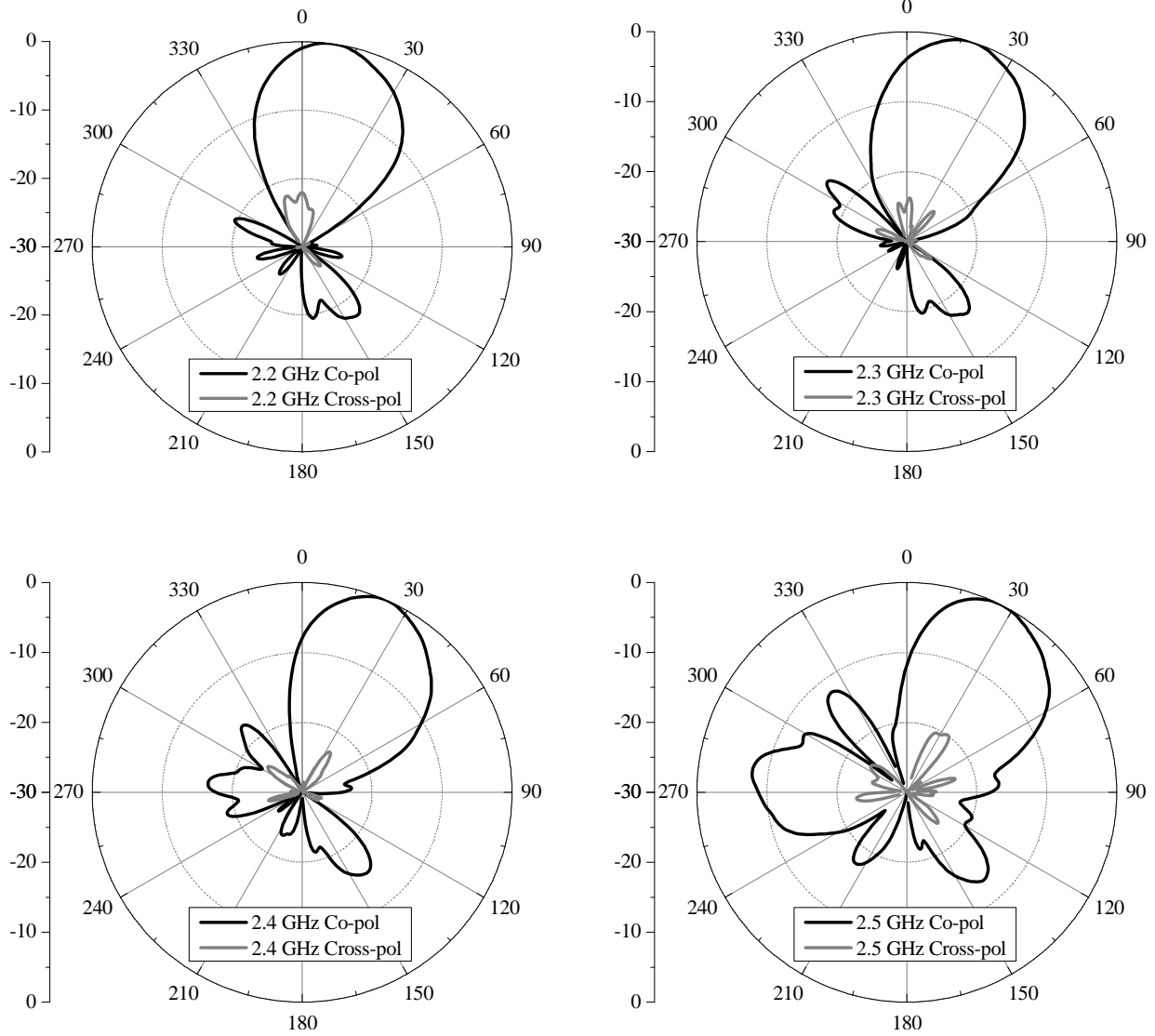
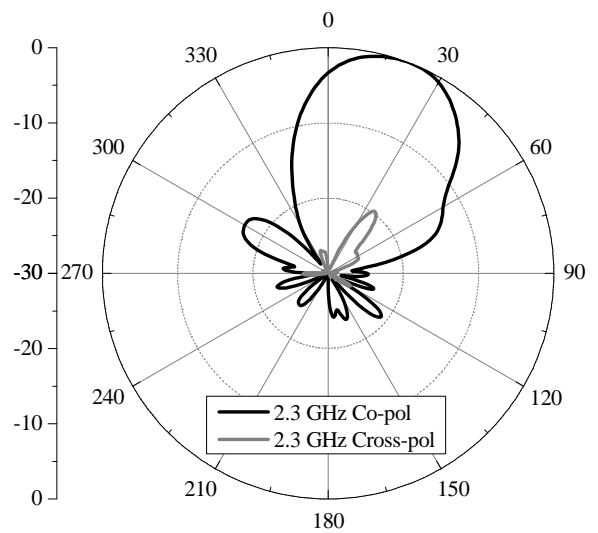
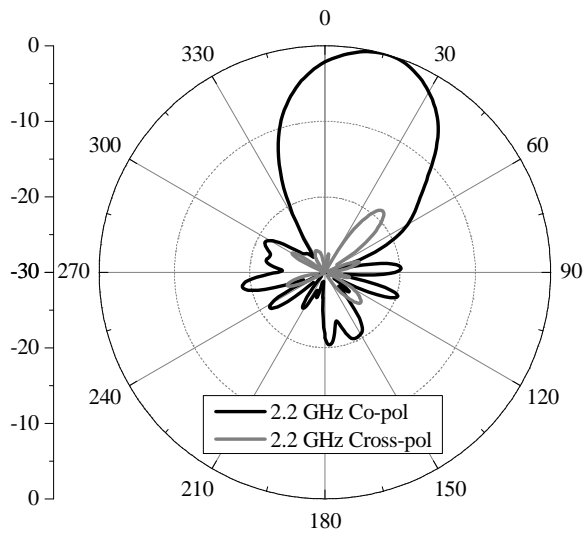
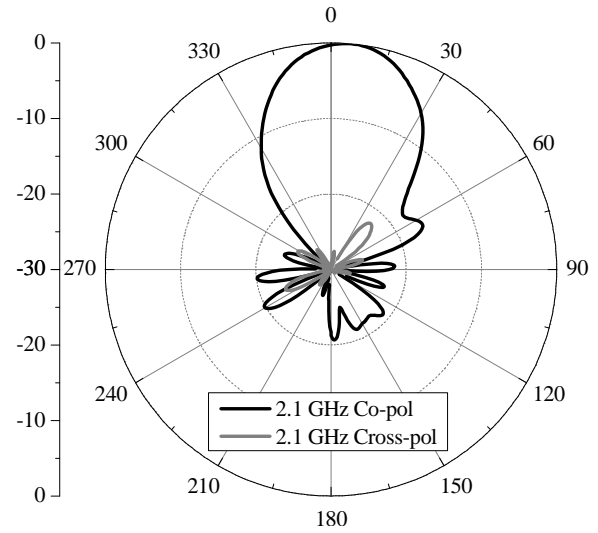
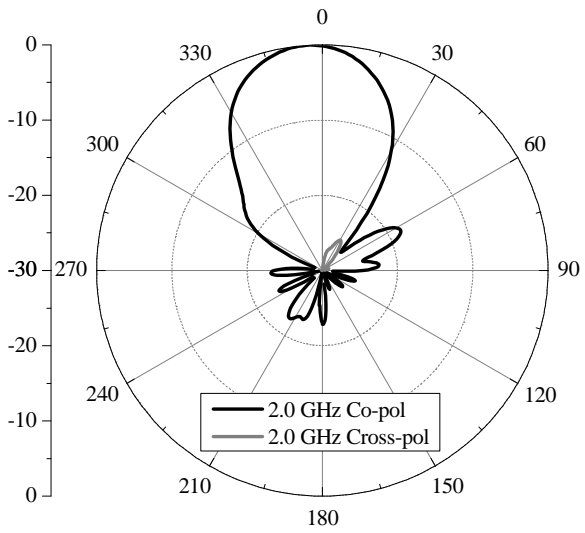
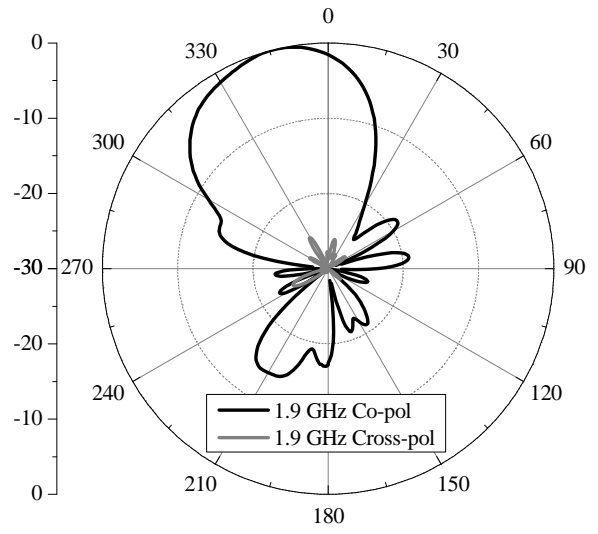
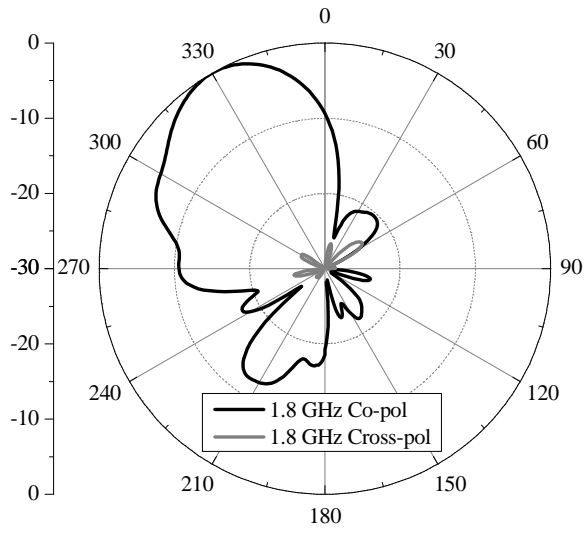


Figure 2-30 Measured four element array normalized E-plane co-pol (black) and cross-pol (gray) radiation patterns in dB scale for frequencies 1.8 GHz to 2.5 GHz using tapered amplitude CRLH phased-array feed network in collinear configuration.



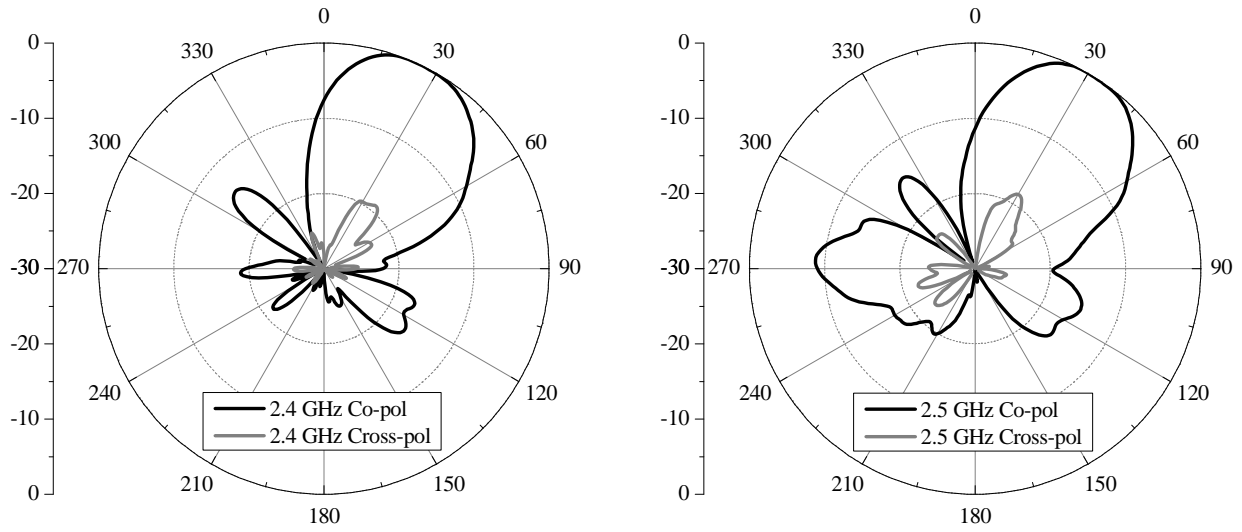


Figure 2-31 Measured four element array normalized H-plane co-pol (black) and cross-pol (gray) radiation patterns in dB scale for frequencies 1.8 GHz to 2.5 GHz using tapered amplitude CRLH phased-array feed network in side-by-side configuration.

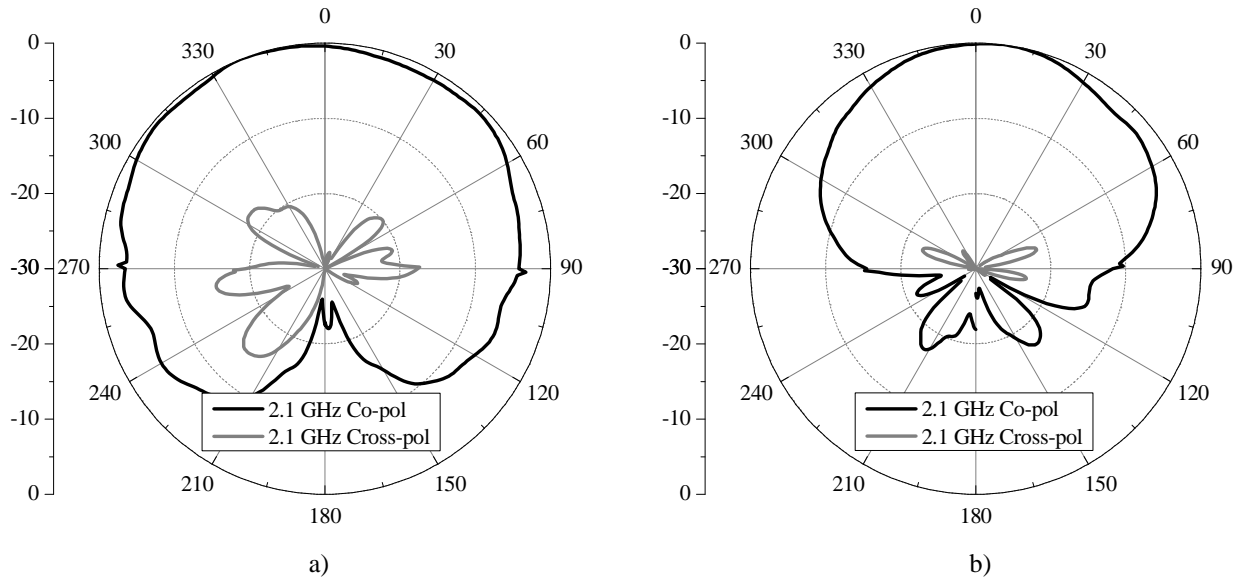


Figure 2-32 Measured four element array normalized co-pol (black) and cross-pol (gray) radiation patterns in dB scale for frequencies 2.1 GHz using tapered amplitude CRLH phased-array feed network for: a) collinear (H-plane) and b) side-by-side configuration (E-plane)..

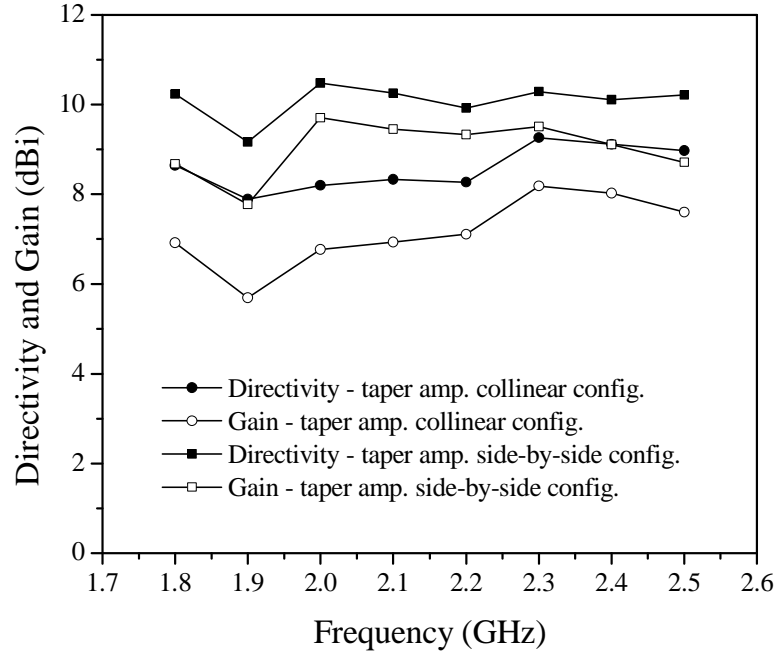


Figure 2-33 Measured directivity and gain of tapered amplitude CRLH phased array.

2.4 CONCLUSION

An all-passive frequency scanning phased-array based on the CRLH feed network provides versatile design freedom that allows easy controllability of radiated parameters including: polarization type, polarization orientation, cross-pol level, directivity, and SLL. The entire circuit can be built using passive components on planar substrates. It can direct the main beam toward the desired elevation angles while allowing bidirectional operation. Simple systematic design approach provides excellent measurement results that match well with the predicted values. The proposed CRLH phased-array network may also be used with any off-the-shelf wideband antennas. Although this method will not replace the CRLH leaky-wave antenna, it may provide benefits for other applications that require more sensitive control of the frequency scanning antenna radiation patterns.

CHAPTER 3

An Alternate Technique in Designing a Low-Profile Two-Pole Bandpass Frequency Selective Surface (FSS) using Aperture Coupling Interlayer

3.1 INTRODUCTION

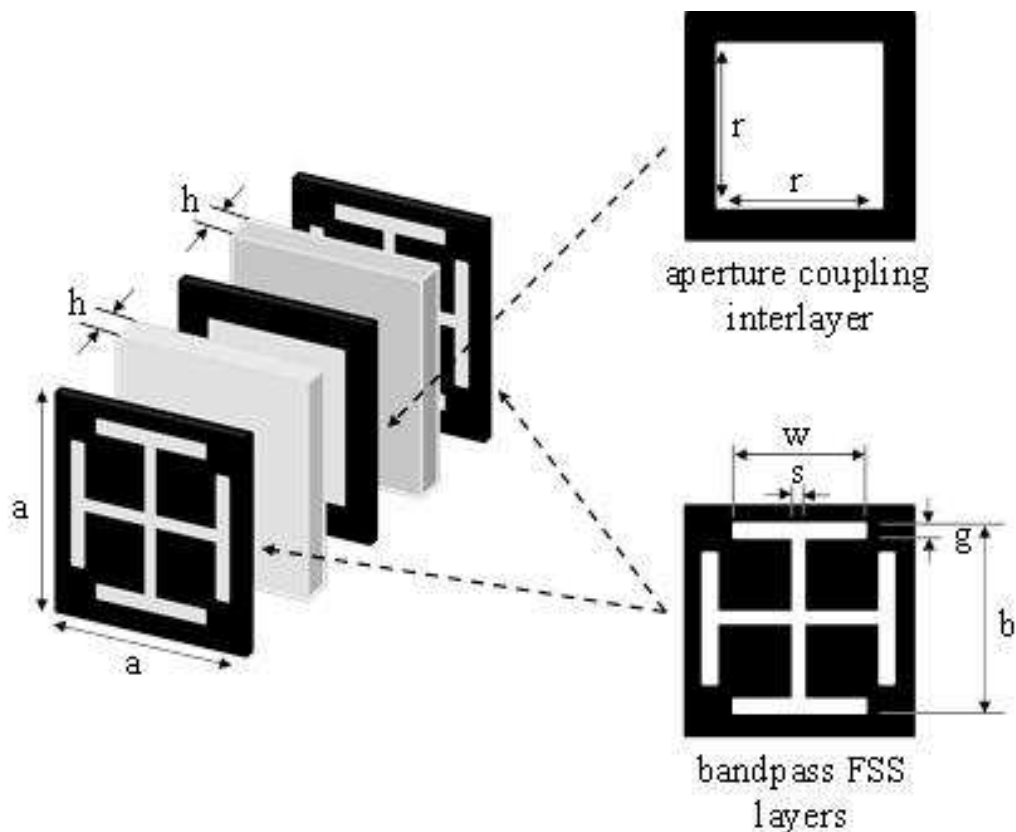


Figure 3-1 Drawing of proposed two-pole FSS based on aperture coupling interlayer. Metal is shown in black color. Dimensions used for this work are: $a = 120$ mil, $b = 115$ mil, $w = 66$ mil, $g = 7$ mil, $s = 2$ mil, $h = 15$ mil, and $r =$ varied.

Frequency Selective Surfaces (FSS) are periodic structures that effectively behave as filters to incident plane waves. In its simplest form, a single layer bandpass FSS can be modeled as a shunt parallel resonator. Multi-pole bandpass FSS can then be designed by stacking single layered bandpass FSS filters. Generally, to minimize the onset of grating lobes and desensitize the filtering response to the oblique angle incidence, FSS unit-element dimensions are miniaturized to dimensions much less than the free-space wavelength (λ_o) of the operating frequency and the spacing between the FSS layers are thinned down as much as possible without degrading the desired filter response [10]. Although $\lambda_o/4$ spacing between the FSSs may ensure a maximally flat bandpass response [52], in doing so, large spacing between the FSS layers increases sensitivity to plane waves incident from oblique angles. Simply reducing the FSS layer separation space cannot be used to solve the oblique plane wave incidence sensitivity; from coupled resonator bandpass filter theory, the stronger the coupling between resonators, the larger the separation between the pole locations [53]. As a result, designing a low-profile multi-pole FSS with flat in-band response is challenging. References [54] and [55] have achieved low-profile bandpass FSS (less than $\lambda_o/30$) with good filtering performance. However, these techniques only apply for those particular FSS unit-element structures. The purpose of this chapter is not to propose a new low-profile multi-pole bandpass FSS structure. Instead, this chapter presents a simple method to improve multi-pole filter response by combining conventional FSS shapes with aperture coupling.

Aperture coupling is well understood in the microwave community. For example, apertures can be used to control the coupling level in waveguide resonators [50]. Since FSSs are essentially resonators, FSSs behave as coupled resonator waveguides to the incident plane wave when stacked together. Therefore, the same concept may be applied to multi-layered FSSs to

control the coupling strength between the FSS resonators, thereby engineering the filtering response. A FSS using aperture coupling has been previously investigated [56]. However, the two-pole response of [12] is designed for a particular FSS structure using resonant elements (patch antennas). Also, the FSS of [12] is designed for linear polarization oriented at a particular direction.

FSSs have been the focus of intensive investigation where varieties of forms and shapes have already been extensively examined; some of the typical element types are summarized in [10]. Therefore, the aperture coupling technique when combined with typical element types may provide an alternate approach in efficiently designing low-profile multi-pole FSS filters, which provide more desirable filter responses that minimize the onset of grating lobes and are less sensitive to oblique angle incidence. In addition, the proposed aperture coupling interlayer is not limited for a particular polarization state and may be applied to any incident polarization. In this chapter, electrically miniaturized complementary Jerusalem cross structures [12] that behave as a parallel shunt tank is chosen to demonstrate the low-profile two-pole bandpass FSS filter design using the aperture coupling interlayer.

3.2 TWO-POLE FSS WITH APERTURE COUPLING INTERLAYER

The unit-element of the two-pole bandpass FSS using the proposed aperture coupling interlayer is shown in (Fig 3-1). When two FSS layers are brought close to each other, strong coupling between the FSS resonator separates the transmission pole locations, which creates undesired in-band insertion loss as shown in (Fig. 3-2). This response is plotted by simulating a two layer FSS separated by 30 mil ($\approx \lambda_o/30$), without the aperture coupling interlayer. The coupled block diagram of the proposed structure is shown in (Fig. 3-3) where P1 and P2

represent the input and output ports, R1 and R2 represent the FSS layers and all other rectangular block represent all possible coupling links between the port and resonant FSS layers. For the proposed design, the major coupling contribution comes between the two resonant FSS layers (C_{R1-R2}).

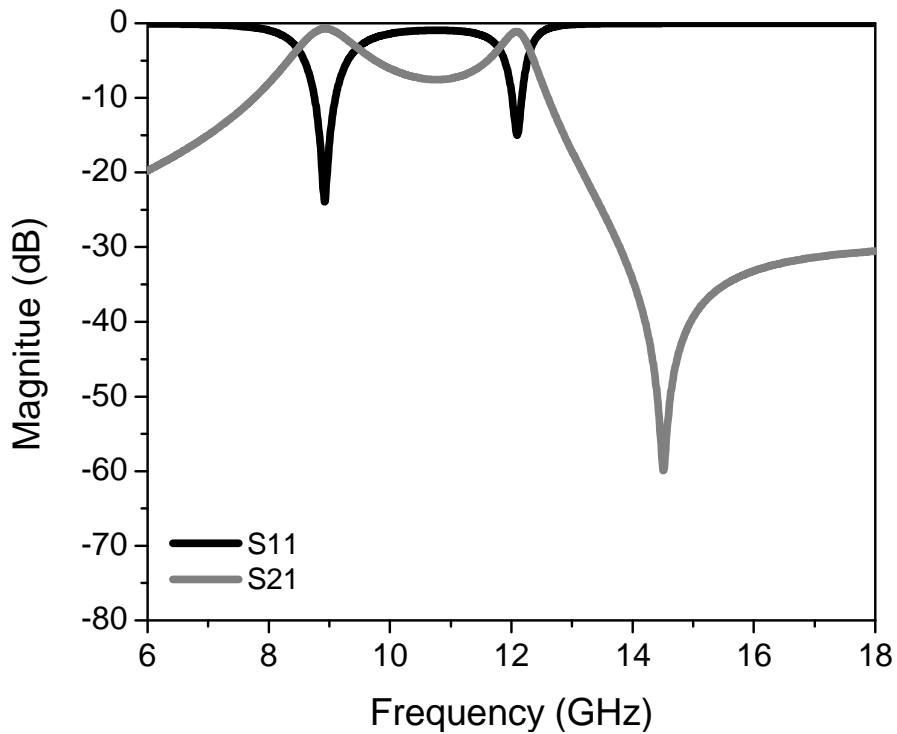


Figure 3-2 Simulated filter response of two layer FSS without the aperture coupling interlayer with $h = 15$ mil.

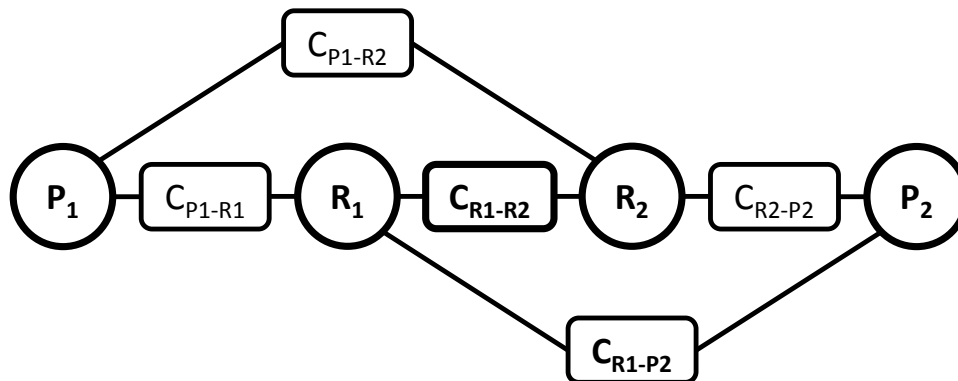


Figure 3-3 Coupling diagram of the proposed dual-pole FSS filter.

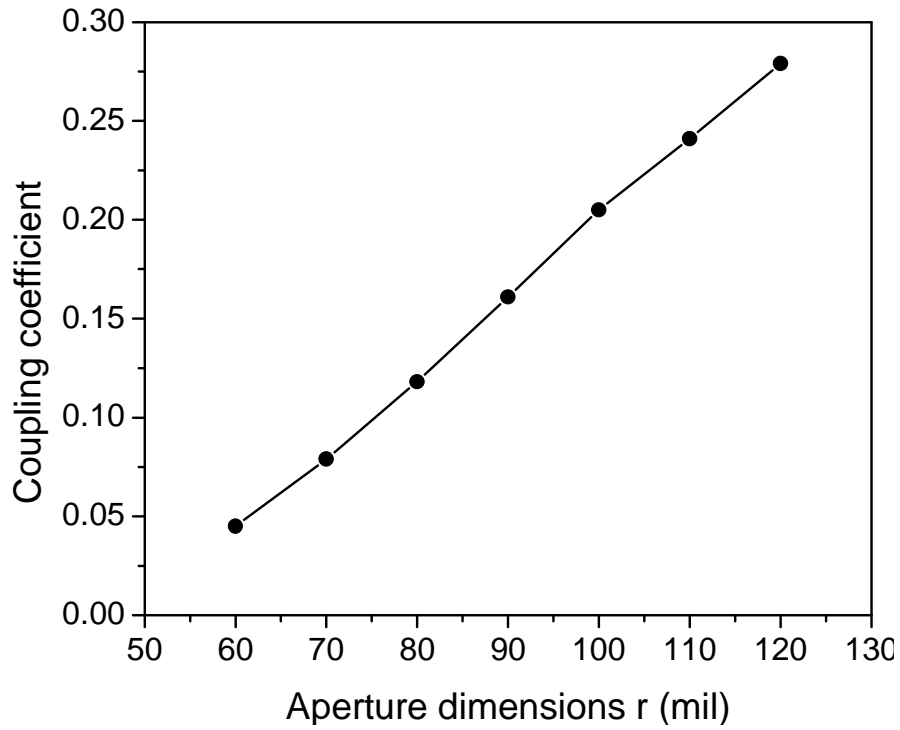


Figure 3-4 Coupling coefficient between the two FSS resonators.

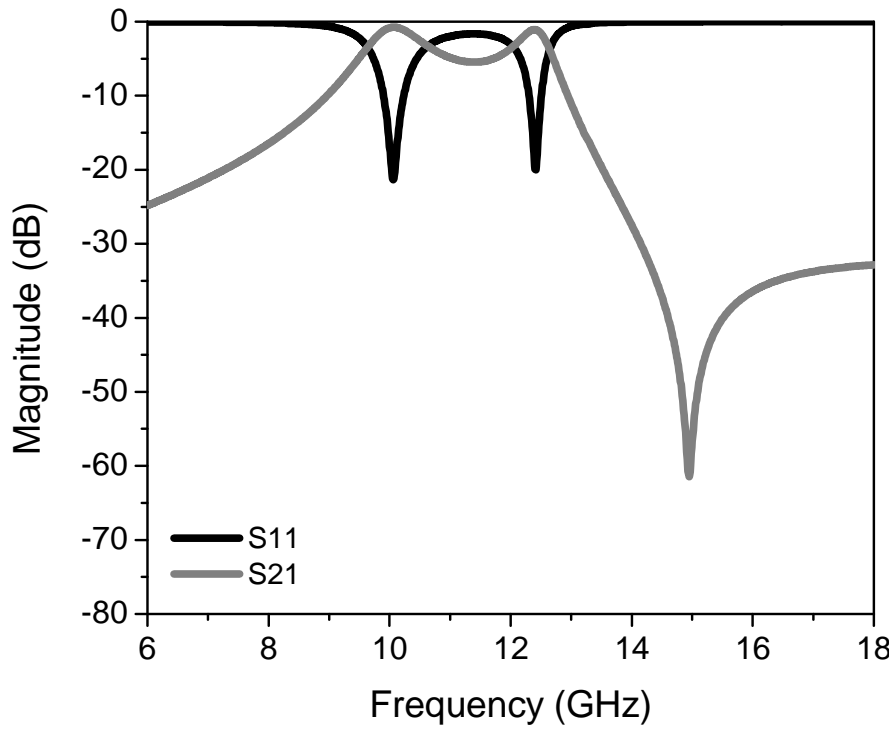


Figure 3-5 Simulated filter response of two layer FSS with the aperture coupling interlayer of aperture dimension $r = 100 \times 100$ mil and the spacing $h = 15$ mil.

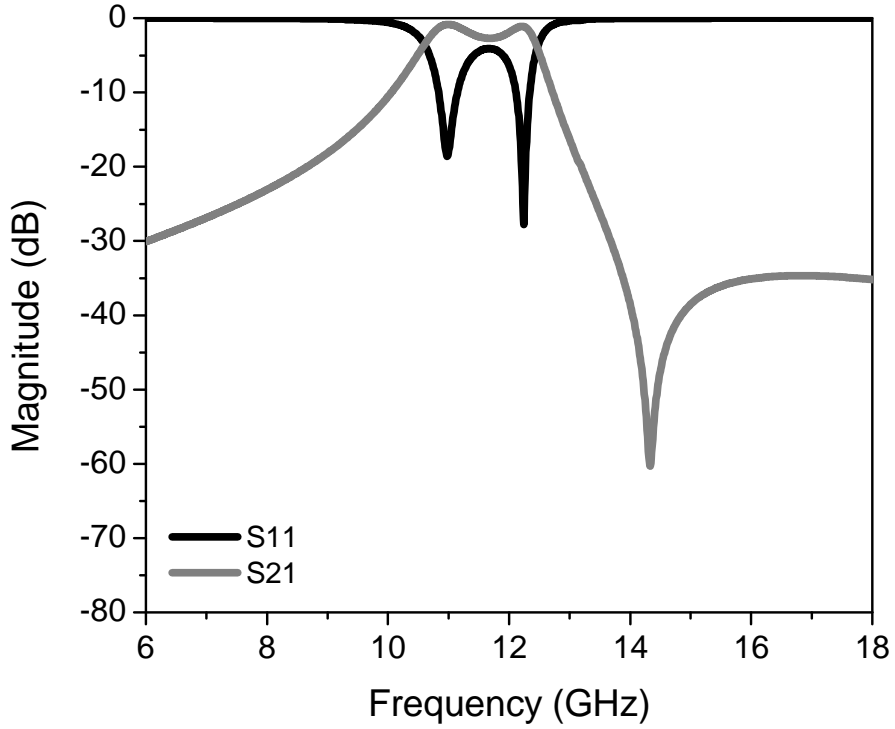


Figure 3-6 Simulated filter response of two layer FSS with the aperture coupling interlayer of aperture dimension $r = 80 \times 80$ mil and the spacing $h = 15$ mil.

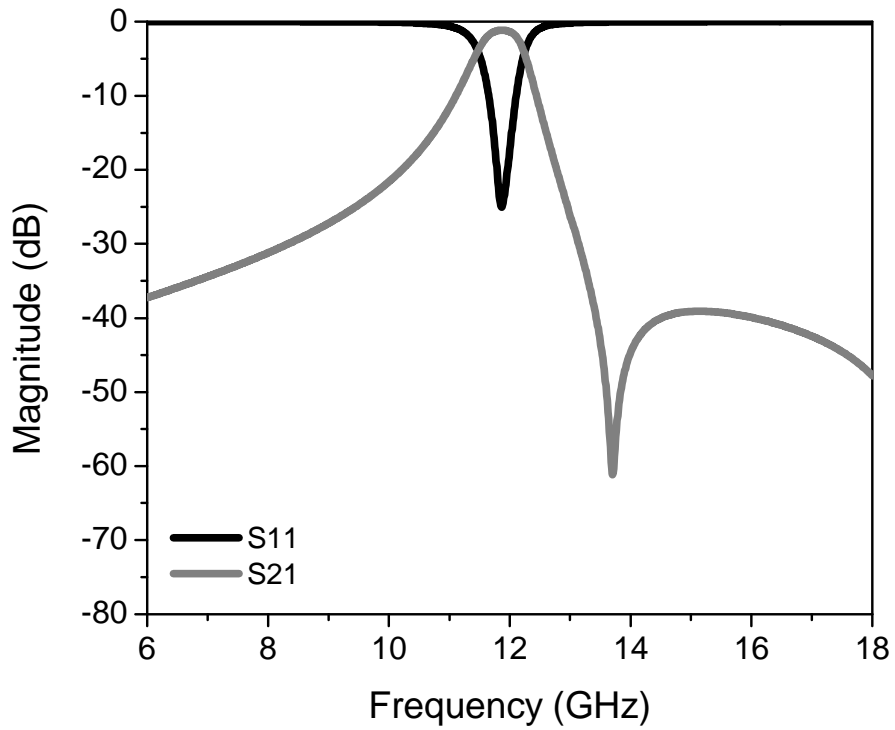


Figure 3-7 Simulated filter response of two layer FSS with the aperture coupling interlayer of aperture dimension $r = 60 \times 60$ mil and the spacing $h = 15$ mil.

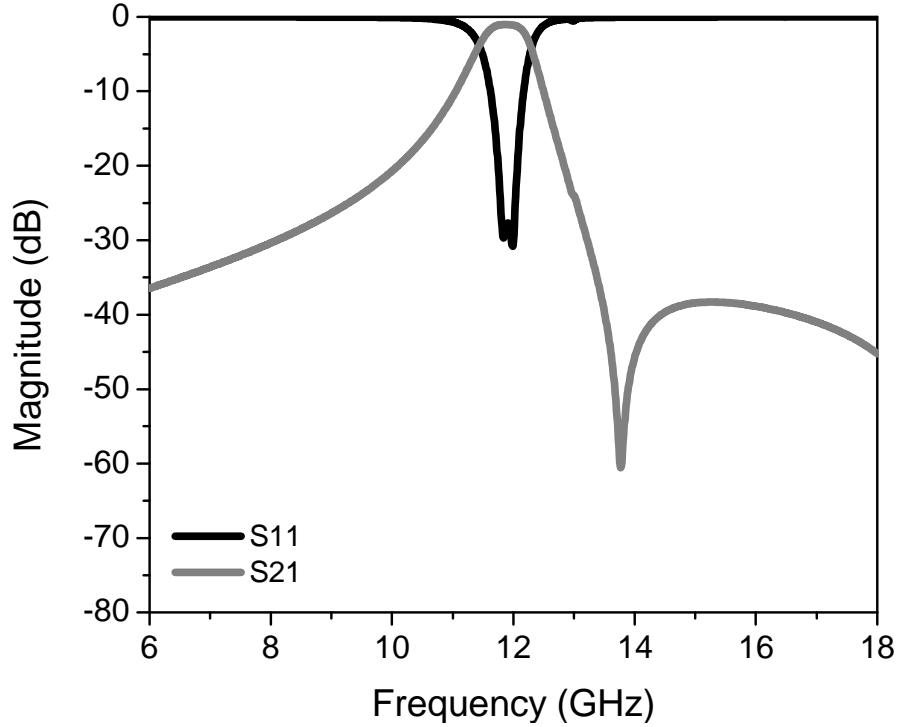


Figure 3-8 Simulated filter response of two layer FSS with the aperture coupling interlayer of aperture dimension $r = 62 \times 62$ mil and the spacing $h = 15$ mil.

Based on conventional filter coupling theory, the coupling coefficient between the two resonant FSS layers are extracted using the transmission pole and transmission zero locations obtained via full-wave simulations (Fig. 3-4). Since the unit-element size of FSS is $a = 120$ mil, the case of $r = 120$ mil in (Fig. 3-2) represents the case with no aperture coupling interlayer. As the aperture dimension of the interlayer is decreased, the coupling strength between the two FSS resonator can be reduced (pole location will converge toward each other). Cases studies of the filter transfer function versus intercoupling aperture dimensions are show the desired filter response can be obtained simply by adjusting the aperture dimension (Fig. 3-5) – (Fig. 3.7). The unit-element dimensions of the FSS used in the proposed circuit is slightly less than $\lambda_o/8$, thus a two-dimensional periodic array effectively delivers metamaterial behavior that is more robust to oblique angle incidence. By increasing the FSS unit-element’s reactance through structural

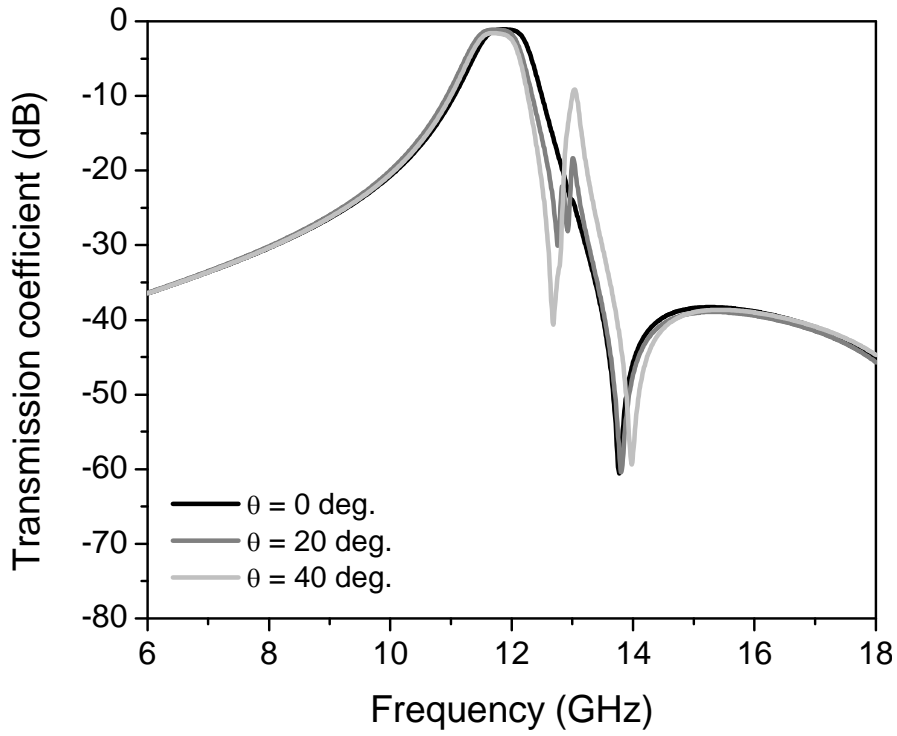


Figure 3-9 Simulated transmission coefficient for various oblique angle incidences with TE-polarizations.

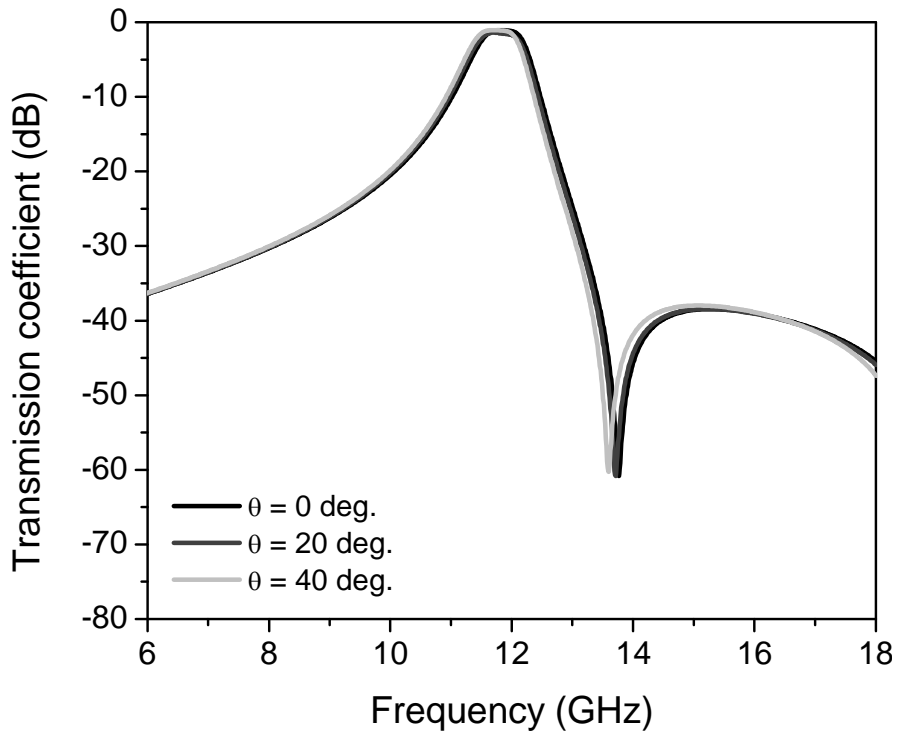


Figure 3-10 Simulated transmission coefficient for various oblique angle incidences with TM-polarizations.

design and using high dielectric substrates, the FSS unit-element can be miniaturized. In this FSS design, the narrow lines and gaps of the FSS are first designed up to the tolerable fabrication limit, then the resonant frequency is further reduced by loading the capacitance with a high dielectric substrate ($\epsilon_r = 10.2$).

3.3 EXPERIMENTAL VERIFICATION AND MEASUREMENT RESULTS

The proposed FSS with the aperture dimension of $r = 62$ mil provides the simulated filter response shown in (Fig. 3-8). Simulated center frequency is 11.9 GHz, in-band insertion loss is 1 dB, -3 dB fractional bandwidth is 8%, and high out-of-band rejection can be obtained. Oblique angle incidence studies are also performed for TE and TM polarized waves (Fig. 3-9)-(Fig. 3-10). For both polarizations, good filter response is maintained when illuminated from various oblique angles. In the TE case, the transmission pole peaking at 13 GHz is due to the bent or “crooked” mode that is inherent in the Jerusalem cross shape [10]. To verify the proposed technique, the above FSS with 42 by 42 unit cells is fabricated on a set of 5 x 5 inch RT duroid/ 6010 substrate ($\epsilon_r = 10.2$, $h = 30$ mil) as shown in (Fig. 3-11). For one of the substrate, the FSS and aperture coupling patterns are etched on each sides of the substrate. For the second substrate the FSS pattern is etched on one side and the metallic layer is completely removed on the opposite side of the substrate. The two substrates are then bonded using an adhesive. Free space measurement of the FSS is carried out in an anechoic chamber (Fig. 3-12). First, a reference transmission coefficient is measured by placing a large highly conductive plate with 5 x 5 inch window (open hole) located at the center. Then the fabricated FSS is placed over the window and the transmission coefficient is measured. The transmission coefficients of the FSS shown in (Fig. 3-13)-(Fig. 3-15) is then plotted by subtracting the measured transmission coefficients (S_{21}) of the

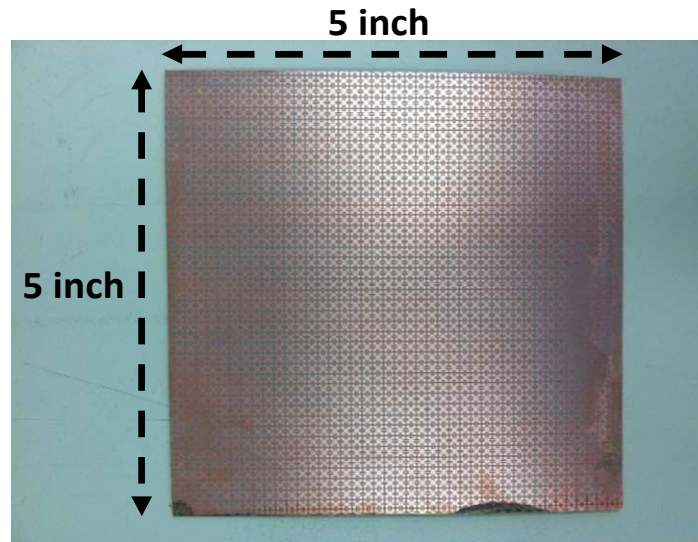


Figure 3-11 Fabricated two-pole FSS based on coupling interlayer.

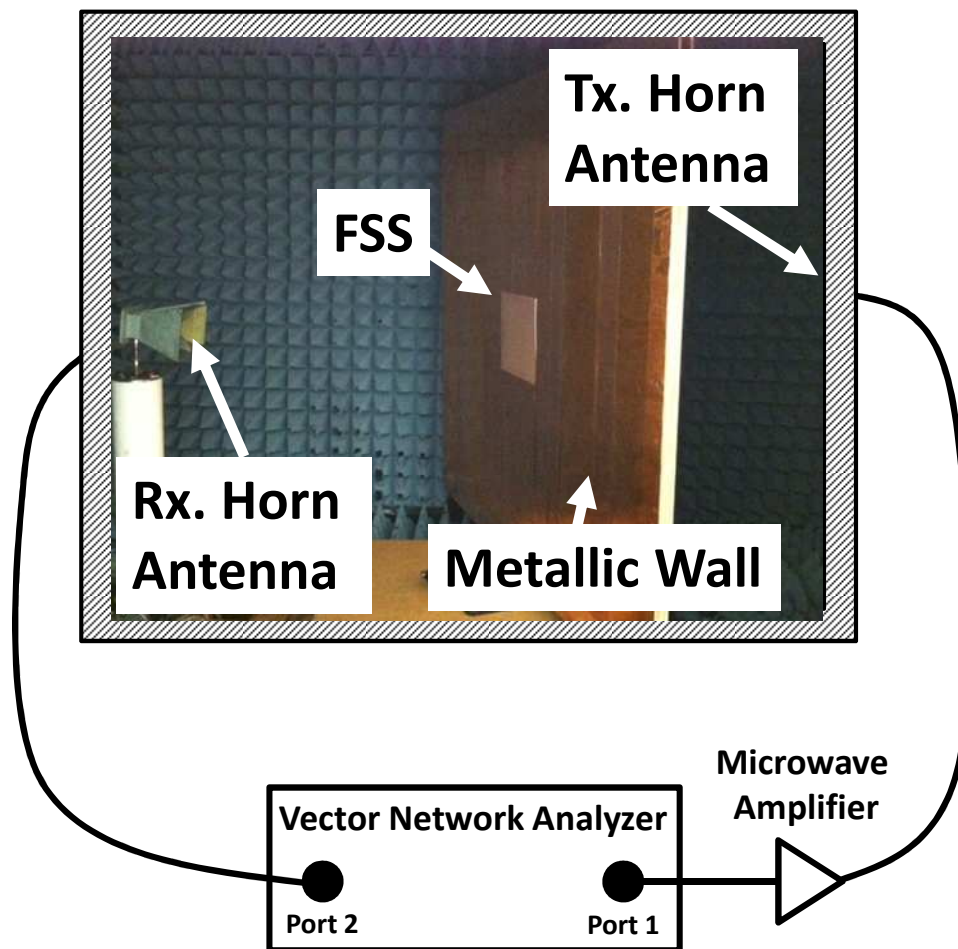


Figure 3-12 Experimental set-up.

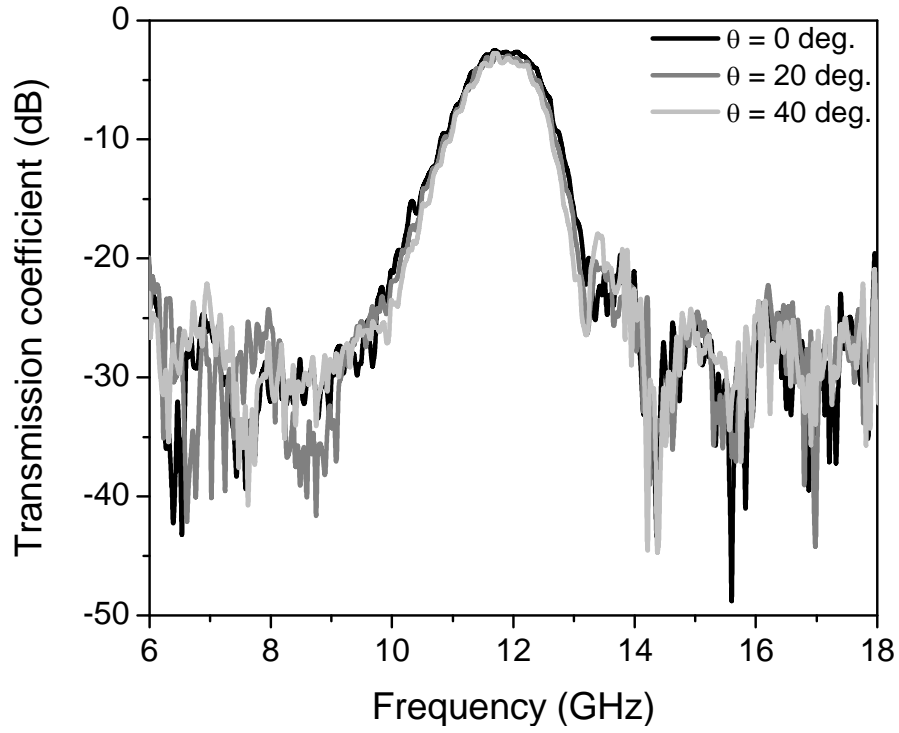


Figure 3-13 Measured transmission coefficient for various oblique angle incidences with TE-polarizations.

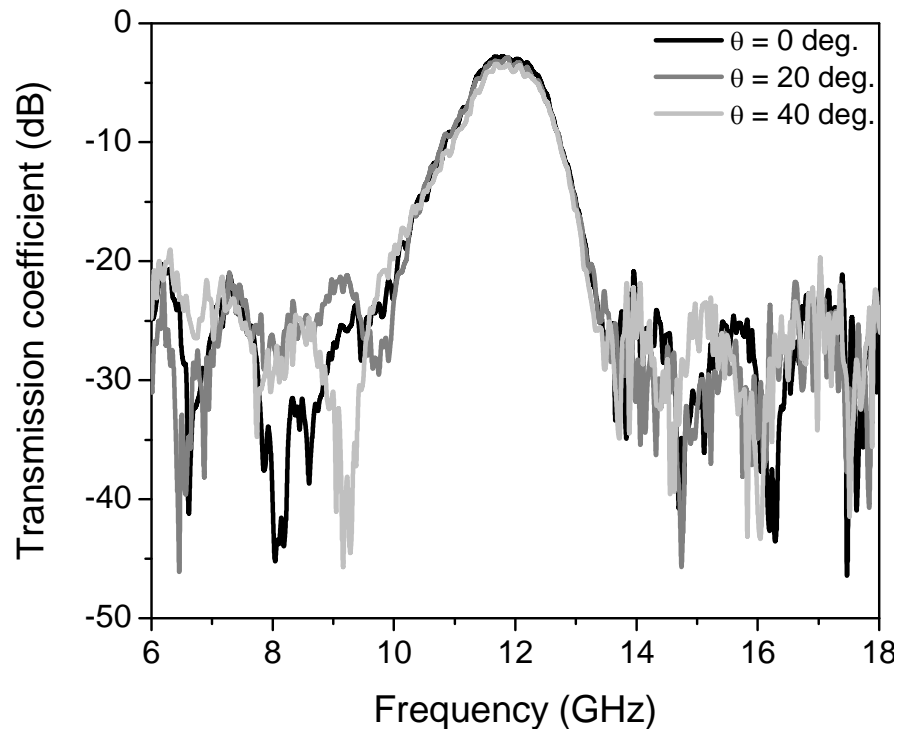


Figure 3-14 Measured transmission coefficient for various oblique angle incidences with TM-polarizations.

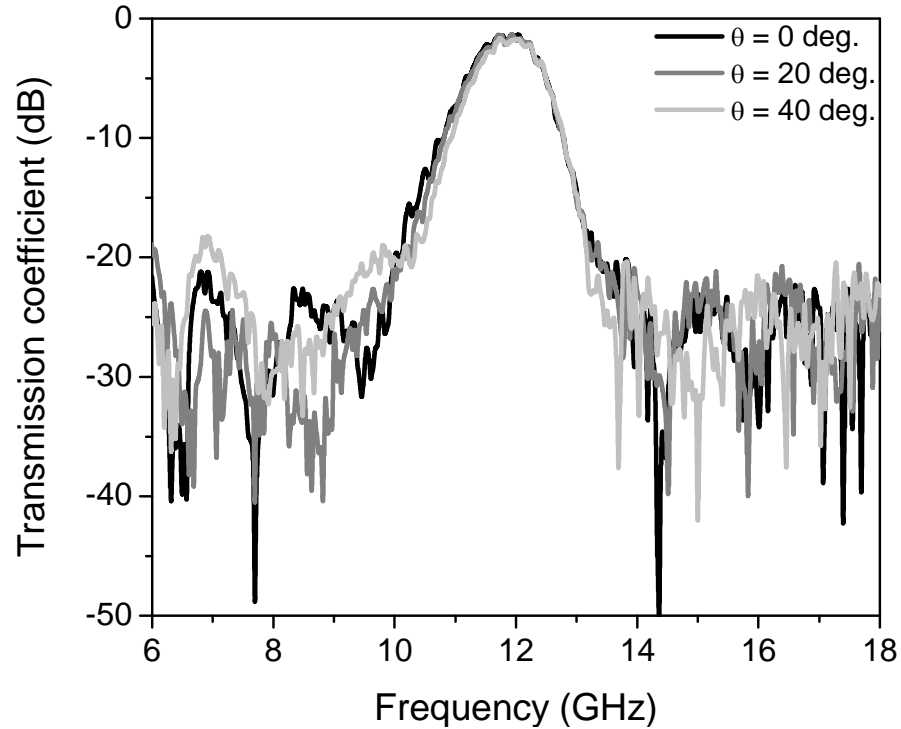


Figure 3-15 Measured transmission coefficient for various oblique angle incidences with Diagonal-polarizations.

metallic plate without the FSS from the measured S_{21} of the metallic plate with the FSS. In the measurement, three polarization cases are investigated: TE, TM, and diagonal polarization. For each case, transmitting and receiving horn antennas are rotated accordingly, then the transmission coefficient is measured for different incident angles. The measurement results show very stable filter response upon oblique angle incidence for all polarization states. Also, high out-of-band rejection can be seen. The measured center frequency is 11.75 GHz, -3 dB fractional bandwidth is 10%, insertion loss range from 1.5 to 2.7 dB for different polarizations. Imperfect alignment between the FSS layers and between the horn antennas, and the lossy adhesive material used to bond the substrates may have lowered the quality-factor of the FSS in the measurement.

3.4 CONCLUSION

The proposed technique enables an alternative approach in designing low-profile multi-pole FSS filters with low in-band insertion loss, selective filter response, and high out-of-band rejection. Given conventional FSS shapes and separation between the FSS layers, an aperture coupling interlayer can be simply inserted between the FSS layers to manipulate coupling strength between the FSS resonators, thereby used to improve the FSS's filter performance. Therefore, the proposed method aids in designing multi-layer FSS filters that are robust for oblique angle incidence by enabling the FSS layers to be positioned closer to each other.

CONCLUSION

Novel microwave devices and systems are realized in the form of periodic arrangements. In the RDA design, periodically spaced array points the rescattered signals back to the original location. In addition to this retrodirective capability, the proposed system can receive any polarization and retransmit a predictable polarization, all in an analog way. Although the presented work is designed to retrodirect with one-dimensional scanning to ease the fabrication difficulties, the same concept can be extended for two-dimensional scanning. Since individual antennas operate independently in the RDA, one of the main advantages over other rescattering techniques is its compatibility to conformal surfaces. In addition, the system allows easier integration with other electronic devices to incorporate signal amplification and modulation. The proposed system may find applications in remote sensors or drones that are subject to constant motion or rotation. If simple modulation is added to the RDA system, it can also serve as a high performance RFID tag for long distance tracking. Also, when operated with linear polarization, the RDA may be especially advantageous when mounted on large metallic background. Specular reflections from the metallic objects are regarded as noise to the retrodirected signals. However, since the proposed RDA always orthogonalizes the reflected polarization, it avoids the large undesired specular reflections from the surrounding environment. This advantage may find applications for example in long distance tracking of large metallic objects such as containers.

In the second chapter, periodicity comes in the form of both array and feeding lines (through CRLH TL). This all passive phased-array can spread the radiated beam to wider spatial angles. Previously, beam spreading was limited to a narrow spatial angle and frequency scanning

was only able to achieve through leaky-wave antennas. However, the proposed approach based on CRLH dispersion engineering provides better design control of the far-field radiated patterns by decoupling the element pattern from the array factor. As a proof of concept, lumped elements are used to design the CRLH based phased-array feed network. For high frequency applications, the same concept can be applied using non-radiating distributed component. Such as vialess CRLH stripline that is recently proposed [57]. Frequency scanning may find important application for the satellite radars or collision avoidance sensor.

Lastly, FSS based on periodic UC-PBG and filter coupled theory is designed to provide robust filtering response to the waves incident from oblique angles with arbitrary polarization at a very thin form factor. This design technique provides a much versatile design freedom in designing high performance multi-pole spatial filter. Although the concept is demonstrated for bandpass filtering, it can be extended to other filter type. Also, the proposed technique works for any arbitrary separation between the FSS layers.

BIBLIOGRAPHY

- [1]. J. Choi, Y. Dong, J. Sun, and T. Itoh, "Polarization Friendly Retrodirective Antenna Array," in *IEEE MTT-S Int. Microw. Symp. Dig.*, Jun. 2012.
- [2]. J. H. Choi, Y. Dong, J. S. Sun, and T. Itoh, "Retrodirective Array Immune to Incident Waves with Arbitrary Polarization." *IEEE Trans. Antennas Propag.*, vol. 61, no. 12, pp. 6006-6013, Dec. 2013.
- [3]. C. A. Balanis, *Antenna Theory: Analysis and Design*. New York: Wiley, 1997.
- [4]. V. Veselago, "The electrodynamics of substances with simulataneously negative values of ϵ and μ ," *Soviet Physics Uspekhi*, vol. 10, no. 4, pp. 509-514, Jan., Feb. 1968.
- [5]. C. Caloz and T. Itoh, *Electromagnetic Metamaterials: Transmission Line Theory and Microwave Applications*. New York: Wiley, 2005.
- [6]. J. Choi and T. Itoh, "Dual-band composite right/left-handed (CRLH) phased-array antenna," *IEEE Antennas Wireless Propag. Lett.*, vol. 11, pp. 732-735, 2012.
- [7]. F. Gross, *Frontiers in Antennas: Next Generation Design & Engineering*, McGraw-Hill, 2011.
- [8]. J. Choi, Y. Dong, and T. Itoh, "Composite right/left-handed (CRLH) phased-array feed network for frequency scanning antenna," in *Eur. Microwave Conf.*, Amsterdam, Netherlands, Oct. 2012, pp. 755-758.
- [9]. J. H. Choi, J. S. Sun, and T. Itoh, "Frequency-Scanning Phased-Array Feed Network Based on Composite Right/Left-Handed Transmission Lines," *IEEE Trans. Microw. Theory Tech.*, vol. 61, no. 8, pp. 3148-3157, Aug. 2013.
- [10]. B. A. Munk, *Frequency Selective Surface: Theory and Design*. New York: Wiley-Interscience, 2000.

- [11]. G. H. H. Sung, K. W. Sowerby, M. J. Neve, and A. G. Williamson, "A frequency selective wall for interference reduction in wireless indoor environment," *IEEE Antennas Propag. Mag.* Vol. 48, no. 5, pp. 29-37, 2006.
- [12]. F.-R. Yang, K.-P. Ma, Y. Qian, and T. Itoh, "A uniplanar compact photonic-bandgap (UC-PBG) structure and its applications for microwave circuit," *IEEE Trans. Microwave Theory Tech.*, vol. 47, pp. 1509-1514, Aug. 1999.
- [13]. J. Choi, J. S. Sun, and T. Itoh, "An alternative technique in designing a low-profile two-pole bandpass frequency selective surface (FSS) using aperture coupling interlayer," in *IEEE MTT-S Int. Micro. Symp. Dig.*, Jun. 2013.
- [14]. D. S. Goshi, K. M. K. H. Leong, and T. Itoh "Recent advances in retrodirective system technology," in Proc. IEEE Radio and Wireless Symp, Jan. 2006, pp. 459-462.
- [15]. L. C. Van Atta, "Electromagnetic reflector," U.S. Patent 2 908 002, Oct. 6, 1963.
- [16]. E. D. Sharp and M. A. Diab, "Van Atta reflector array," *IRE Trans. Antennas Propagat.*, vol AP-8, pp. 436-438, July 1960
- [17]. J. A. Vitaz, A. M. Buerkle, and K. S. Sarabandi, "Tracking of metallic objects using a retro-reflective array at 26 GHz," *IEEE Trans. Antennas Propag.*, vol. 58, no. 11, pp. 3539-3544, Nov. 2010.
- [18]. W.-J. Tseng, S.-J. Chung, and K. Chang, "A planar Van Atta array reflector with retrodirectivity in both E-plane and H-planes," *IEEE Trans. Antennas Propag.*, vol. 48, no. 2, pp. 173-175, Feb. 2000.
- [19]. S.-J. Chung, S.-M. Chen, and Y.-C. Lee, "A novel bi-directional amplifier with applications in active Van Atta retrodirective arrays," *IEEE Trans. Microw. Theory Tech.*, vol. 51, no. 2, pp. 542-547, Feb. 2003.
- [20]. C. Y. Pon, "Retrodirective array using the heterodyne technique," *IEEE Trans. Antennas Propag.*, vol. AP-12, pp. 176-180, Mar. 1964.
- [21]. K. M. K. H. Leong, R. Y. Miyamoto, and T. Itoh, "Moving forward in retrodirective antenna arrays," *IEEE Potentials*, vol. 22, no. 3, pp. 16-21, Aug.-Sep. 2003.

- [22]. K. M. K. H. Leong, R. Y. Miyamoto, S.-S. Jeong, Y. Wang, and T. Itoh, "A frequency autonomous retrodirective array transponder," in *IEEE MTT-S Int. Microwave Symp. Dig.*, vol. 2, June 2003, pp. 1447-1450.
- [23]. C. Lei, S. Xiao-Wei, Z. Tian-Ling, C. Chang-Yun, and L. Hao-Jia, "Design of a dual-frequency retrodirective array," *IEEE Antennas Wireless Propag. Lett.*, vol. 9, pp. 478-480, 2010.
- [24]. R. Y. Miyamoto and T. Itoh, "Retrodirective arrays for wireless communications," *IEEE Microwave Mag.*, pp. 71-79, Mar. 2002.
- [25]. B. T. Murakami, J. D. Roque, S. S. Sung, G. S. Shiroma, R. Y. Miyamoto, and W. A. Shiroma, "A quadruple subharmonic phase-conjugating array for secure picosatellite crosslinks," in *IEEE MTT-S Int. Microwave Symp. Dig.*, Jun. 2004, pp. 1687-1690.
- [26]. S. Lim, K. M. K. H. Leong, and T. Itoh, "Adaptive power controllable retrodirective array system for wireless sensor server applications," *IEEE Trans. Microw. Theory Tech.*, vol. 53, no. 11, pp. 3735-3743, Dec. 2005.
- [27]. C. Luxery and J.-M. Laheurte, "A retrodirective transponder with polarization duplexing for dedicated short-range communications," *IEEE Trans. Microwave Theory Tech.*, vol. 47, pp. 1910-1915, Sept. 1999.
- [28]. S. L. Karode and V. F. Fusco, "Self-tracking duplex communication link using planar retrodirective antennas," *IEEE Trans. Antennas Propagat.*, vol. 47, pp. 993-1000, June 1999.
- [29]. C. W. Pobanz and T. Itoh, "A conformal retrodirective array for radar applications using a heterodyne phased scattering element," in *IEEE MTT-S Int. Microwave Symp. Dig.*, Orlando, FL, June 1995, pp. 905-908.
- [30]. R. Y. Miyamoto, Y. Qian, and T. Itoh, "An active integrated retrodirective transponder for remote information retrieval-on-demand," *IEEE Trans. Microwave Theory Tech.*, vol. 49, pp. 1658-1662, Sept. 2001.
- [31]. T. Brabetz, V. F. Fusco, and S. Karode, "Balanced subharmonic mixers for retrodirective-array applications," *IEEE Trans. Microwave Theory Tech.*, vol. 49, pp. 465-469, Mar. 2001.

- [32]. W. L. Stutzman and G. A. Thiele, *Antenna Theory and Design*, 2nd ed. New York: Wiley, 1998.
- [33]. I.-H. Lin, M. DeVincentis, C. Carloz, and T. Itoh, "Arbitrary dual-band components using composite right/left-handed transmission lines," *IEEE Trans. Microw. Theory Tech.*, vol. 52, no. 4, pp. 1142-1149, Apr. 2004.
- [34]. P. Chi and T. Itoh, "Miniaturized dual-band directional couplers using composite right/left-handed transmission structures and their applications in beam pattern diversity systems," *IEEE Trans. Microw. Theory Tech.*, vol. 57, no. 5, pp. 1207-1215, May 2009.
- [35]. C.-H Tseng and T. Itoh, "Dual-band bandpass and bandstop filters using composite right/left-handed metamaterial transmission lines," in *IEEE MTT-S Int. Dig.*, pp. 931-934, 2006.
- [36]. D. Parker and D. Z. Zimmermann, "Phased arrays-Part I: Theory and architectures," *IEEE Trans. Microw. Theory Tech.*, vol. 50, no. 3, pp. 678-687, Mar. 2002.
- [37]. Y. Qian, W. R. Deal, N. Kaneda, and T. Itoh, "A uniplanar quasi-Yagi antenna with wide bandwidth and low mutual coupling characteristics," in *IEEE AP-S Int. Symp. Dig.*, vol. 2 Orlando, FL, July 1999, pp. 924-927.
- [38]. W. Menzel, "A new-traveling wave antenna in microstrip," *Arch. Eleckton. Uebertrag. Tech.*, vol. 33, no. 4, pp. 137-140, Apr. 1979.
- [39]. A. Oliner and K. Lee, "Microstrip leaky wave strip antenna," *Proc. IEEE Int. Antennas Propagat. Symp. Dig.*, pp. 443-446, Jun. 1986.
- [40]. C. Caloz and T. Itoh, "Array factor approach of leaky-wave antennas and application to 1-D/2-D composite right/left-handed (CRLH) structures," *IEEE Microw. Wireless Comp. Lett.*, vol. 14, no. 6, pp. 274-276, Jun. 2004.
- [41]. L. Lei, C. Caloz, and T. Itoh, "Dominant mode leaky-wave antenna with backfire-to-endfire scanning capability," *Electron. Lett.*, vol. 38, no. 23, pp. 1414-1416, Nov. 2002.
- [42]. A. Grbic and G. V. Eleftheriades, "A backward-wave antenna based on negative refractive index L-C networks," in *Proc. IEEE Antennas Propagat. Soc. Int. Symp. Dig.*, vol. 4, pp. 340-343, Jun. 2002.

- [43]. M. R. M. Hashemi and T. Itoh, "Coupled composite right/left-handed leaky-wave transmission-lines based on common/differential-mode analysis," *IEEE Trans. Microw. Theory Tech.*, vol. 58, no. 12, pp. 3645-3656, Dec. 2010.
- [44]. F. P. Casares-Miranda, C. Camacho-Penalosa, and C. Caloz, "High-gain active composite right/left handed leaky wave antenna," *IEEE Trans. Antennas Propag.*, vol. 54, no. 8, pp. 2292-2300, 2006.
- [45]. Y. Dong and T. Itoh, "Composite right/left-handed substrate integrated waveguide and half mode substrate integrated waveguide leaky-wave substrate," *IEEE Trans. Antenna Propag.*, vol. 59, no. 3, pp. 767-775, Mar. 2011.
- [46]. C. Caloz, T. Itoh, and A. Rennings, "CRLH metamaterial leaky-wave and resonant antennas," *IEEE Antennas Propag. Mag.*, vol. 50, no. 5, pp. 25-39, Oct. 2008.
- [47]. S. Paulotto, P. Baccarelli, F. Frezza, and D. R. Jackson, "Full-wave modal dispersion analysis and broadside optimization for a class of microstrip CRLH leaky-wave antennas," *IEEE Trans. Microw. Theory Tech.*, vol. 56, no. 12, pp. 2826-2837, Dec. 2008.
- [48]. W. R. Deal, N. Kaneda, J. Sor, Y. Qian, and T. Itoh, "A new quasi-Yagi antenna for planar active antenna arrays," *IEEE Trans. Microw. Theory Tech.*, vol. 48, no. 6, pp. 910-918, Jun. 2000.
- [49]. C. J. Lee, C. Caloz, K. M. K. H. Leong, S. M. Han, and T. Itoh, "A planar broadband antenna for UWB pulse transmission," in *Proc. 34th Eur. Microw. Conf.*, vol. 3, pp. 1329-1331, Oct. 2004.
- [50]. D. M. Pozar, *Microwave Engineering*, 3rd ed. Hoboken, NJ: Wiley, 2005.
- [51]. H.-R. Ahn and I. Wolff, "General design equations of three-port unequal power-dividers terminated by arbitrary impedances," in *IEEE MTT-S Int. Microwave Symp. Dig.*, June 2000, pp. 1137-1140.
- [52]. K. Sarabandi and N. Behdad, "A frequency selective surface with miniaturized elements," *IEEE Trans. Antennas Propag.*, vol. 55, no. 5, pp. 1239-1245, May 2007.
- [53]. J. S. Hong and M. J. Lancaster, *Microstrip Filter for RF/Microwave Application*. New York: Wiley, 2001.

- [54]. M. Al-Joumayly and N. Behdad, "A new technique for design of low-profile, second-order, bandpass frequency selective surfaces," *IEEE Trans. Antennas Propag.*, vol. 57, no. 2, pp. 452-459, Feb. 2009.

- [55]. F. Bayatpur and K. Sarabandi, "Multipole spatial filters using metamaterial-based miniaturized-element frequency-selective surface," *IEEE Trans. Microw. Theory Tech.*, vol. 56, no. 12, pp. 2742-2748, Dec. 2009.

- [56]. R. Pous and D. M. Pozar, "A frequency-selective surface using aperture-coupled microstrip patches," *IEEE Trans. Antennas Propag.*, vol. 39, pp. 1763-1769, Dec. 1991.

- [57]. J. Choi, C. Wu, H. Lee, and T. Itoh, "Vialess composite right/left-handed stripline and its applications for broadband 3-dB and tunable couplers," in *Eur. Microwave. Conf.*, *Accepted for publication*, 2014.